DEVELOPMENT OF MULTI-METAL OXIDE PHOTO-ELECTRODES FOR ENERGY APPLICATIONS

A Thesis Submitted to the Graduate School of İzmir Institute of Technology in Partial Fulfillment of the Requirements for the Degree of
MASTER OF SCIENCE
in Chemistry

by
Ecem Ezgi ÖZKAHRAMAN

August 2020
İZMİR

ACKNOWLEDGMENTS

Throughout the writing of this thesis I have received a great deal of support and assistance.

Firstly, I would like to thank my supervisor Assoc. Dr. Engin Karabudak for his guidance and encouragement during my research.

I appreciate my lab-mates for all their help with the experiments and discussions as well as creating a fun and friendly environment.

I would also like to thank my parents Esin and Teoman for their unconditional love and support. It wouldn’t be the same without their encouragement.

I would like to thank my friends; Salih Tola, Leyla Akbalık, Buse Çakır, Özge Sevin Keskin, Rabia Önen and Melahat Bozkuş; they made these two years full of fun and joyful moments.

Last but not least, I would like to thank my feline companion, Luna, for never leaving my side during the writing process and keeping me sane with her silliness.

ABSTRACT

Development of Multi Metal Oxide Photo-Electrodes for Energy Applications

Water splitting via artificial photosynthesis uses only sunlight and water to produce hydrogen and oxygen. Hydrogen can be used as a green energy source. To be able this reaction to occur there is a catalyst needed as reaction center. Platinum and Iridium are the state-of-art catalyst used for water splitting reactions. The goal of this study is to develop an earth abundant, highly stable and efficient catalyst as an alternative to noble metal catalysts. For this purpose, ABO3 type perovskites was chosen to study for their abundancy and proven electrochemical efficiencies. BSCF was chosen as the starting point of this study because it is known for its great catalytic activity compared to state-of-art catalysts such as Iridium Oxide. To enhance the stability and catalytic activity of synthesized perovskite oxides, several foreign atoms (dopants) were introduced to their structure from B-site. Each perovskite was synthesized by the EDTA-Citrate complexing Sol-Gel method. Also, for dopants, cost-efficient and electron conductive elements was chosen in each study. As HER catalysts, manganese, zinc, and copper were introduced to BSCF structure as dopant, while for OER, silver was used as a dopant. In this study, catalytic activities and stabilities were tested by electrochemical methods. All electrochemical measurements were performed in alkaline media by three-electrode configurations. Perovskite oxides were prepared by the coating of their inks on Ni foam substrates by drop coating for HER and OER activity measurements by electrochemical methods. For the bulk and surface characterization of synthesized perovskite oxide powders, SEM, XRD, XPS, and BET analysis was performed.

ÖZET

Enerji Uygulamaları İçin Çoklu Metal Oksit Foto-Elektrotların Geliştirilmesi

Yapay fotosentez ile suyun ayrıştırılması yöntemi, su ve güneş ışığı enerjisini kullanarak yenilenebilir enerji kaynağı olan hidrojen elde edilmesini sağlar. Suyun elektrolitik ayrıştırılması yöntemi mekanizma olarak yavaş ve verimi düşük olduğundan markette halihazırda kullanılmakta olan fosil yakıtlarla yarışmakta yetersiz kalır. Bu sebepten dolayı, katalizörler kullanılmaktadır. Bu çalışmanın amacı katalizör olarak kullanılan iridyum ve platin gibi soy metaller yerine yer yüzünde bulunma yüzdesi fazla olan ve düşük maliyetli katalizörler sentezlemektir. ABO_3 tipi perovskit yapıları bu kritere uymakla birlikte elektrokimyasal aktiviteleri açısından da daha önceki çalışmalarda kendilerini kanıtlamışlardır. Özellikle $Ba_{0.5}Sr_{0.5}Co_{0.8}Fe_{0.2}O_{3-\delta}$ (BSCF), su ayrışması katalizörleri arasında en verimlisi olarak kabul edilen iridyum oksitten daha yüksek verim sağladığından dolayı bu çalışmanın ana konusu olarak tercih edilmiştir. BSCF'nin kararlılık ve katalitik aktivitesini arttırmak için, kristalin B atom grubuna yabancı atomlar eklenmiştir. Hidrojen çıkış reaksiyonlarına yönelik aktivitenin arttırılması için yapıya mangan, çinko ve bakır eklenirken, oksijen çıkış reaksiyonlarına yönelik aktivite çalışmalarında gümüş atomları eklenmiştir. Çalışmada kullanılan bütün perovskitler Sol-Jel metoduna göre sentezlenip, kompleksleştirici olarak EDTA – Sitrat kullanılmıştır. Elektrokimyasal karakterizasyonlar için, sentezlenen toz yapıları mürekkep haline getirildikten sonra nikel köpüğün üzerine damlatılarak kaplanmıştır. Elektrokimyasal ölçümler alkali ortamda alınırken üçlü elektrot konfigürasyonu kullanılmıştır. Yapısal ve yüzeysel karakterizasyonlar için XRD, XPS BET ve SEM analizleri kullanılmıştır.

TABLE OF CONTENTS

LIST OF FIGURES

Figure **Page**

LIST OF TABLES

Table **Page**

CHAPTER 1

INTRODUCTION

1.1. Sustainable Energy

The world's energy need is growing every day with the growing population and increasing demand by industry. Currently, this energy need is supplied up to %85 percent from fossil fuels. Fossil fuels such as oil and coal are among the main reasons for greenhouse gases such as carbon dioxide which causes global warming on a great scale. Also because of the carbon dioxide emission, ocean water becomes more acidic and this creates a harmful environment for living creatures in the oceans. To be able to eliminate further irreversible effects on environment, it is a necessity to halve down the carbon dioxide emission by 2050. [1] Besides its harms to the environment, according to estimates by the International Energy Agency, the world's oil reserves will decline by 40-60 % in the next twenty years.[2] If the consumption of coal increases at a rate of 5%, the world's coal sources are expected to be run out in 100 years. Also, BP Statistical Review of World Energy specifies when energy sources are expected to run out as; Coal - year 2169, Natural Gas - year 2068, Crude Oil - year 2066. [3] To supply enough energy to the world requires the support of other sources such as nuclear energy and renewable energies.

Renewable energy takes its sources from the earth and converts it into a form that we can use, which is electricity. Wind power, hydropower, solar energy, geothermal energy, and bioenergy are types of renewable energy. Most used renewable energy sources are wind power and hydropower since they can provide large amounts of energy. According to the statistics of the European Statistics Office, among the renewable energy sources, hydropower (%36,9) and wind power (%31,8) was the most used ones in 2016. Although these sources are clean and reliable, they need large areas and environmental conditions must be convenient to build these facilities. Since hydropower and wind power require sophisticated equipment and engineering, they have high investment and maintenances costs. Hydropower requires larger area use in comparison to wind power

and it is considered harmful to the ecosystem that it is built. The efficiency of an energy source can be calculated by the cost of the fuel it uses and production and the recovery costs of its harms to the environment. When these points considered, wind power is the most efficient among all renewable energy sources with a % 1164 efficiency percentage.

Solar energy requires least area use among all the renewable energy types and has the least greenhouse gas emission. One of the common problems of most used energy sources such as wind, hydro, and solar is that they cannot provide continuous energy. Since most of the renewable energies take its source from the earth, their efficiency is dependent on the environment therefore it is not reliable. But their intermittent nature doesn't mean humans cannot rely on these sources. Since the world has great potential by these sources, by the right ways of usage and convention we can produce reliable green energy.

Solar energy is clean and supplies unlimited energy. Every 30 minutes the Earth absorbs enough sunlight to supply the whole world a yearlong with energy. Solar energy sources supply energy larger than 20 TW and it covers the worlds energy need for today's conditions. [4] If today's technology was able to collect solar energy for a single year and convert it to electricity, it would cover global energy consumption for the next 6000 years. [5] To produce electricity from sunlight, solar cells are used. Solar cell is a device which uses solar energy to produce electrical energy. They are called *photovoltaic cells* or *photoelectric cells* also. Solar cells are made of silicon which is a semiconductor. The problem with that is its efficiency is very low and the electricity produced can't be stored. Instead of using excited electrons of the cell to produce electricity, artificial photosynthesis uses the current to split water. Hydrogen is produced in the negative electrode (cathode) and oxygen is produced in the positive electrode (cathode) from the splitting of water. Hydrogen can be used as an alternative source to fossil fuels in the areas such as heating and transportation. According to the expectations of international energy agency, solar energy will be % 25 of the energy market.

1.2. Solar Water Splitting

Artificial photosynthesis aims to produce solar fuels by using solar radiation energy as an electron source. In this study, artificial photosynthesis is used to produce

hydrogen and oxygen gas from the electrochemical splitting of water.[6] The challenge of producing hydrogen and oxygen through photoelectrochemically splitting of water is finding a suitable catalyst to work as a reaction center which is stable in water and cheap so that it can be in the market as an alternative to other energy sources. The earliest research about water splitting was done by Baur and Rebmann in 1921 by using UV light and AgCl/TlCl as a catalyst to split the pure water.[7] Large scale hydrogen production requires solar to chemical efficiency to be at least % 10. The mechanism of artificial photosynthesis is the same as the natural photosynthesis. When sunlight hits the electrode surface, the energy of the photons excites electrons in the crystalline structure and causes electrons to jump from valence band to conduction band, leaving positive or negative holes behind. Overall water splitting reaction requires $\Delta G0 = 237.13$ kJ/mol so the reaction cannot occur spontaneously. For this reason, catalysts are required to overcome water splitting reactions energy barrier. $\Delta G0 = 237.13$ kJ/mol) and thus cannot occur spontaneously.

Electrons and holes generated in CB and VB by electron excitations can be used for catalytic surface reactions for their strong reduction and oxidation potentials.[8] Band positions are an important property of the semiconductor. Conduction bands minimum energy must be lower than the hydrogens reduction potential which is 0 V and valence bands maximum energy must higher than the water oxidation energy which is 1.23 V., therefore, a bandgap of minimum 1.23 eV is needed. To be able to excite an electron, the wavelength of incident light must correspond to the energy gap between valence and conduction band. Since the energy required to excite the electrons is absorbed from sunlight, the solar spectrum is another limiting factor for the determination of semiconductor band positions. In terms of energy, sunlight at Earth's surface is around 52 to 55 percent infrared (above 700 nm), 42 to 43 percent visible (400 to 700 nm), and 3 to 5 percent ultraviolet (below 400 nm). [9] In consideration of the solar spectrum, bandgap should be narrower than 3.1 eV to achieve more light absorption. This way semiconductor is suitable to oxidize organic compounds and split water to hydrogen and oxygen by harvesting sunlight energy. The reaction of splitting water can be written as;

$$4\,H^+ + 4\,e^- = 2\,H_2 \quad (1.1)$$

$$2\ H_2O + 4\ H^+ = O_2 + 4\ H^+\ (2)\ E° = 1.23\ V\ vs\ RHE \quad (1.2)$$

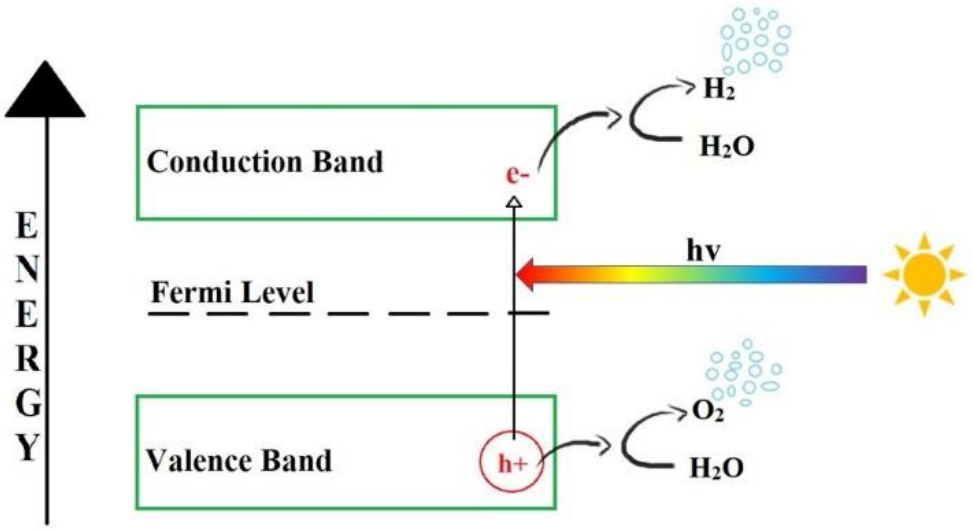

Figure 1.1. Water splitting reaction via artificial photosynthesis mechanism.

1.2.1. Materials Used in Solar Water Splitting

Materials are divided into three main groups according to their electrical conductivity; conductors, semiconductors, and insulators. For water-splitting reactions, semiconductors play a crucial role because of their band position tunability. There are valence bands are formed by bonding energy levels and conduction bands are formed by antibonding energy levels. At zero kelvin, the valence band is occupied by electrons, and the conduction band is empty. [10] Electrons and holes generated by excitation of the atom acts as a charge carrier and makes it possible for water to split into oxygen and hydrogen. Production of solar fuels via artificial photosynthesis requires three main components;

1-Reaction center which can absorb sunlight

2-Water oxidation complex where water splits into hydrogen and oxygen

3-Another catalytic system to use reduction equivalents to make fuels

A study on TiO2 as a water-splitting catalyst by Fujishma and Honda in 1972 led to greater investigations on semiconductors for water splitting reactions.[11] Exciting semiconductors with solar radiation to split water has become the basis of solar fuel studies. There are several materials used as catalysts for water splitting. These materials include carbons, nitriles, various transition metals, metal macrocycles, and metal oxides. In the latest studies especially one type of metal oxides attracts attention, which is called perovskites. This attention is due to their high electrocatalytic activity and cheap costs.

While choosing a suitable semiconductor there are some important qualifications such as bandgap and overpotential. Since high mobility of charge carriers are desired, the bandgap of selected semiconductor is an important property. The bandgap is the energy difference between the valence band and conduction bands of the material. Semiconductors have bandgap between 1 eV and 5 eV. [12] The Stability of the chosen material also depends on the band positions. Elements with empty d orbitals tend to bond with Oxygen 2p orbitals and form stable oxides under conditions required for water splitting reactions. Because of their d orbital characteristics, their valence bands have low energy and their band gaps are too large for solar energy harvesting. [4] Another important qualification needed for the semiconductors is that they have a naturally occurring electric field inside which is called the space charge region. Space charge prevents the recombination of excited electrons and holes and causes band bending. Band bending is the change of energy on the edges of the bands of a semiconductor. Band bending and space charge effect depend on the junction of a semiconductor with another semiconductor, a metal, or a dopant. Bands can bend upward or downward depending on the pH of the electrolyte. In strong oxidizer solutions, bands bend upward. It is very useful to determine the position of the band edges because they determine the reduction and oxidation power of the material. Also, band bending is the key to understand ohmic contact and the Schottky barrier.

The Schottky barrier is the energy barrier for electrons at a junction of semiconductors with metal or electrolytes. The Schottky barrier is used in device productions such as DC power supplies.

Ohmic contact means an electrical junction between two conductor materials, it supplies current flow. It refers to a metal-semiconductor junction. In this contact type, current flows both ways of the junction. In the fabrication of devices such as photodiodes and photodetectors, ohmic contact is essential to increase the performances.

While designing a photoelectrochemical cell some important points are listed as;

- Optimum range for bandgap of semiconductor is 1.9-3.1 eV. [10]
- Electrode surface must be suitable to absorb visible light efficiently.
- Designed photoelectrode should be highly stable in both dark and light conditions to prevent photo corrosion.
- Band edges of semiconductor catalysts should be in a suitable position to enable the reduction/oxidation of water by the photo generated holes /electrons.
- Semiconductor must have low overpotentials for reduction and oxidation reactions which also means high catalytic activity.
- Solar – to – hydrogen efficiency must be at least 10 % for large scale hydrogen production. [11]

- Best catalysts for OER: Ir and Ru

- Best catalyst for HER: Pt

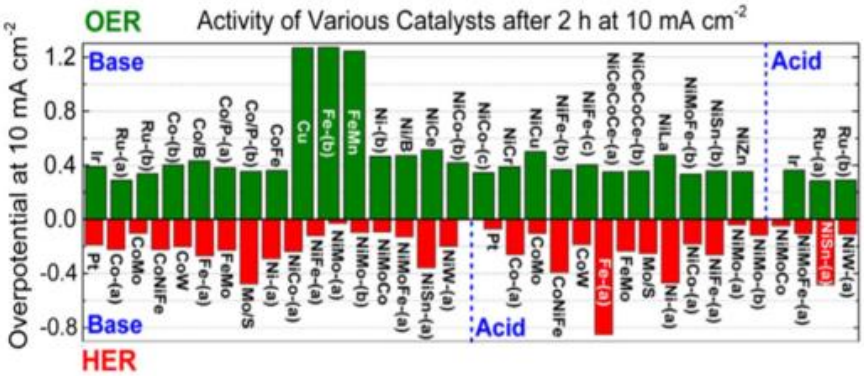

Figure 1.2. Activity of various catalysts for HER and OER.

For increasing the efficiency of solar to hydrogen energy conversion and lowering the overpotentials of chosen materials, electrocatalysts are used in both oxygen evolution

reactions (OER) and hydrogen evolution reactions (HER Since the oxygen evolution reaction is a 4-electron mechanism, it is accepted as sluggish step of water splitting reactions. Also, high overpotentials are needed for the O-H bond breaking and O-O bond formation.[12] Therefore, the development of an OER catalyst is important for the overall efficiency of water splitting.

1.2.2. Hydrogen Evolution Reactions

Hydrogen evolution reaction is the cathodic half-reaction of water splitting reactions. Platinum and Carbon supported Pt based catalyst are reported as the best HER catalyst in literature. [13] Pt-based catalysts are not suitable for large scale use because of their high costs and long-term stability in acidic media. Both in acidic and alkaline media were used as electrolyte solutions for HER tests in earlier studies and it has been shown that activities were greater in acidic media. [14–17] Tafel slopes of Pt/C catalyst for HER was reported in acidic media as 30 mV [18] and 125 mV [19] in basic media. Although their better HER catalytic activities, most non-precious metal catalysts show poor stabilities in acidic media. Stability issues forced the scientific community to investigate better catalysts in alkaline or neutral media for hydrogen evolution reactions. Perovskites was investigated for their ORR/OER activities, but their HER mechanism is unknown to detail. Various literature studies suggested that B-site of perovskites are active sites because of their adsorption with reaction intermediates such as OH. [20] A catalysts activity towards HER is dependent on metal- adsorbed hydrogen (H_{ad}) bond energy, nature of proton source and the presence of surface spectators (OH_{ad}, H_{ad}, H_2O). [21] Also pH has an important effect on the activity on catalyst. It is proved that the kinetics of HER mechanism are more slower in alkaline media than in acidic media. [22]

In acidic media HER reaction proceeds in three steps. [23] M denotes the HER active surface of metal.

<u>Volmer step:</u> $H^+ + e^- + M^* / MH^*$ (1.3)

<u>Heyrovsky step:</u> $H^+ + e^- + HM^* / H2 + M^*$ (1.4)

Tafel step: $2HM^* / H_2 + 2M^*$ (1.5)

In alkaline media HER reactions proceed as followed;

Volmer step: $H_2O + e^- + M^* / MH^* + OH^-$ (1.6)

Heyrovsky step: $H_2O + e^- + MH^* / H_2 + OH^- + M^*$ (1.7)

1.2.3. Oxygen Evolution Reaction

Mechanism of OER reactions cannot be understood as well as HER because of the complication of 4 electron involving steps. OER activities of catalysts are depend on oxygen adsorption strengths of O containing intermediates and oxygen binding strengths of the surface of catalyst material. [23] Ir and Ru has proven the best catalytic activities for OER in the literature as noble metal oxides.[24] Although they have great catalytic activities, their costs were not suitable for large scale applications. [13] To be able to use a catalyst in large scale productions, cost effective materials such as transition metals and alkaline earth metals was considered. Metal oxides have good catalytic activities in acidic media, but their stability fails to be considered for long-term uses. In alkaline media, their catalytic activity decreases in comparison to acidic media but stabilities increase. Surface modifications and dopant additions are used to enhance metal oxide catalysts characteristics are one of the most important research subjects for their usability in large pH range. Other than precious metal studies, transition metals were investigated for their cost efficiencies. In recent studies, especially ABO3 type of perovskites was investigated for their promising OER activity and tunability from A and B sites. It has shown that highest catalytic activity of perovskites can be achieved by closed to unity occupancy of e_g orbitals. Suntivich et al. described the relation between eg occupancy and OER catalytic activity in a volcano curve. [25]

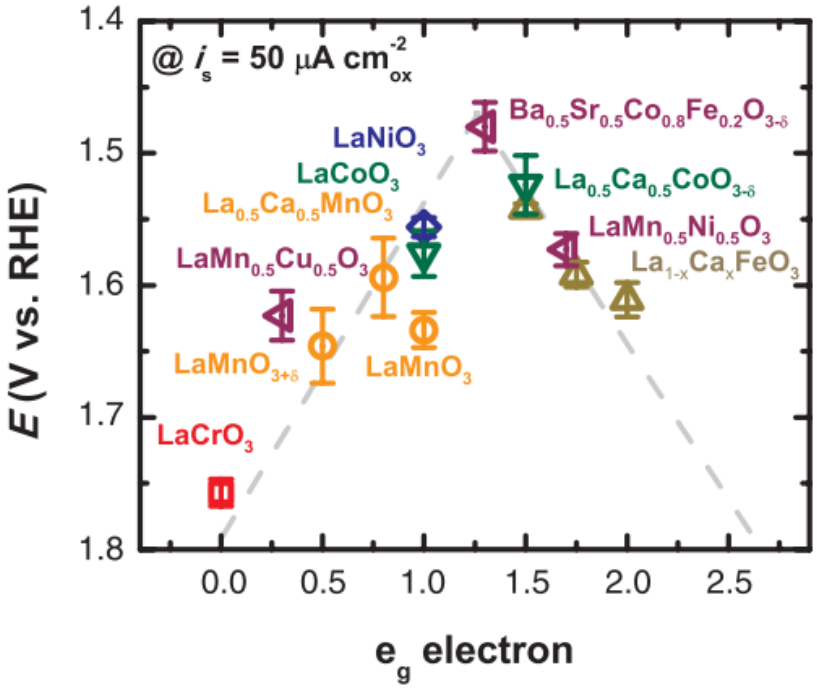

Figure 1.3. Volcano curve showing the relationship between eg occupancy and catalytic activity of various perovskites. (Copyright © 2011, American Association for the Advancement of Science.)

Ba0.5Sr0.5Co0.8Fe0.2O3-d (BSCF) is a ABO3 type perovskite which fulfills this criterion and was investigated for its oxygen reduction reaction (ORR) [26] and OER [27] characteristics in alkaline media.

In alkaline media;

$$OH^- + M^* / HOM^* + e^- \quad (1.8)$$

$$HOM^* + OH^- / OM^* + H_2O + e^- \quad (1.9)$$

$$O^- + OH^- / HOOM^* + e^- \quad (1.10)$$

$$HOOM^* + OH^- / O_2 + H_2O + e^- + M^* \quad (1.11)$$

In acidic media;

$$H_2O + M^* / HOM^* + H^+ + e^- \quad (1.12)$$

$$HOM^* / OM^* + H^+ + e^- \quad (1.13)$$

$$OM^* + H_2O / HOOM^* + H^+ + e^- \quad (1.14)$$

$$HOOM^* / O_2 + H^+ + e^- + M^* \quad (1.15)$$

1.3. About This Study

1.3.1. Perovskite Oxide Catalysts

The latest researches are focused on multi-metal oxides for their high abundance and good catalytic activities. One class of multi-metal oxide is highly investigated due to their flexibility of chemical and physical properties. The general formula of perovskites is ABO_3. An ideal ABO_3 type perovskite has cubic symmetry with a pm3m space group. A site is occupied by an alkaline earth element in 12-fold coordination and the B site is occupied by a transition metal element in 6-fold coordination to the oxygen atoms. Deviations from cubic symmetry can be observed in orthorhombic, rhombohedral, or tetrahedral symmetry formations. [28] Generally, the B site of the perovskite is identified as an oxygen evaluation reaction center. There is no detailed information about the mechanism of hydrogen evaluation and oxygen evolution reactions of perovskites. According to the latest studies, HER and OER efficiency stabilities, Fermi level, bandgap energy, and the density of states in conduction and valence bands of perovskites can be improved by dopants either to A site or B site.

BSCF is a $SrCoO_{3-\delta}$ type perovskite which was firstly developed for high temperature oxygen permeation membrane applications. Based on Shao's studies, introducing Ba and Sr atoms in 50% percentage to $Co_{0,8}Fe_{0,2}$ provided the best stability for perovskite structure and gained it remarkable oxygen permeation properties. By

doping $Co_{0,8}Fe_{0,2}$ structure with Ba and Sr atoms, oxygen vacancies increased therefore increasing its performance. [29]

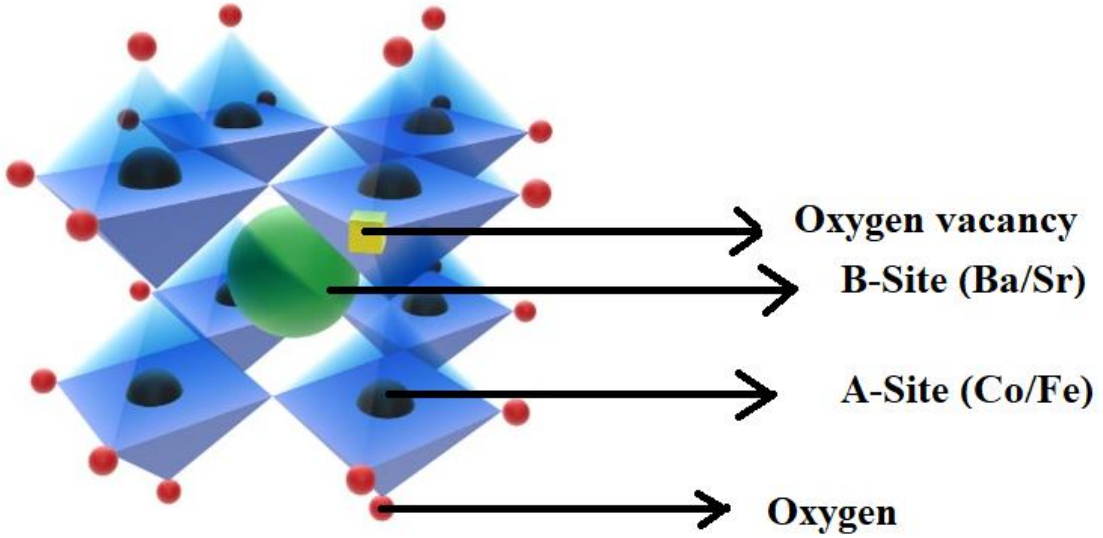

Figure 1.4. ABO3 type perovskite structure showing A-Site and B sites atoms with oxygen vacancy.

BSCF was firstly first use as an energy material is for fuel cell applications by Shao and Haile Nature. In this study, BSCF has shown to be a promising candidate as cathode material for its ORR activities.[30] Fe doping effects was investigated by Chen et al. and they found that $Ba_{0.5}Sr_{0.5}Co_{1-y}Fe_yO_{3-1}$ cathodes at y = 0.2 showed the best ORR catalytic activity and increase in Fe percentage concludes in decrease of electrical conductivity. [31] Molecular dynamic simulation studies done by Fisher et al. proved that the 50 % percentage doping of Ba Sr atoms conclude in the best oxygen vacancy content and ionic conductivity. [32]

In the later researches, for its high electrochemical performance BSCF is considered for water splitting catalysts too. According to studies of Suntivich et al**.** BSCF shows better current densities than state-of-art IrO_2 for oxygen evolution reactions. [27]

Activity of BSCF towards ORR and OER reactions can be tuned by electrode preparation techniques. Fabbri et al. showed that addition of acetylene black to electrode coating material can boost BSCF activity by chancing the electronic configuration. Change in electronic configuration of BSCF is caused by the reduction of Co oxidation

states by carbon addition. [33] In further studies, Fabbri et al. also showed the effect of ball milling of perovskite powder enhances its OER activity by providing smaller crystalline sizes. [34] Another work on electrode preparation was done by using Ni foam and ITO as substrate and chancing the film thickness of BSCF on Ni foam. Increase of film thickness enhanced the durability of catalyst in alkaline media and the study proved that Ni foam serves as a better substrate by tuning the oxidation states of perovskite for OER. [35]

Hydrogen evolution catalyst characteristics of perovskites was not investigated in detail in alkaline solutions due to complicate HER mechanisms and overpotential losses due to slow kinetics of reaction. Xu et al. firstly investigated the HER activity of BSCF and Pr doped BSCF for its known OER popularity among perovskites and showed that Pr doped BSCF has 237 mV overpotential at 10 mA cm^{-2} and BSCF showed 342 mV overpotential. This drop in overpotential is explained in facilitated electron transfer by Pr doping and proved that BSCF is a promising candidate as a HER catalyst. [21] Li, Xiangnan et al reported. the HER activity dependency of BSCF to Ba^{+2} ions. According to their study, Ba^{+2} ion deficiency doping improved electrochemical and physical properties in addition of Zr and Y atoms to structure by showing smaller Tafel slopes and lower overpotentials in alkaline media. [36]

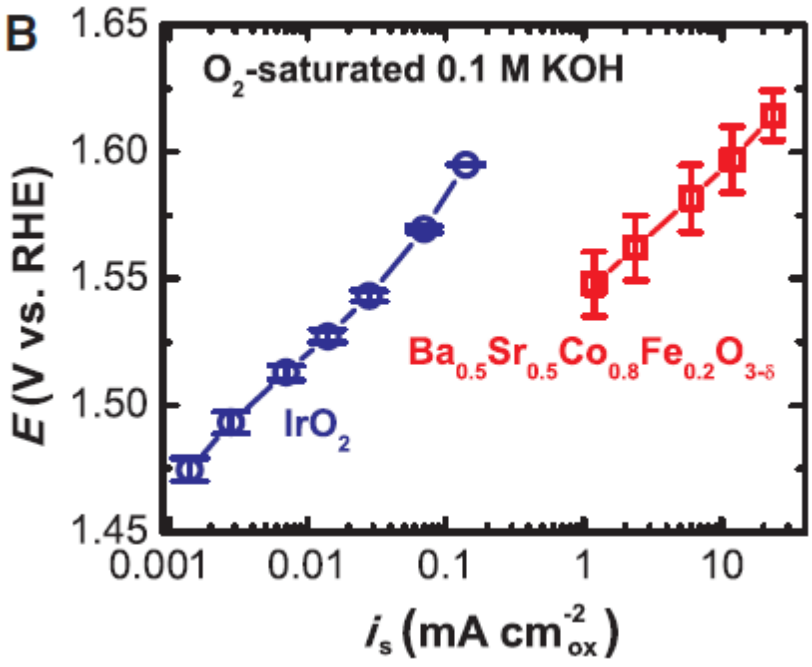

Figure 1.5. OER activity comparison of BSCF to IrO_2. (Copyright © 2011, American Association for the Advancement of Science.)

Several synthesis routes was studies for perovskites such as sol-gel synthesis [37,38], solid state reactions [39], co-precipitation and hydrothermal synthesis, flame spray synthesis [40,41], solution combustion synthesis [42], glycine nitrate process [43] concluding different crystalline sizes, surface and bulk characteristics and therefore ionic conductivity, OER/ORR/HER activities. Among these methods, Sol-Gel synthesis by EDTA-citrate complexing method is the most commonly used route for providing homogeneity on molecular level which enhance electrochemical performance and fast reaction kinetics. [44]

Laing et al. compared solid state reaction, Pechini method and sol-gel synthesis of BSCF in their studies and reported that the BSCF synthesized by sol-gel method has higher conductivities by 90% than solid state reaction and 42% Pechini method. [39]

Xu et al. synthesized BSCF as a membrane material to test the differences on oxygen permeability performance caused by synthesis methods. In the study, they compared solid-state reaction, modified citrate process and EDTA - citrate complexing method. They observed that the smallest grain size was obtained by EDTA-citrate method with 0,1 μm. [44]

May et al. studied the structural effects on electrochemical activity of BSCF in alkaline media and they showed that surface amorphization increased with increasing cycling number leading to better catalytic activities for OER. [45]

1.3.2. Experimental and Characterization Methods

1.3.2.1. Sol-Gel Synthesis

Sol-Gel is the most preferred method for the synthesis of perovskites. This method provides homogeneity of elemental composition among the perovskite and ability to control stoichiometric ratios of desired metals. Another important aspect of sol-gel synthesis is that it can be done under low temperatures (< 100 °C). Although the formation of fine crystalline structures by the sol-gel route is unknown by detail, this formation is important for the performance of synthesized powders in the energy applications. There are three phases of sol-gel synthesis including; hydrolysis of metal precursors to form metal hydroxides followed by condensation to form gels and the final step is drying. [46] Especially EDTA-Citrate complexing method was investigated for its

known ability to form cubic structures of complex metal oxides such as perovskites. In this method, both EDTA and Citric Acid are being used as gelation and complexation agents. Since the synthesis of perovskites precursors are dissolved in water, it is called aqueous sol-gel method. In the aqueous sol-gel method, needed oxygen in the synthesis of metal oxides is supplied by water. There are some difficulties in the sol-gel method such as control of particle morphology. This problem arises from the simultaneous occurrence of hydrolysis, condensation, and drying steps. But in the bulk synthesis of materials, this problem is not much of importance. For all the perovskite oxide catalysts studied in this work, EDTA- citrate complexing method was used.

1.3.2.2. X-Ray Diffraction and Rietveld Analysis

X-ray diffraction is one of the most common methods to study the morphology of the materials. By this method crystal structure, unit cell dimensions, and lattice parameters can be determined. Its working principle depends on the interaction between the atoms of the crystal structure and X-rays generated from the cathode ray tube. Scattered X-rays produce constructive interferences and diffracted rays that form the unique XRD pattern of the crystal. Bragg's law is used to find the lattice spacing (d) from obtained data. In Bragg's equation, n is the reflection order, λ is the wavelength of incident light and θ is the angle between the incident X-ray and the normal to the reflecting plane. Each mineral has unique d spacing which is used for the identification of unknown samples. [47]

$$2dsin\theta = n\lambda \quad (1.16)$$

One of the important outcomes of XRD data is calculation of crystal size (D) by Scherrer equation. In Scherrer's equation D is the crystallite size, λ is the wavelength of the incident light , β is the peaks full width at half maximum (FWHM) and θ is the angle between the beam and normal of the reflection plane, k is a dimensionless shape factor which is approximately 0,9.

$$D = (K\lambda) / (\beta Cos\theta) \quad (1.17)$$

For this study Copper is used as anode material with Cu K(α1) = 1.5400 Å because of its high energy. Angles from 20 ° (Start Position [°2θ]) to 90 ° (End Position [°2θ]) was scanned by Step Size [°2θ] = 0,0170. Rietveld analysis was done to calculate the lattice parameters from obtained XRD data. For all the calculations and elemental structural determinations, X'Pert HighScore Plus program was used. For Rietveld analysis, Profex program was used.

1.3.2.3. X-Ray Photoelectron Spectroscopy

X-ray photo electron spectroscopy reveals the atomic composition of the surface of sample and gives information about the binding states in sample structure by bombarding the sample surface with X-rays in vacuum. Emitted photoelectron energy by elements in the sample is unique and helps to for identification. For the binding energy calculations, chemical shifts observed on the XPS spectra is used because shell electron energies are sensitive to the chemical bonding between atoms. [48] XPS was used for the determination of electronic states present in the synthesized perovskites in this work by analyzing binding energies.

1.3.2.4. Scanning Electron Microscope and Energy Dispersive X-Ray Spectroscopy

Scanning electron microscope uses an electron beam bombardment on sample surface to produce a topological image and surface composition. From the bombardment, secondary electrons (SE), backscattered electrons (BSE) and characteristic X-Rays are produced. From secondary electrons information's about roughness and texture of sample can be obtained. BSE also gives information about topography of the sample, but it uses contrast image dependent on the atomic numbers of elements present in the sample which

is why it usually preferred for high atomic number elements. EDX uses emitted X-rays for the element identification from this unique information. [49] SEM was used for surface screening to observe the porosity and agglomerations and bulk analysis to investigate elemental compositions by EDX for synthesized perovskites in this work.

1.3.2.5. Brunauer – Emmett – Teller Analysis

Electrochemical reactions occur at the surface of an electrode. Therefore, it is important to determine the surface areas of subjected materials for further improvements of the reaction characteristics. Brunauer-Emmett-Teller analysis is a surface area determination method based on adsorption of nitrogen gas. [50] From adsorption measurements, important physical properties of materials such as total surface area, pore volume and pore size can be calculated. BET analysis was performed for BSCF powder.

1.3.2.6. Electrochemical Characterizations

Current-Voltage measurements are the most widely used methods for electrochemical performances of materials. Since there is no direct determination of HER and OER performance for materials, lineer sweep voltammetry (LSV) and cyclic voltammetry (CV) are both used for catalytic performance measurements. In both cases, applied voltage is swept between a range and the electrolytic current which flows through the electrolyte between the working (W) and counter (C) electrodes are saved.[51] Their main difference is that, cyclic voltammetry cannot be used in irreversible reactions. This data is plotted as current (I) vs applied potential (E). From the data obtained from CV, oxidation and reduction potentials, reaction rates, reversibility of the reaction [52] and transferred electron stoichiometry can be determined. For experimental applications, three electrode configurations are used. For counter electrode, a material chosen with better electrochemical activity than working electrode to prevent resistance issues.

Tafel slope is an important term for electrochemical activity measurements. Tafel plots can be derived from measured LSV or CV data. It is plotted by; base 10 logarithm

of current is on the x axis and potentials or overpotentials are on the y axis. In this work, Tafel plots were determined from LSV measurements. It gives information about onset potential, exchange current density and overpotentials of catalyst materials. Overpotential is the potential that exceeds the equilibrium potential to achieve thermodynamic energy barrier of a reaction to occur.[53] For water splitting reactions, equilibrium potential is 1,23 V. Every overpotential for materials used in water splitting is calculated in compared to this potential value. Onset potential is defined as the voltage corresponding to 1 mA/cm^2 current density. It is the thermodynamic barrier for a reaction should exceed to be able to continue. As the onset potential gets smaller, this barrier means to get smaller too. As conclusion of this, smaller onset potentials mean higher catalytic activity. Exchange current density is the current passing when oxidation and reduction reactions of a redox reaction are in equilibrium. It is a descriptor of the reaction kinetics. Exchange current shows how easily of charge transfer is occurring in the material. Materials with larger exchange current densities have faster reaction kinetics.[54] The slope of the Tafel plot is another descriptive term which gives information about the rate of the reaction. If the Tafel slope of a material is smaller, it means that the less potential or overpotential is required to achieve the same current with this material. Unit of Tafel slope is mV/dec, dec meaning the decade. Since x axis is in terms of logarithm, Tafel slope gives the information about how much of more potential should be applied to increase the reaction rate by 10 factors.

Chrono methods was used to test the stability of prepared electrodes and synthesized powders in alkaline media. Chronopotentiometry is the time dependent analysis of the stability at constant current of an electrode. This method measures the potential value while keeping the current constant. Generally, for water splitting reactions, 10 mA/cm^2 is used as constant current value. On the other hand, chronoamperometry is the measure of current stability of an electrode among time. For this method, potential is kept constant while the current is measured for a determined time. For water splitting reactions, potential that is kept constant is chosen as potential which corresponds to 10 mA/cm^2 current density from cyclic voltammetry of lineer sweep voltammetry data. Both chrono methods are expected to be in consistency with LSV or CV measurements for an electrode with ideal stability.

For reference electrode, an electrode with known potential is used. In this work, Pt mesh was used as counter electrode and Ag/AgCl electrode was used as reference

electrode in three electrode configurations. For all electrochemical measurements 1 M KOH solution was used as electrolyte solution, therefore, all catalytic activities were measured in alkaline media.

CHAPTER 2

EXPERIMENTAL RESEARCH

2.1. Equipment and Materials

Table 2.1. Materials and chemicals used in the electrochemical tests.

Materials used for electrochemical characterizations	From
Platinum mesh	Siz Plus
Ag/AgCl reference electrode	Referans Kimya, Turkey
Potassium Hydroxide	Tekkim, Turkey

2.1.1. Equipment and Materials for Perovskite Oxide Catalyst Studies

Table 2.2. Materials used for electrode fabrications in the electrochemical testing of perovskite oxide catalysts.

Materials used for electrode fabrication	From
Nickel foam	SİZ Plus

Table 2.3. Chemicals used in the synthesis of perovskite oxide catalysts.

Chemicals used for perovskite oxide synthesis	From
Barium (II) Nitrate	ZAG Chemicals, Turkey
Strontium (II) Nitrate	ZAG Chemicals, Turkey
Cobalt (II, III) Nitrate	ZAG Chemicals, Turkey
Iron (III) Nitrate	ZAG Chemicals, Turkey

Nickel (II) Nitrate	ZAG Chemicals, Turkey
Zinc (II) Nitrate	ZAG Chemicals, Turkey
Manganese (II) Nitrate	ZAG Chemicals, Turkey
Silver Nitrate	ZAG Chemicals, Turkey
EDTA	Sigma Aldrich, Germany
Citric Acid	ZAG Chemicals, Turkey
Ammonium Hydroxide	Tekkim, Turkey

Table 2.4. Chemicals used in the ink preparation for electrochemical tests of synthesized perovskite oxide catalysts.

Chemicals used for ink preparation from perovskite oxide powders	**From**
Nafion	Sigma Aldrich, Germany
Carbon Black	Tekkim, Turkey
Ethanol	Tekkim, Turkey

Table 2.5. Equipment used in the characterizations of synthesized perovskite oxide catalysts.

Equipment used	**From**
Drying oven	Karabudak Research Lab
Metroohm PG-208 – Potentiostat / Galvanostat	Karabudak Research Lab
XPS	DAYTAM
Philips X'Pert Pro - XRD	İYTE MAM
Philips XL 30S FEG and FEI QUANTA 250 FEG - SEM	İYTE MAM
Mikromeritics Gemini V - BET	İYTE MAM

2.2. Hydrogen Evolution Reaction: Synthesis and Characterization of Perovskite Oxide Catalysts

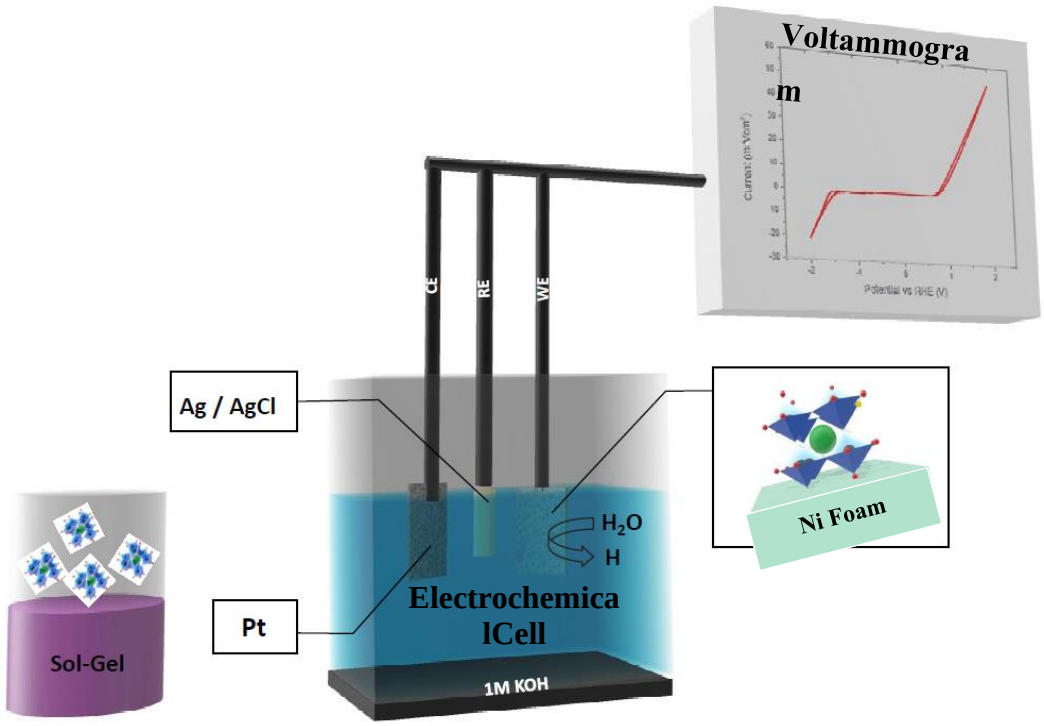

Figure 2.1. Graphical abstract of experimental steps of perovskite oxide studies.

2.2.1. Synthesis of perovskite oxides

Perovskite powders were synthesized by sol-gel method as previously mentioned in the literature.[44] EDTA and citrate was used as complexing agents. NH4OH was added to set the pH. Figure 7. shows the general synthesis route followed for the synthesis of perovskites in this study.

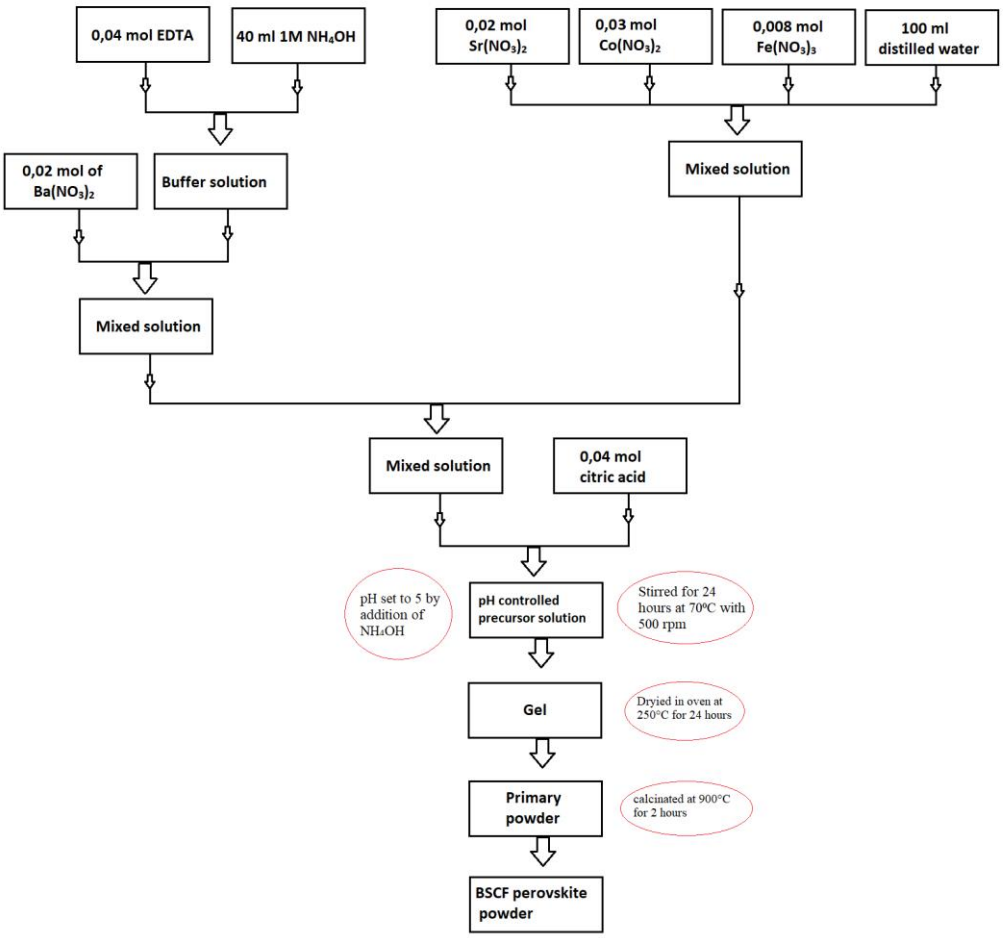

Figure 2.2. Synthesis route followed for the all perovskite synthesis in this work.

2.2.1.1. Synthesis of BSCF

- 0,04 mol of EDTA dissolved in 40 ml 1M NH_4OH solution.
- 0,02 mol of $Ba(NO_3)_2$ mixed with EDTA-NH_3 solution.
- 0,02 mol of $Sr(NO_3)_2$ 0,03 mol of $Co(NO_3)_2$ and 0,008 mol of $Fe(NO_3)_3$ were dissolved in 100 ml of water.
- $Ba(NO_3)_2$ -EDTA- NH_3 mixture and solutions of $Sr(NO_3)_2$, $Co(NO_3)_2$ and $Fe(NO_3)_3$ was added together to form precursor solution.
- 0,04 mol of citric acid was added to the mixed solution and pH was set to 5 by addition of NH_4OH.
- Final solution was stirred for 24 hours at 75ºC with 500 rpm.

- The gelled samples obtained were baked in a drying oven at 250°C for 24 hours.
- Finally, primary powder was calcinated at 800°C for 2 hours.

2.2.1.2. Synthesis of BSCF-Mn

- 0,04 mol of EDTA dissolved in 40 ml 1M NH_4OH solution.
- 0,02 mol of $Ba(NO_3)_2$ mixed with EDTA-NH_3 solution.
- 0,02 mol of $Sr(NO_3)_2$ 0,03 mol of $Co(NO_3)_2$ and 0,008 mol of $Fe(NO_3)_3$ were dissolved in 100 ml of water.
- $Ba(NO_3)_2$ -EDTA- NH_3 mixture and solutions of $Sr(NO_3)_2$, $Co(NO_3)_2$ and $Fe(NO_3)_3$ was added together to form precursor solution.
- $Mn(NO_3)_2$ was added to final precursor solution by 0,3 mol.
- 0,04 mol of citric acid was added to the mixed solution and pH was set to 5 by addition of NH_4OH.
- Final solution was stirred for 24 hours at 75ºC with 500 rpm.
- The gelled samples obtained were baked in a drying oven at 250°C for 24 hours.
- Finally, primary powder was calcinated at 800°C for 2 hours.

2.2.1.3. Synthesis of BSCF-Cu

- 0,04 mol of EDTA dissolved in 40 ml 1M NH_4OH solution.
- 0,02 mol of $Ba(NO_3)_2$ mixed with EDTA-NH_3 solution.
- 0,02 mol of $Sr(NO_3)_2$ 0,03 mol of $Co(NO_3)_2$ and 0,008 mol of $Fe(NO_3)_3$ were dissolved in 100 ml of water.
- $Ba(NO_3)_2$ -EDTA- NH_3 mixture and solutions of $Sr(NO_3)_2$, $Co(NO_3)_2$ and $Fe(NO_3)_3$ was added together to form precursor solution.
- $Cu(NO_3)_2$ was added to final precursor solution by 0,3 mol.
- 0,04 mol of citric acid was added to the mixed solution and pH was set to 5 by addition of NH_4OH.
- Final solution was stirred for 24 hours at 75ºC with 500 rpm.

- The gelled samples obtained were baked in a drying oven at 250°C for 24 hours.
- Finally, primary powder was calcinated at 800°C for 2 hours.

2.2.1.4. Synthesis of BSCF-Zn

- 0,04 mol of EDTA dissolved in 40 ml 1M NH_4OH solution.
- 0,02 mol of $Ba(NO_3)_2$ mixed with EDTA-NH_3 solution.
- 0,02 mol of $Sr(NO_3)_2$ 0,03 mol of $Co(NO_3)_2$ and 0,008 mol of $Fe(NO_3)_3$ were dissolved in 100 ml of water.
- $Ba(NO_3)_2$ -EDTA- NH_3 mixture and solutions of $Sr(NO_3)_2$, $Co(NO_3)_2$ and $Fe(NO_3)_3$ was added together to form precursor solution.
- $Zn(NO_3)_2$ was added to final precursor solution by 0,1, 0,3 and 0,5 mol proportions concluding three different Zn-doping percentages.
- 0,04 mol of citric acid was added to the mixed solution and pH was set to 5 by addition of NH_4OH.
- Final solution was stirred for 24 hours at 75ºC with 500 rpm.
- The gelled samples obtained were baked in a drying oven at 250°C for 24 hours.
- Finally, primary powder was calcinated at 800°C for 2 hours.

2.2.1.5. Doping of BSCF with Various Transition Metals

Electrochemical and structural stability of perovskites can be tuned by A-site or B-site dopants. İt is previously mentioned that B-site is the catalytic active site of BSCF. In this study, B-Site of BSCF was doped with transition metals to enhance its electrochemical activity and stability. For this purpose, Copper, manganese and zinc elements was added to BSCF structure as foreign atoms. In the earlier literature studies, BSCF was doped with zinc to investigate its oxygen separation capacities in membrane applications. In this study Zhang et al. showed that concentration of Zn atoms increased the oxygen vacancies [55], which is directly proportional to the OER and ORR activities.

From this starting point, BSCF was doped with other transition metals including Cu and Mn for comparison of their HER activities.

2.2.2. Bulk and Surface Characterizations of Synthesized Perovskite Oxide Powders

2.2.2.1. Scanning Electron Microscope and Energy Dispersive X-Ray Spectroscopy

Scanning Electron Microscopy (SEM) images were obtained via FEI QUANTA 250 FEG instrumentation to investigate surface morphologies, elemental compositions and homogeneities of perovskite oxide powders. For SEM, backscattered electron detector was used while for EDX analysis, X-Ray detector was used. All images were taken at 2500x zooming.

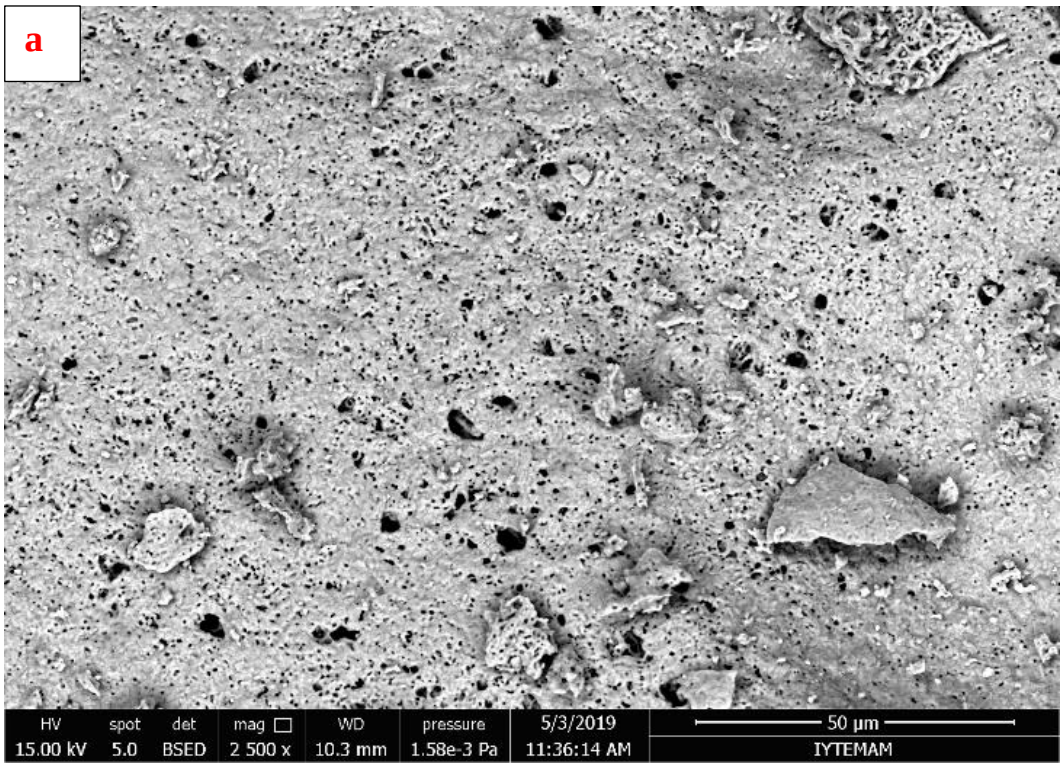

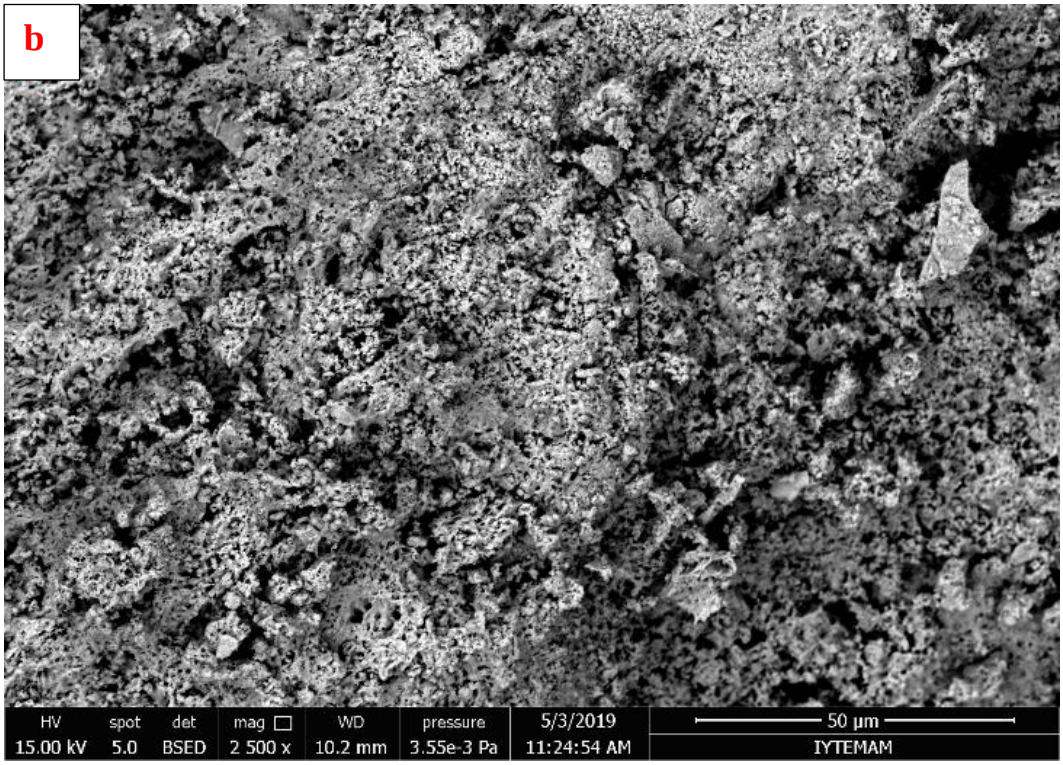
b
HV
15.00 kV
spot
5.0
det
BSED
mag
2 500 x
WD
10.2 mm
pressure
3.55e-3 Pa
5/3/2019
11:24:54 AM
50 µm
IYTEMAM

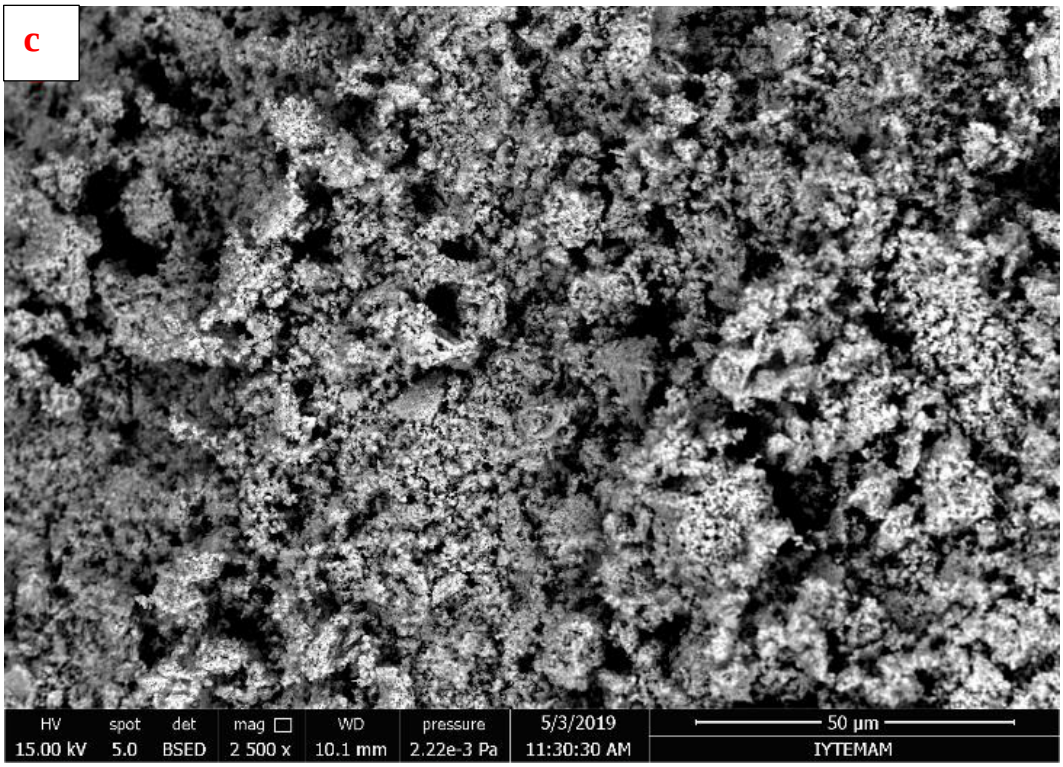
c
HV
15.00 kV
spot
5.0
det
BSED
mag
2 500 x
WD
10.1 mm
pressure
2.22e-3 Pa
5/3/2019
11:30:30 AM
50 µm
IYTEMAM

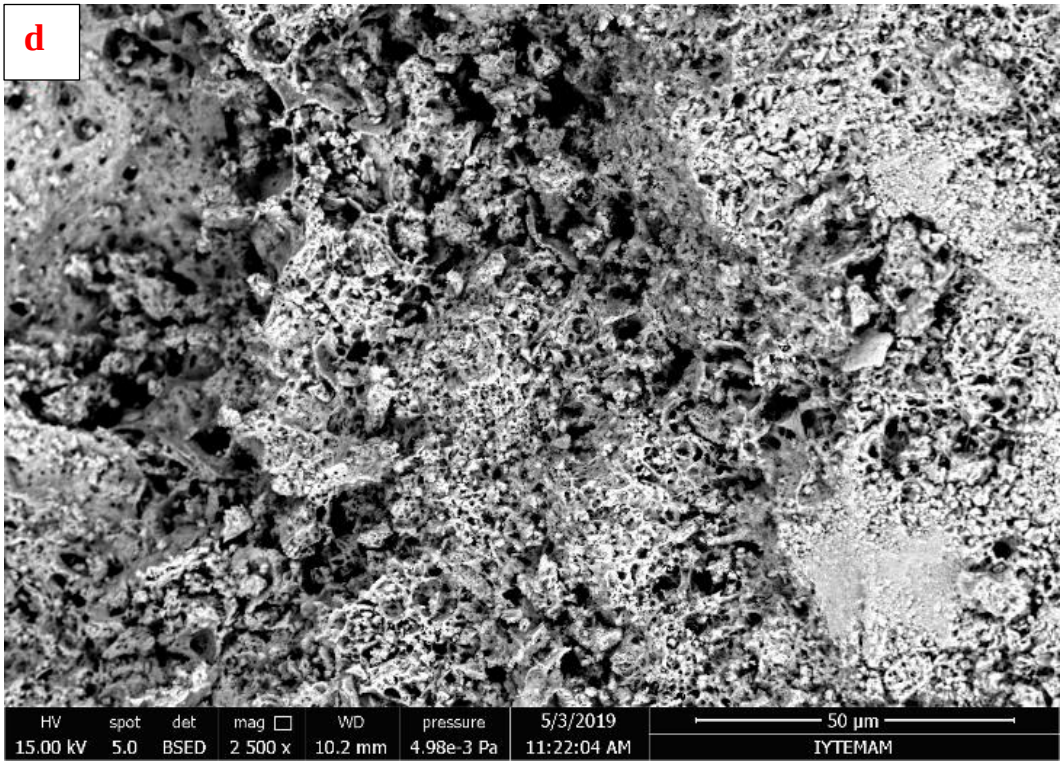

Figure 2.3. SEM images of a) BSCF b) BSCF-Cu c) BSCF-Mn d) BSCF-Zn powders at 50 µm 2500x zoom.

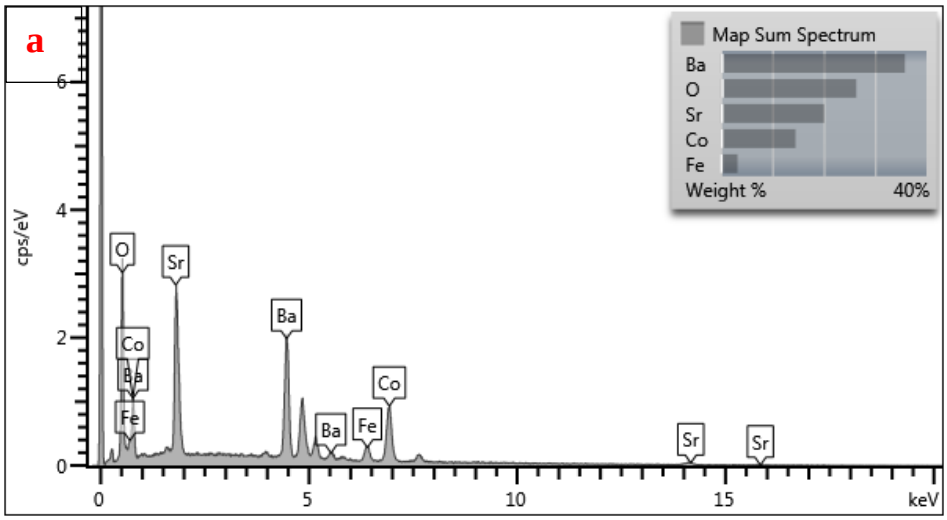

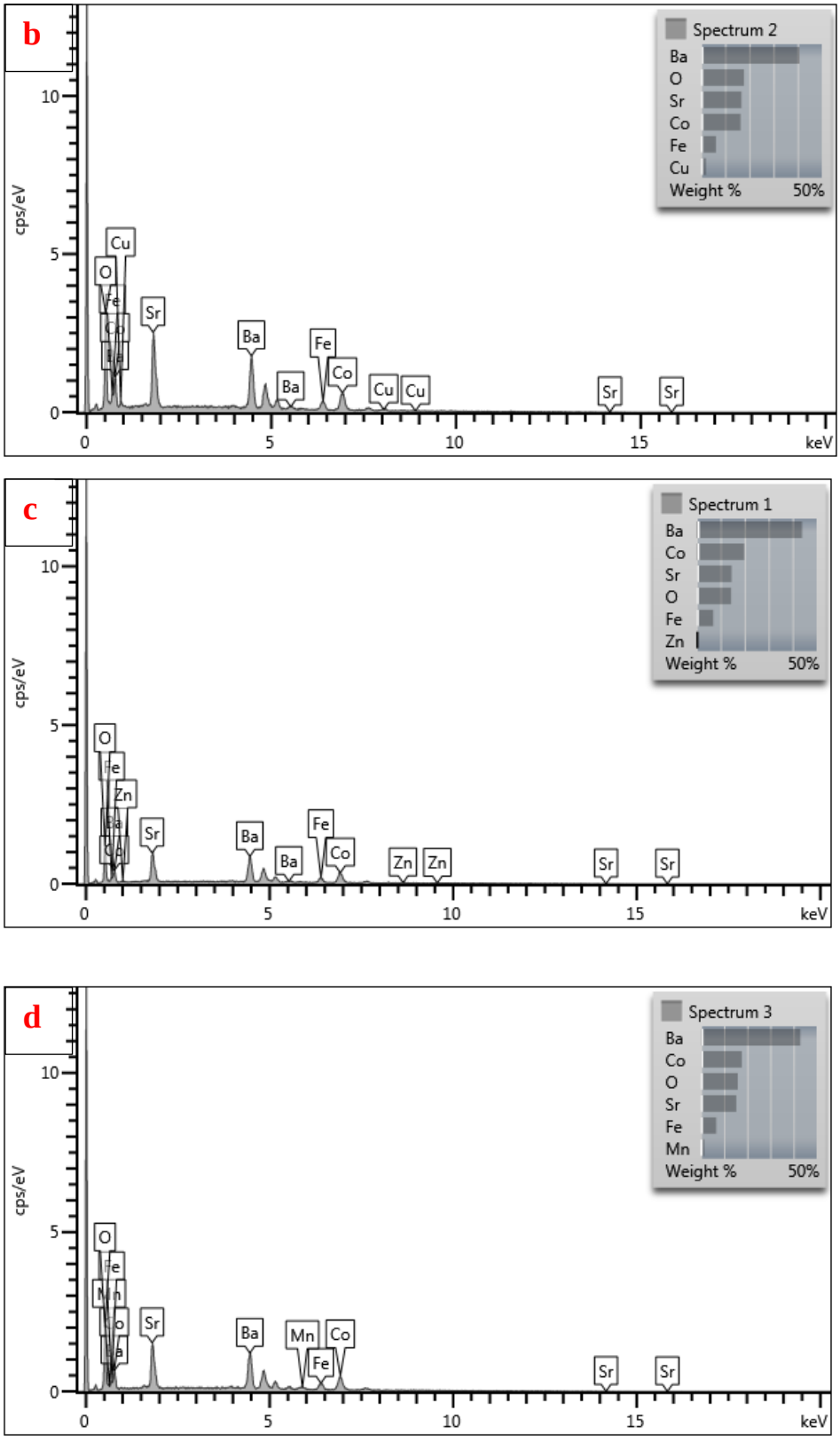

Figure 2.4. EDX Map Spectrum analysis of a) BSCF, b) BSCF-Cu, c) BSCF-Zn and d) BSCF-Mn

2.2.2.2. X-Ray Diffraction Crystallography

For X-ray diffraction analysis (Philips X'Pert Pro) of BSCF, BSCF-Ag, BSCF-Cu, BSCF-Mn, and BSCF-Zn measurements were carried out by using Cu Kα radiation (λ=1.5418 Å) with a tube voltage 40 kV and current of 35 mA at room temperature. Measurement data were obtained by step scanning in a 2θ range of 20-90° with intervals of 0.02°. Obtained XRD patterns show that powders consist of single crystallized perovskite structures after calcination in air at 850 oC for 5 h.

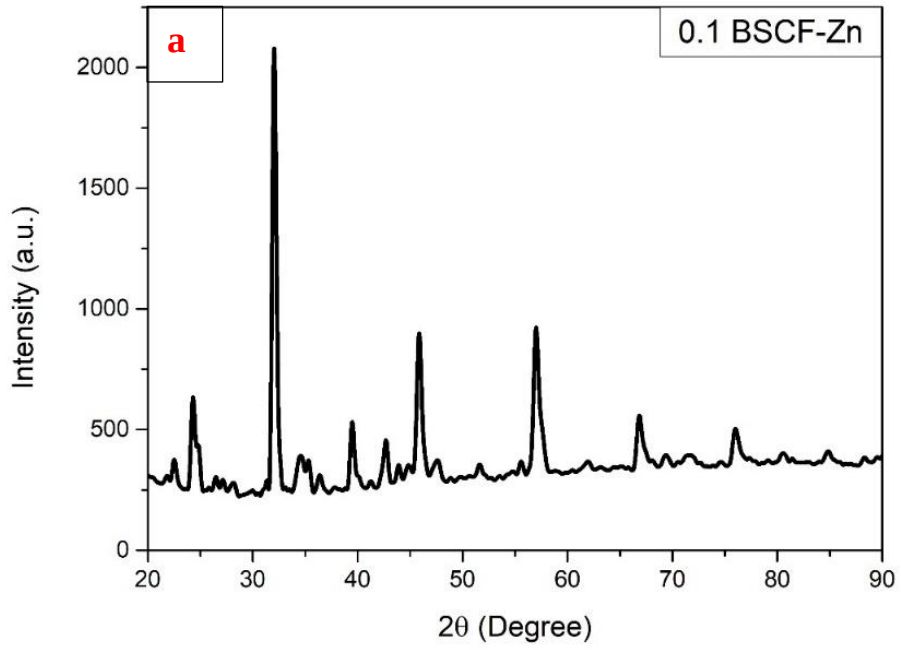

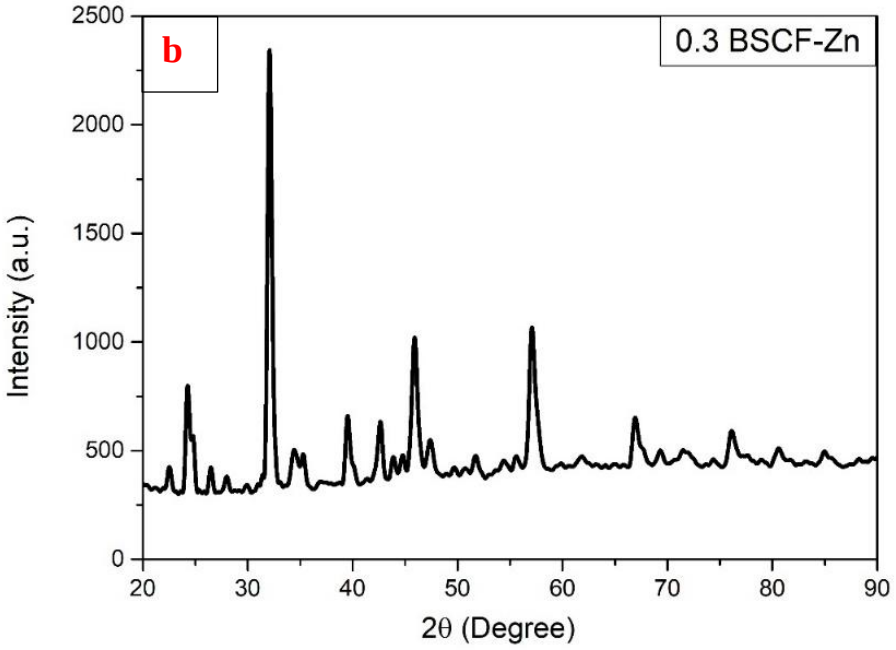
b
0.3 BSCF-Zn
Intensity (a.u.)
2θ (Degree)
0
500
1000
1500
2000
2500
20
30
40
50
60
70
80
90

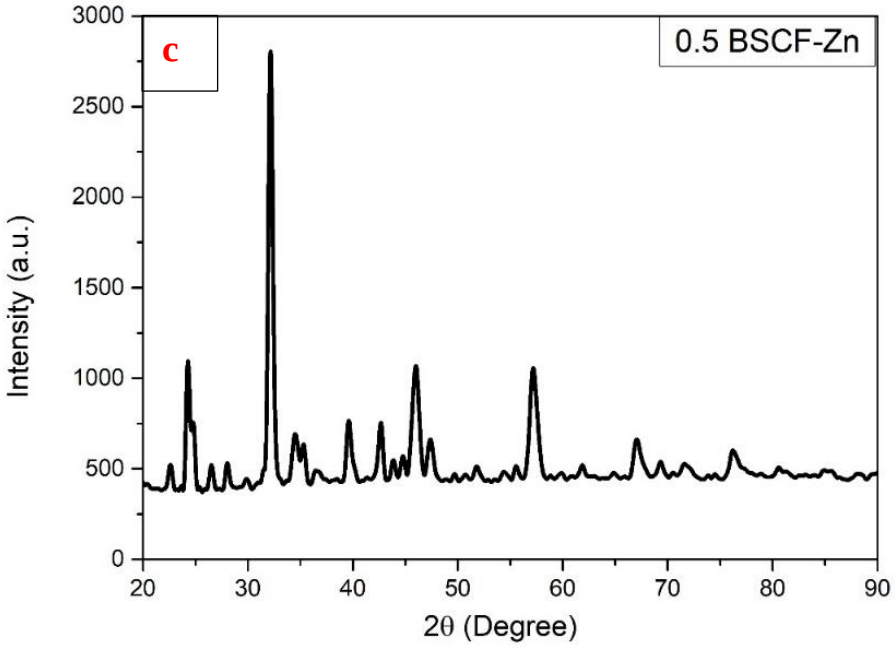
c
0.5 BSCF-Zn
Intensity (a.u.)
2θ (Degree)
0
500
1000
1500
2000
2500
3000
20
30
40
50
60
70
80
90

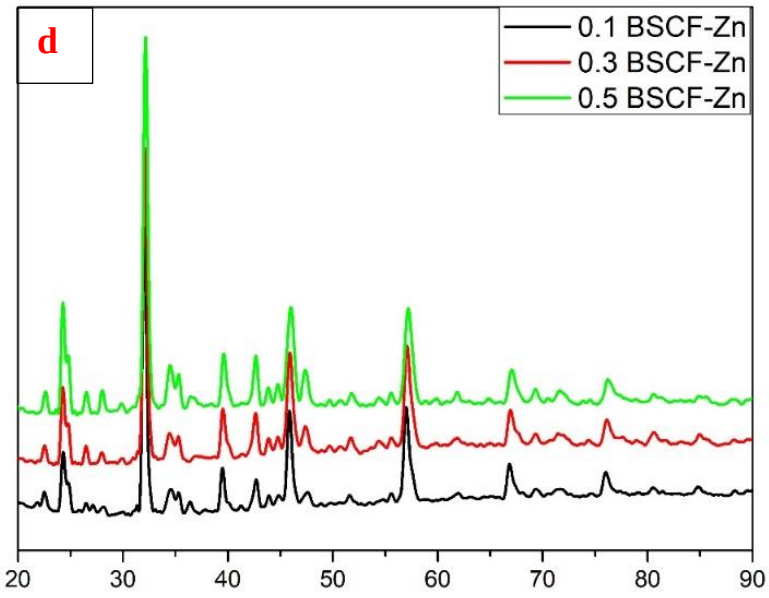

Figure 2.5. XRD patterns of as-synthesized BSCF -Zn perovskite oxide powders. a) 0,1 mol Zn doped BSCF, b) 0,3 mol Zn doped BSCF and c) 0,5 mol Zn doped BSCF. d) Overlapping of characteristic peaks of BSCF-Zn powders.

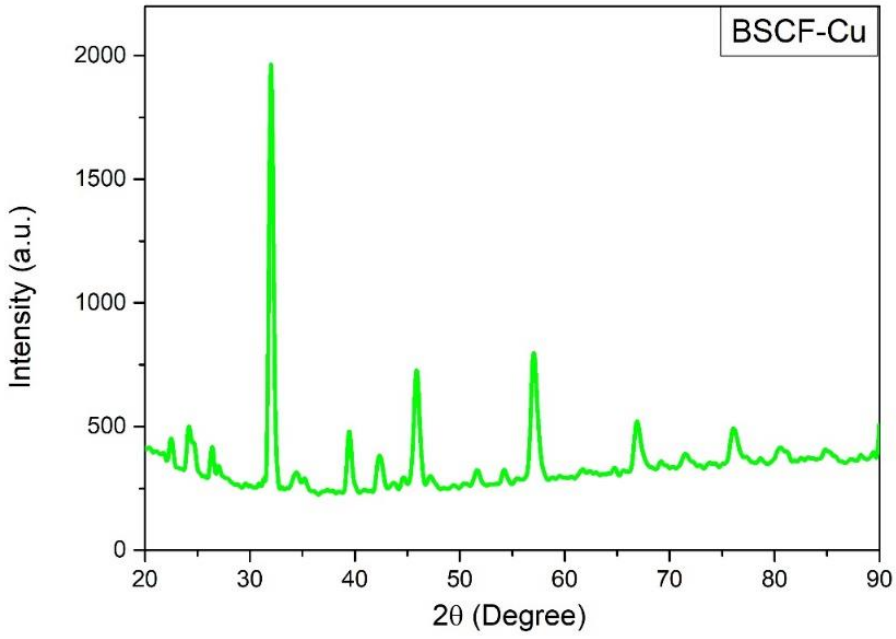

Figure 2.6. XRD pattern of Cu doped BSCF showing the characteristic peak.

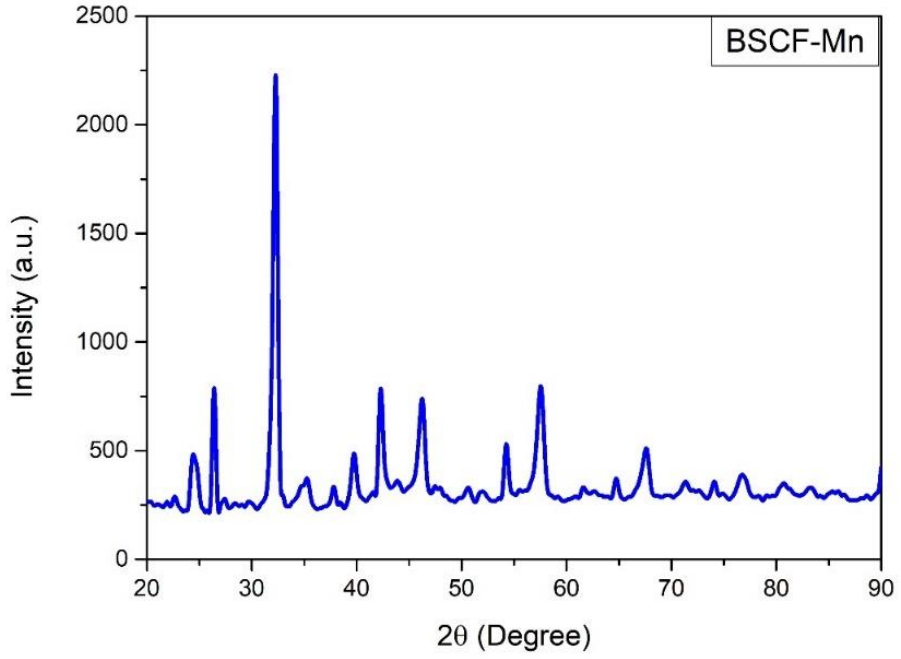

Figure 2.7. XRD pattern of Mn doped BSCF showing characteristic peak.

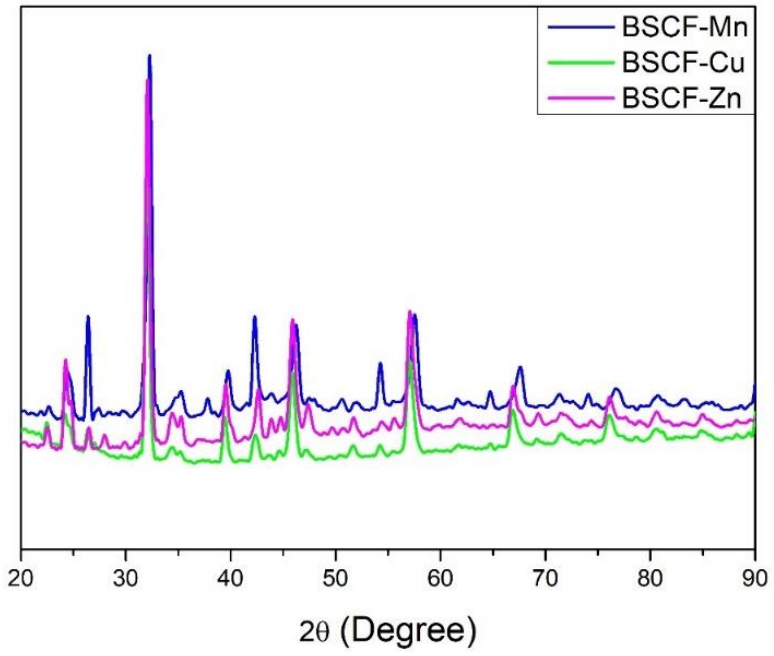

Figure 2.8. XRD peak comparison of BSCF-Zn, BSCF-Mn and BSCF-Cu. Figure showing the overlapping of main peaks and their slightly shifted 2 theta angles.

Table 2.6. Crystallite size comparisons of synthesized perovskites according to Scherrer equation.

Perovskite Type	Crystallite Size (nm)
BSCF	28,7
BSCF – Cu	20,7
BSCF – Zn	51,6
BSCF – Mn	35,0

Crystallite sizes in the table 2.6 were calculated according to Scherrer equation using the data obtained from XRD measurements. According to table 2.6., Zn has the biggest crystallite size since it has the biggest atomic radius. Crystallite sizes are sorted from highest to lowest as followed; BSCF-Zn > BSCF-Mn > BSCF > BSCF-Cu.

2.2.2.3. X-Ray Photoelectron Spectroscopy

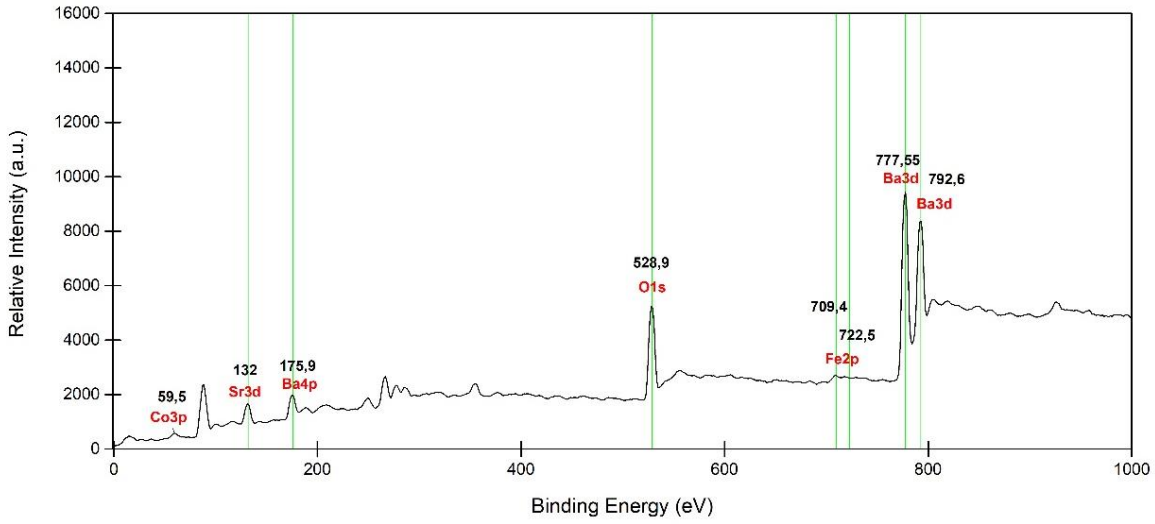

Figure 2.9. XPS graph of pure BSCF powder. Straight lines showing the positions of binding energies of Ba, Sr, Co, Fe and O orbitals.

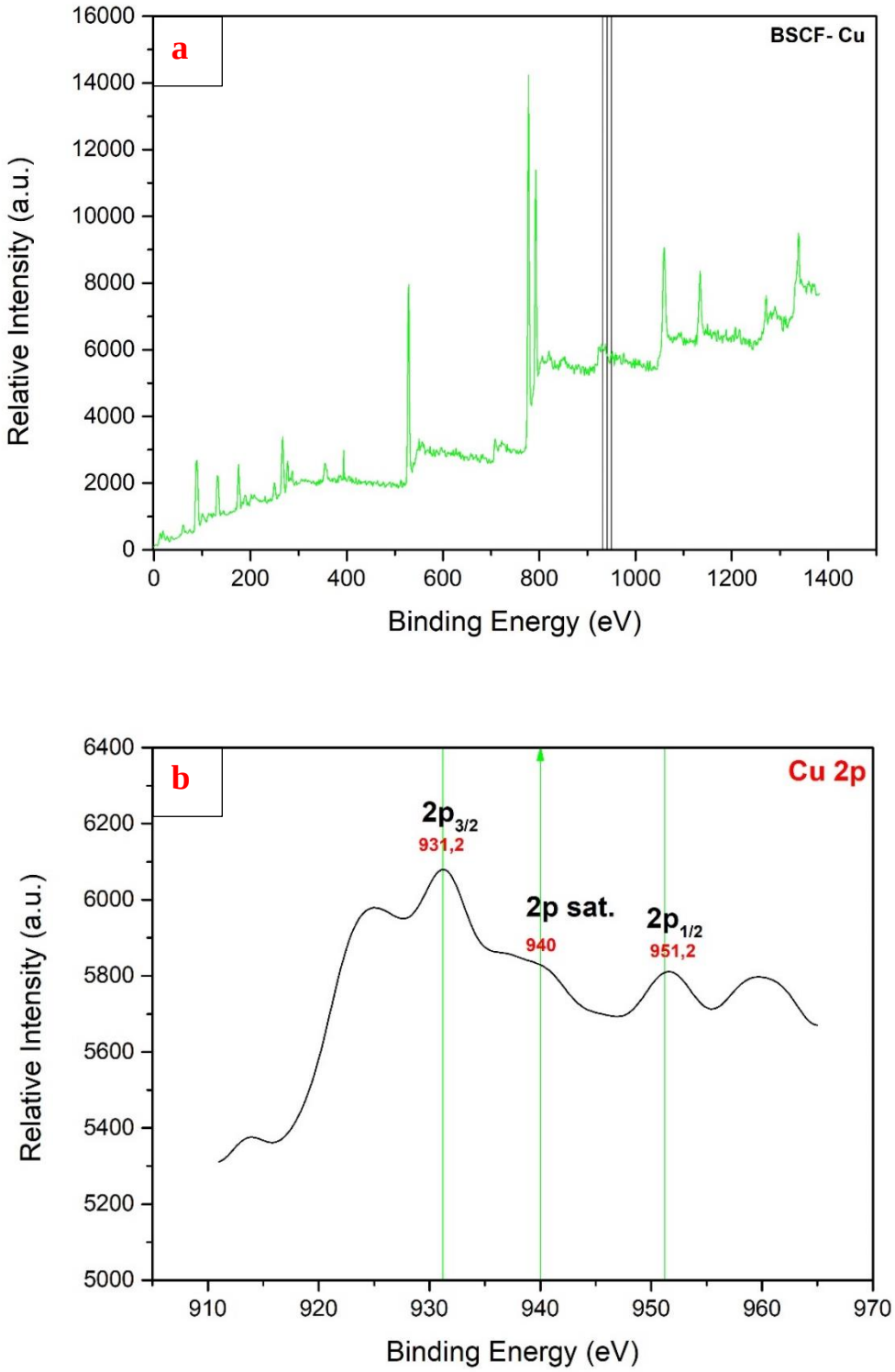

Figure 2.10. XPS graph of a) BSCF-Cu. Straight lines showing the Cu 2p orbitals. b) Detailed Cu 2p orbitals binding energies in the structure.

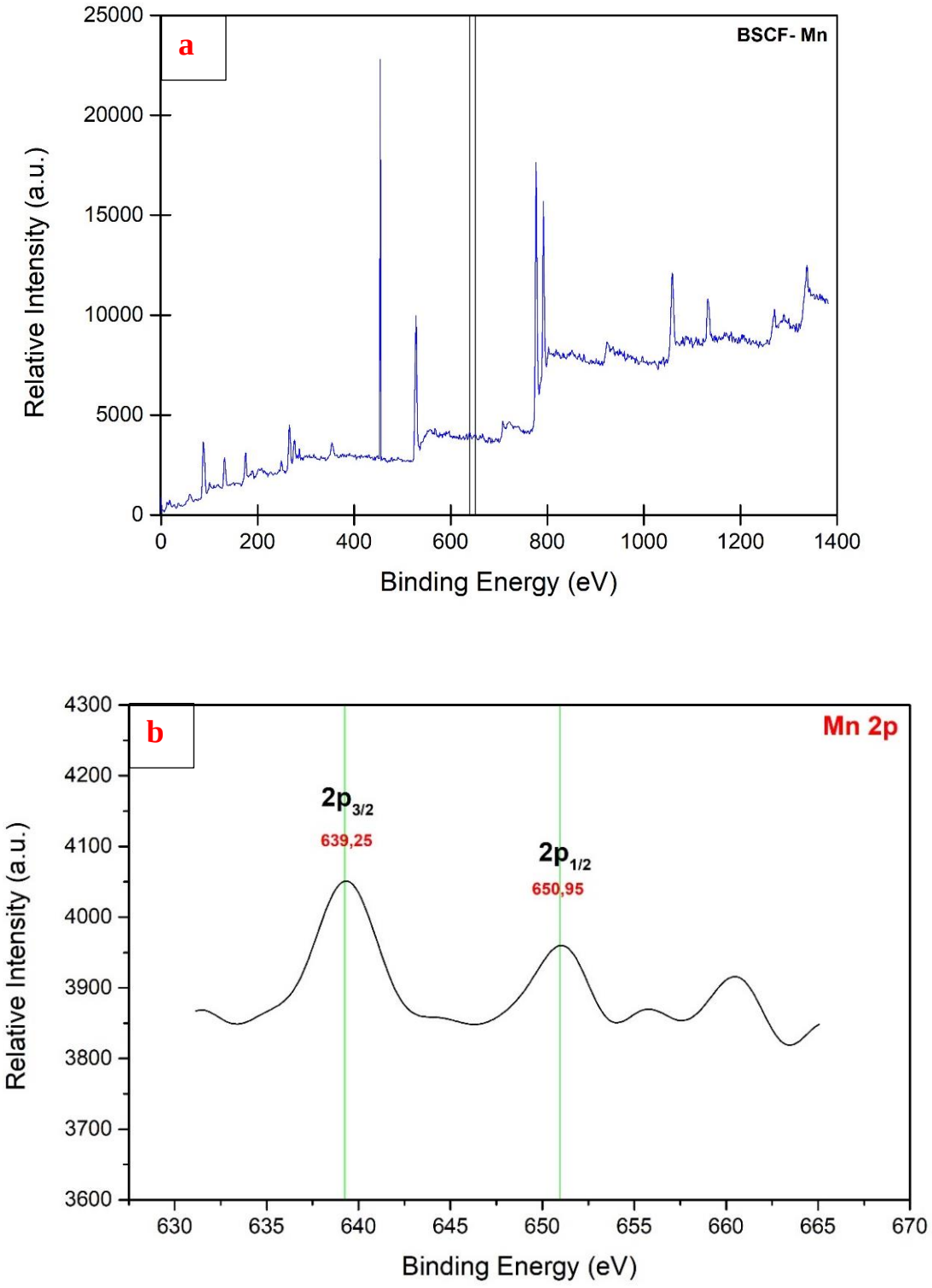

Figure 2.11. XPS graphs of a) BSCF-Mn powder. Straight lines showing the Cu 2p orbitals. b) Detailed Mn 2p orbitals binding energies in the structure.

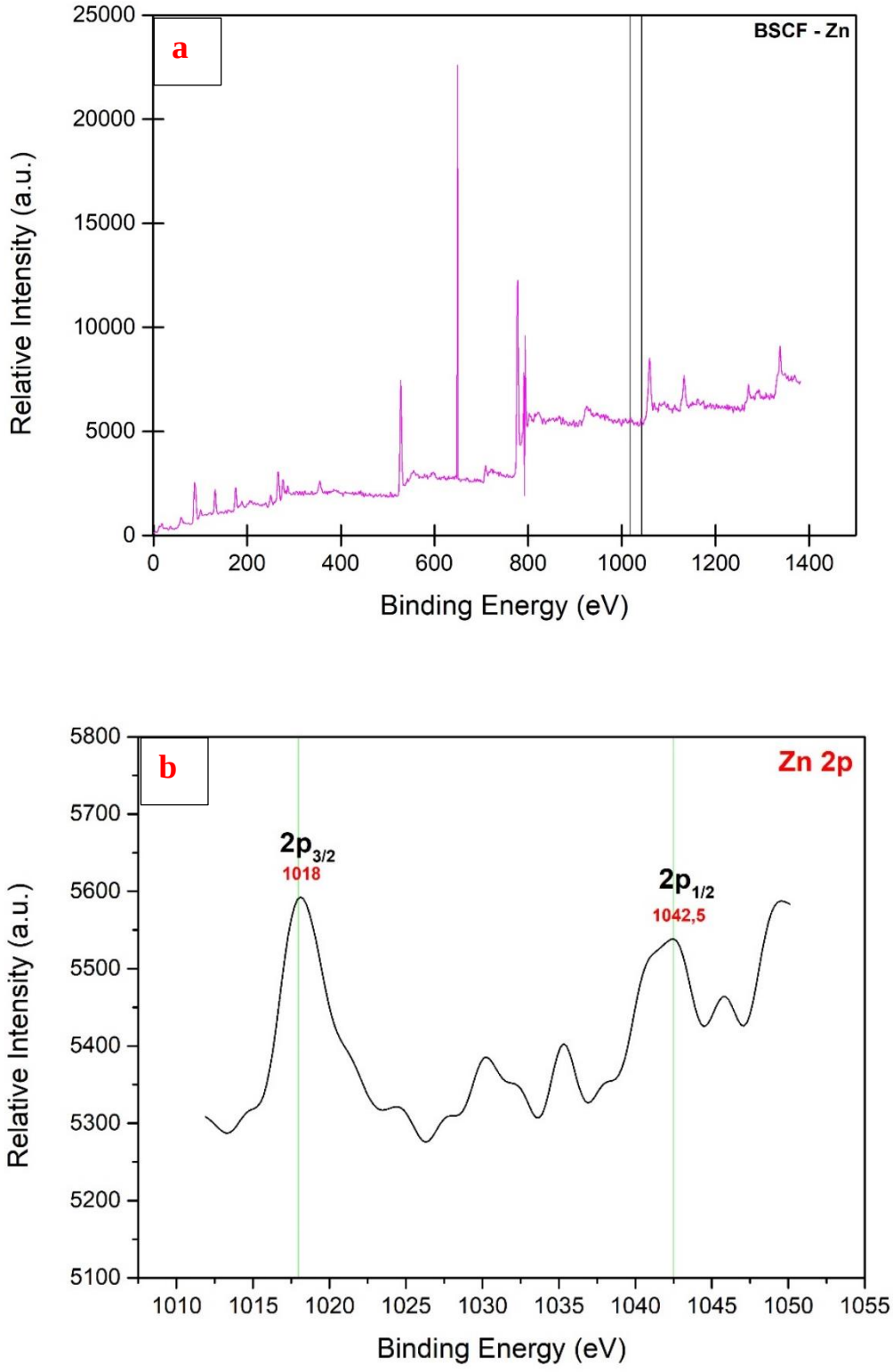

Figure 2.12. XPS graphs of a) BSCF-Zn. Straight lines showing the Zn 2p orbitals. b) Detailed Zn 2p orbitals binding energies in the structure.

2.2.2.4. Brunauer – Emmett – Teller Analysis

Table 2.7. BET analysis results of BSCF, BSCF-Cu, BSCF-Zn and BSCF-Mn.

Perovskite Type	Surface Area (m^2/g)	Pore Size (Å)	Pore Volume (cm^3/g)
BSCF	1,07	186,08	0,005
BSCF-Cu	1,35	122,47	0,004
BSCF-Zn	1,70	104,44	0,004
BSCF-Mn	4,30	135,76	0,015

According to table 2.7., Mn doping provided the best increase in surface area. Although the pore sizes are smaller than pure BSCF, Mn doping again provided the highest pore size among other doped BSCF types. Since Mn doping increases surface area, it is expected to have greater catalytic activity among other doped BSCF structures.

2.2.3. Electrochemical Characterization

Electrochemical characterizations were done by three electrode system in 1 M KOH solution as electrolyte with potentiostat. In the three-electrode configuration, Ag-AgCl was used as reference electrode while Pt mesh was used as counter/auxiliary electrode. Electrodes prepared in this study was positioned as working electrode in the system. Since all the measurements were done in alkaline media, voltage values were normalized with pH value according to Nernst equation. pH was accepted as 14 for 1 M of KOH solution. According to Nernst equation, for per pH change, potential changes about 60 mV. Also, E° is accepted as 0,205 (in 3,5 mol/kg KCl at 25°C) for Ag/AgCl reference electrode. Calculation below applied to all voltammetry measurements. LSV measurements were performed between 0.1 - -0,5 V. Cyclic voltammetry measurements were performed with 20, 60, 100, 140 and 180 mV/s. between 0,12 – 0,17 V.

$$E = E° + 0{,}0592\text{pH at } 25°C \qquad (2.1)$$

$$E = 0{,}205 + 0{,}0592*14 \quad (2.2)$$

$$E \approx 1{,}03 \quad (2.3)$$

2.2.3.1. Ink Preparation from Synthesized Perovskite Oxide Powders

Ink solution was prepared by mixing 10 mg of BSCF powders with 100 µl of nafion and 1 ml of ethanol and 10 mg of carbon black.

Addition of carbon black was known to tune the electronic states of perovskite structures. Especially, it is proven that Carbon reduces the Co states in BSCF. Since Co is accepted as the active site, Carbon addition increases catalytic activity. But for OER working potentials carbon is known to be oxidize easily. In the previous studies, it is shown that addition of carbon to structure does not affect OER activity directly, but it facilitates the Co reduction in the structure. [56] Nafion was added to mixture as a binder, also, it eases the transport of dissolved oxygen to the catalyst surface. It is known that as the reaction intermediate binding increases, activity of a catalyst increases also.

2.2.3.2. Coating and Preparation of Electrodes

Ink solutions were prepared by the same manners as mentioned above for all synthesized powders. For BSCF-Cu, BSCF-Mn and BSCF-Zn, nafion was used as an immobilizing binder and carbon black was used as Co reducing initializer. Each electrode was prepared by cutting Ni Foam 1 cm x 5 cm dimensions. Prepared ink solutions were drop coated on Ni foam substrates with a loading of ~ 232 µg/cm^2. Coated Ni foams were annealed at 80 ° C for 5 h. This way, it is expected to increase the stability of electrodes. Drop coating was chosen as coating method because the bulk performance of each prepared ink was investigated. As the loading of catalyst increases to a limit, activity is expected to increase also.

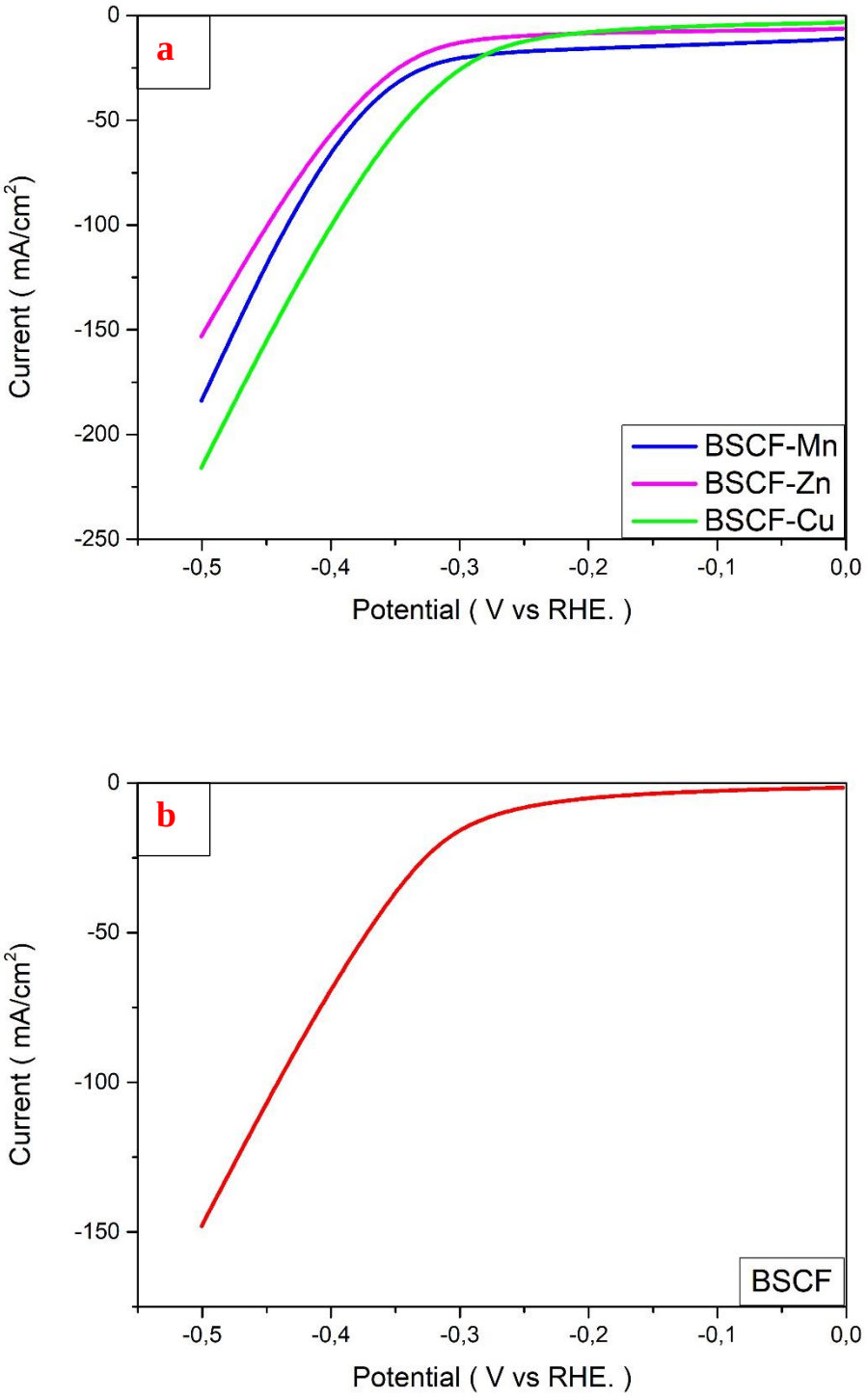

Figure 2.13. a) LSV comparison of BSCF-Zn, BSCF-Mn and BSCF-Cu and b) BSCF between 0 - - 0,5 V in 1 M KOH

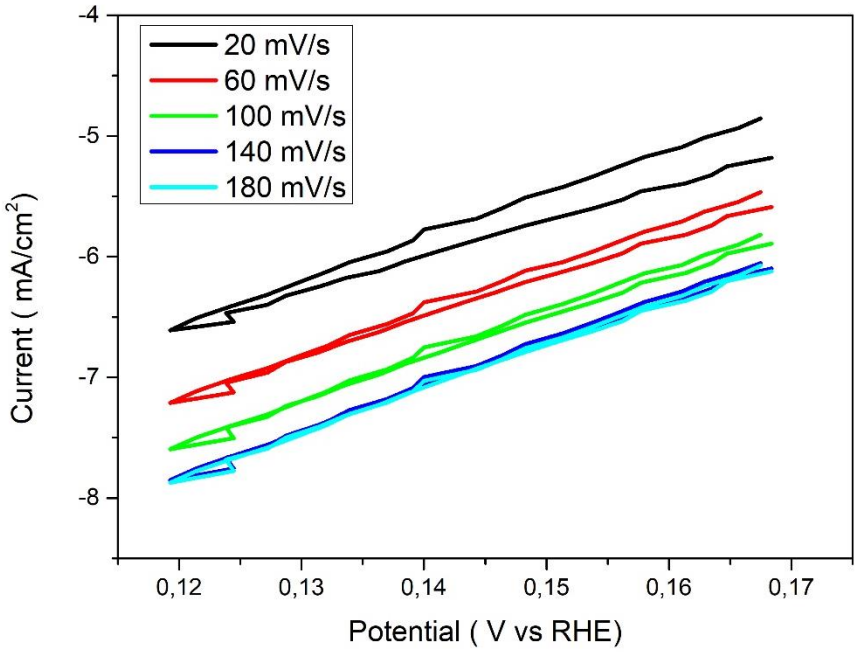

Figure 2.14. Cyclic voltammetry graphs of BSCF at 20, 60, 100, 140 and 180 mV/s scan rates between 0,25 – 0,17 V in 1 M KOH.

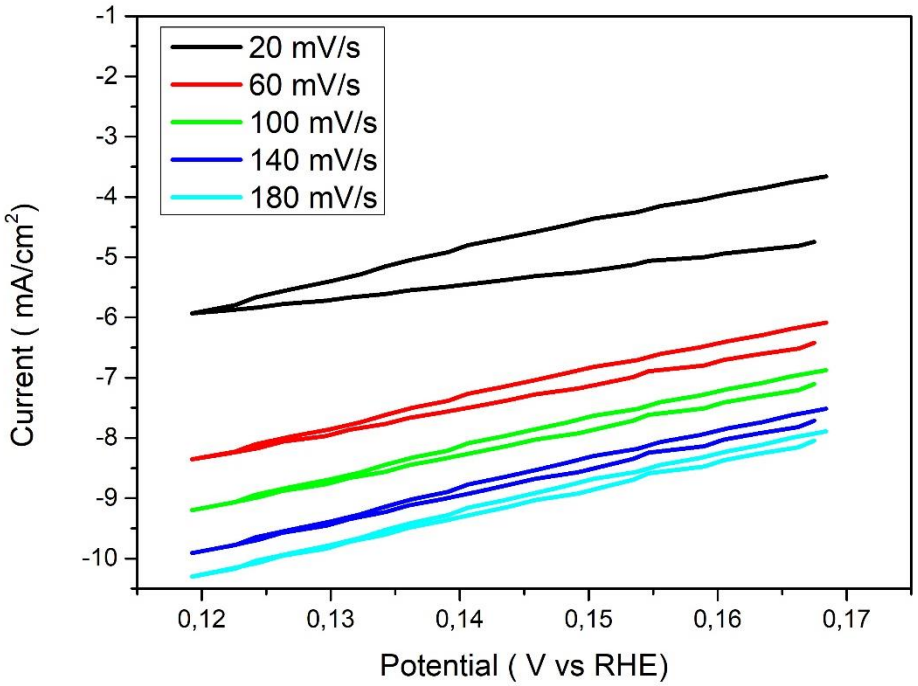

Figure 2.15. Cyclic voltammetry graphs of BSCF-Cu at at 20, 60, 100, 140 and 180 mV/s scan rates between 0,25 – 0,17 V in 1 M KOH.

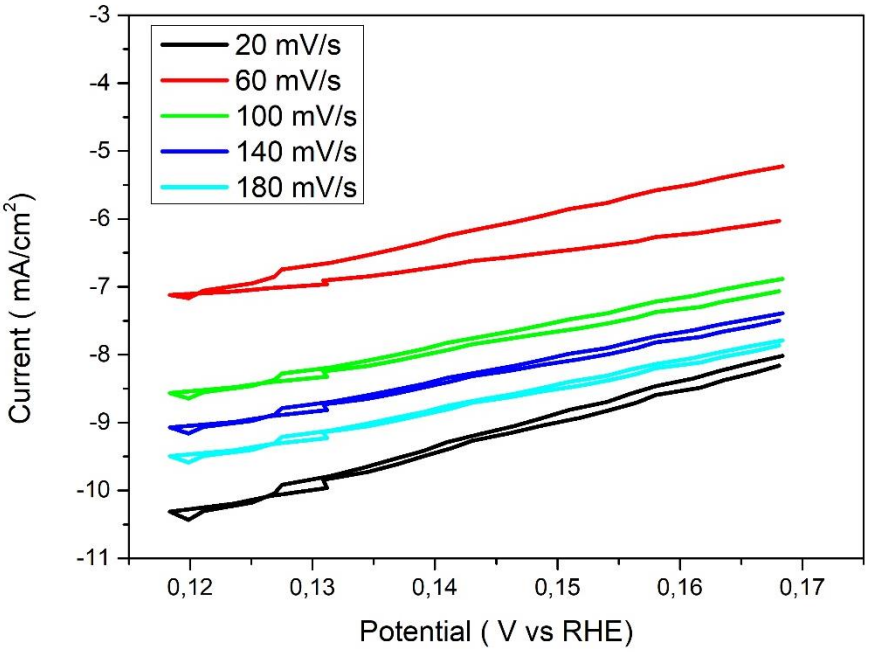

Figure 2.16. Cyclic voltammetry graphs of BSCF-Mn at 20, 60, 100, 140 and 180 mV/s scan rates between 0,25 – 0,17 V in 1 M KOH.

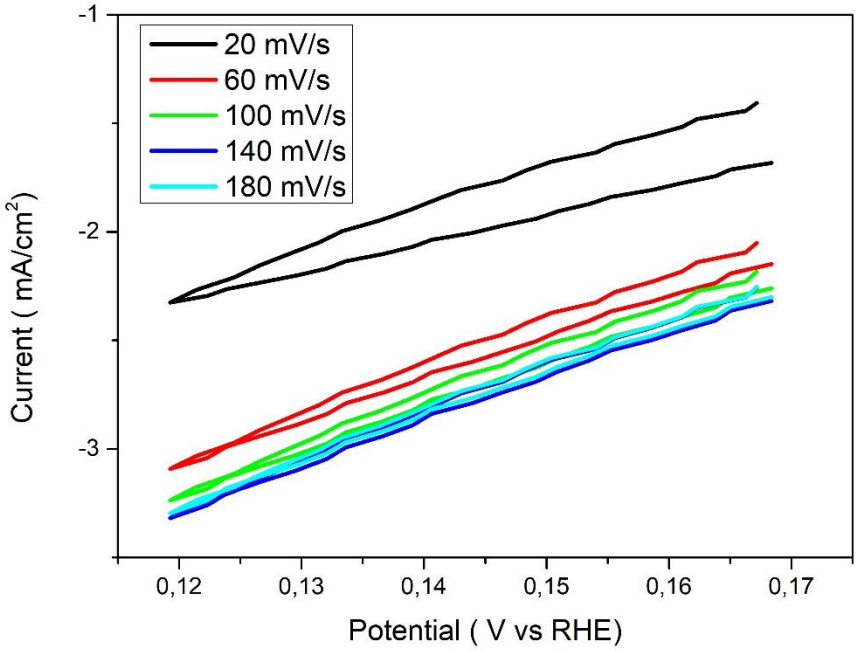

Figure 2.17. Cyclic voltammetry graphs of BSCF-Zn at at 20, 60, 100, 140 and 180 mV/s scan rates between 0,25 – 0,17 V in 1 M KOH.

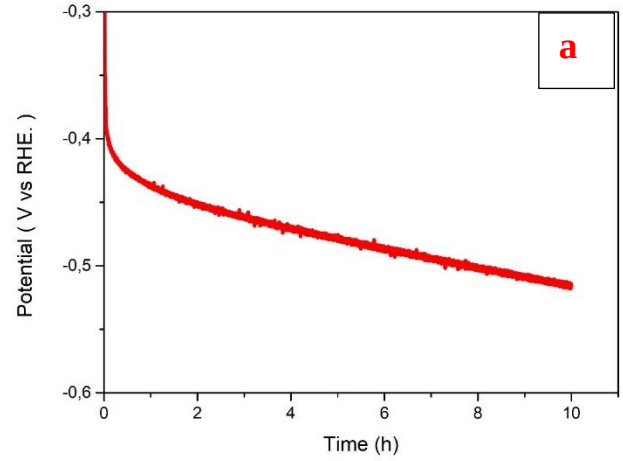
a
Potential (V vs RHE.)
Time (h)
-0,3
-0,4
-0,5
-0,6
0
2
4
6
8
10

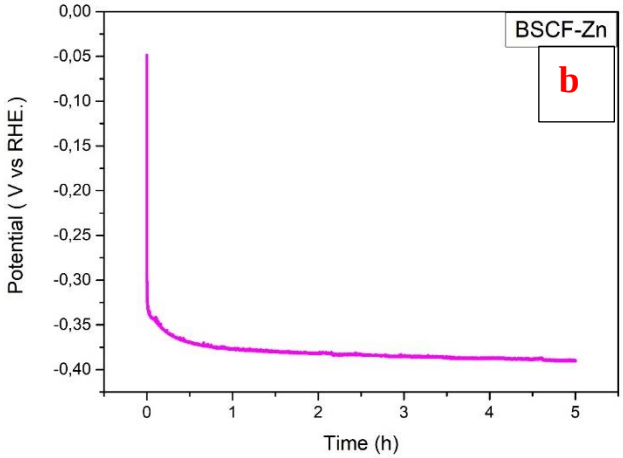
BSCF-Zn
b
Potential (V vs RHE.)
Time (h)
0,00
-0,05
-0,10
-0,15
-0,20
-0,25
-0,30
-0,35
-0,40
0
1
2
3
4
5

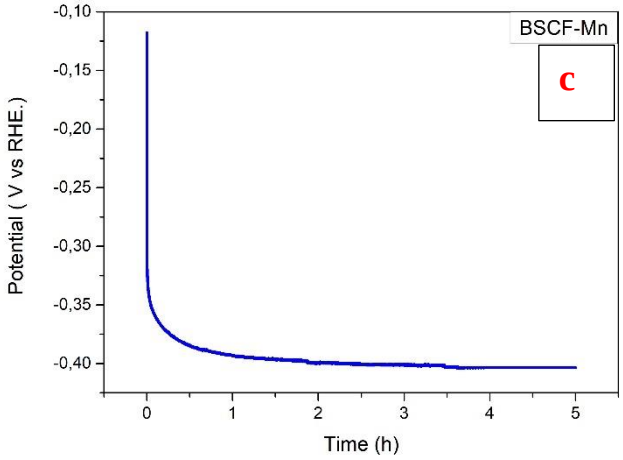
BSCF-Mn
c
Potential (V vs RHE.)
Time (h)
-0,10
-0,15
-0,20
-0,25
-0,30
-0,35
-0,40
0
1
2
3
4
5

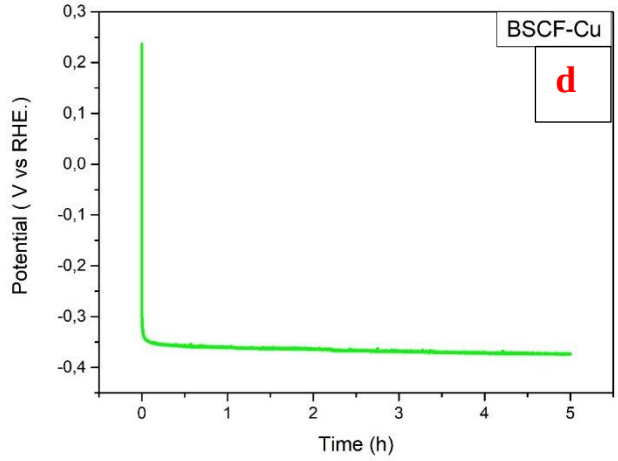

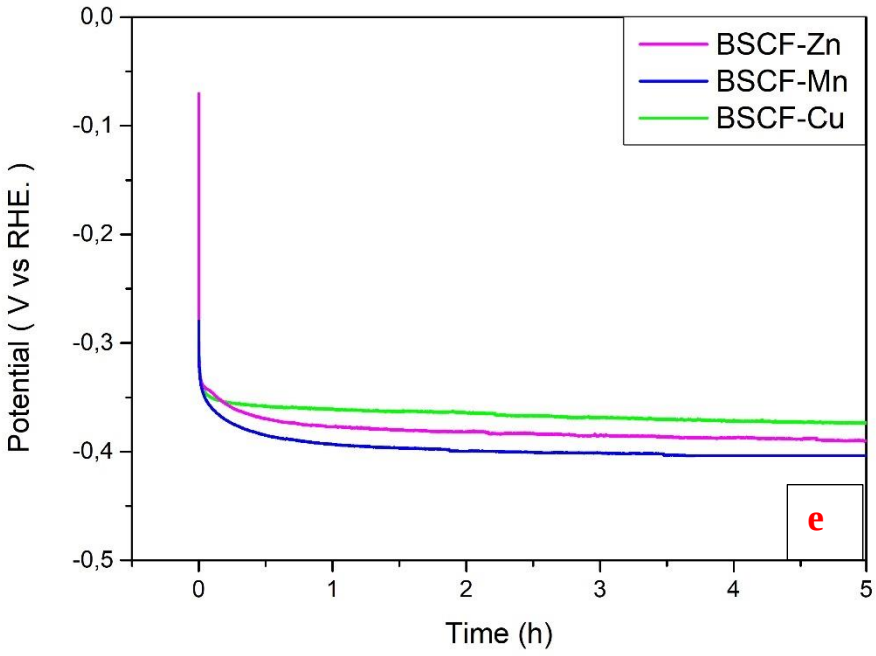

Figure 2.18. Chrono potentiometric measurements of a) Pure BSCF, b) BSCF-Zn and c) BSCF-Mn d) BSCF-Cu and e) Comparison of the stabilities at 50 mA of synthesized perovskites for 5 hours.

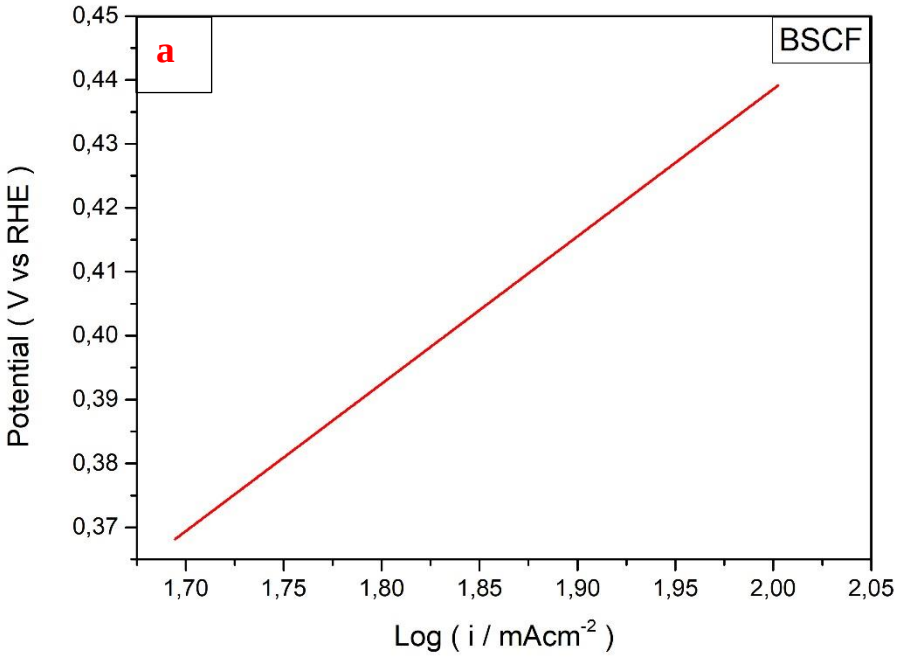
a
BSCF
Potential (V vs RHE)
0,45
0,44
0,43
0,42
0,41
0,40
0,39
0,38
0,37
1,70
1,75
1,80
1,85
1,90
1,95
2,00
2,05
Log (i / mAcm-2)

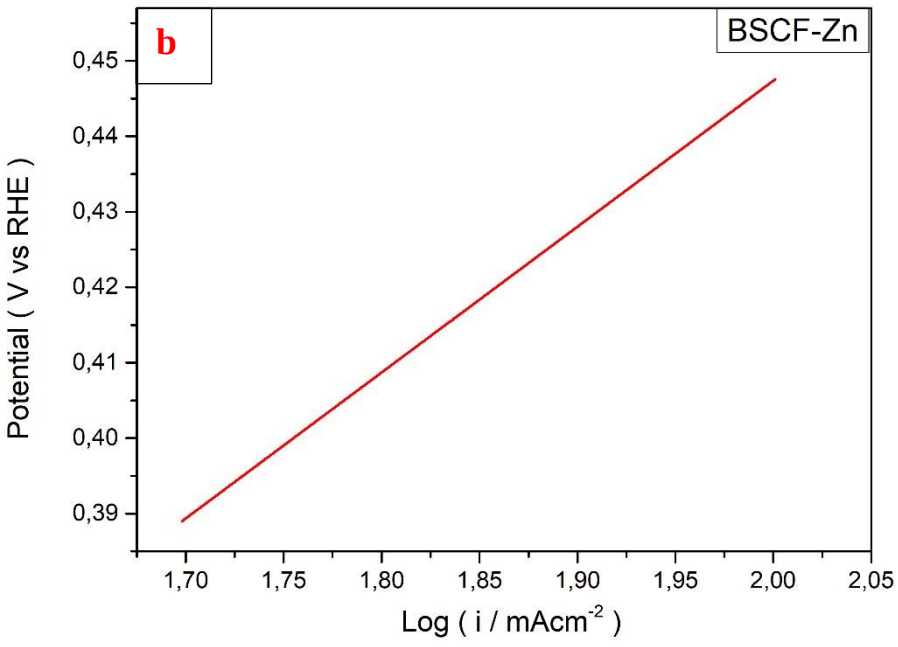
b
BSCF-Zn
Potential (V vs RHE)
0,45
0,44
0,43
0,42
0,41
0,40
0,39
1,70
1,75
1,80
1,85
1,90
1,95
2,00
2,05
Log (i / mAcm-2)

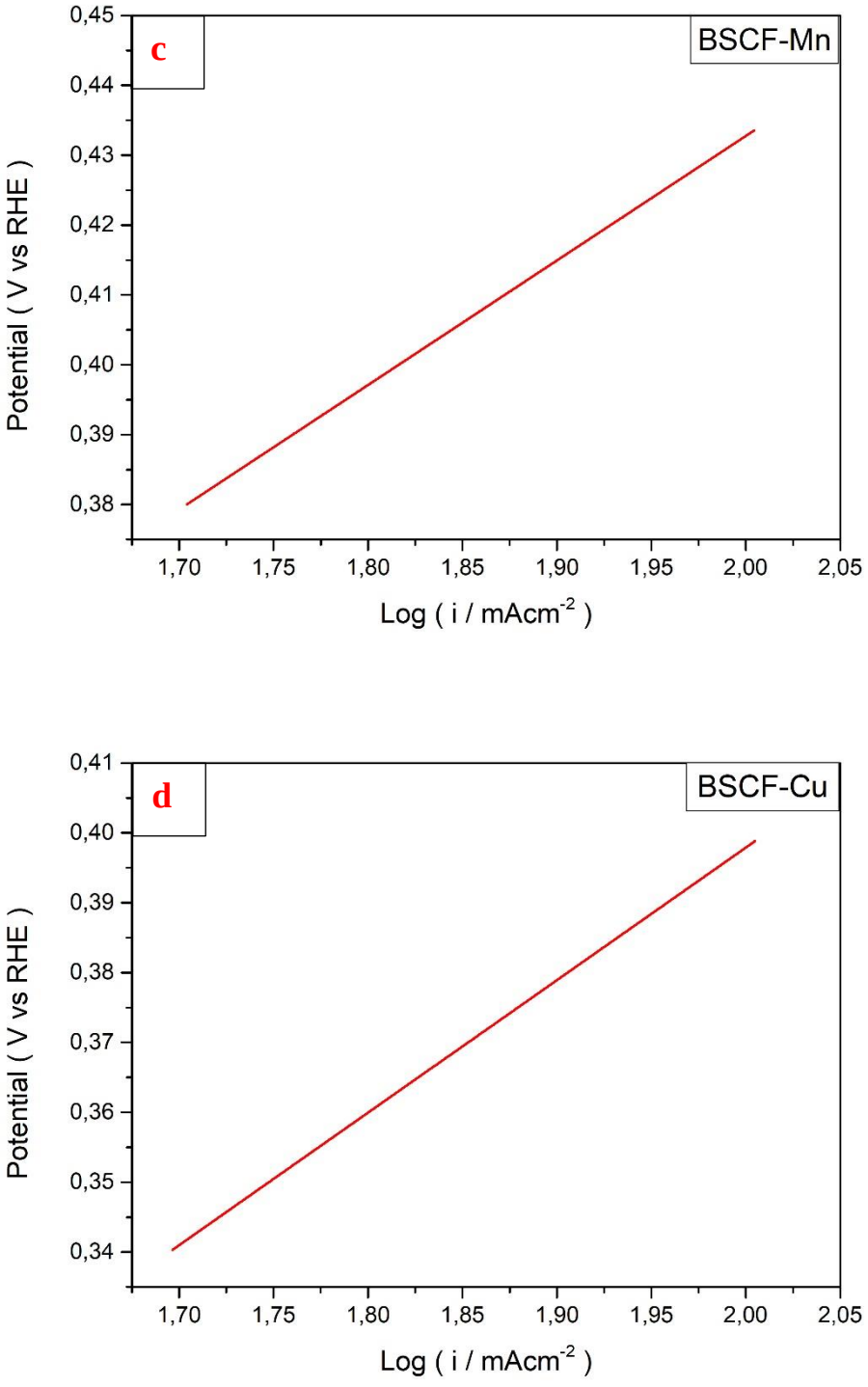

Figure 2.19. Tafel curves of a) BSCF, b) BSCF-Zn, c) BSCF-Mn and d) BSCF-Cu between 50 mA - 100 mA.

Table 2.8. Tafel slopes and overpotentials of synthesized perovskites.

Perovskite type	Tafel Slope (mV/dec)	Overpotential (mV)
BSCF	231	373
BSCF-Cu	190	340
BSCF-Mn	178	380
BSCF-Zn	193	390

Table 2.8. shows the data calculated from Tafel plots of each synthesized perovskite oxide. Tafel slopes and overpotentials gives information about the thermodynamic and kinetic rates. According to the table 2.8., Mn doping has the fastest kinetics and Cu doping has the best thermodynamically favorable structure for HER catalyst.

2.2.4. Results and Discussion

XPS, SEM, XRD and BET were used as characterization methods for synthesized perovskites. According to SEM images, metal doping increases the surface area of BSCF powder as expected. X-ray photoelectron spectroscopy was used to show the existing electronic states of metals included in the crystal structure. XPS graphs of undoped BSCF gives peaks at 59,3 eV for Co 3p; 132 eV for Sr 3d; 175,9 eV for Ba 4p; 528,9 eV for O 1s; 709,4 eV and 722,5 eV for Fe 2p; 777,55 eV and 792,6 eV for Ba 3d. There are doublet peaks for Fe 2p and Ba 3d orbitals due to the orbital degeneracy. Degeneracy of electronic states also observed for Cu 2p Mn 2p and Zn 2p orbitals too. In the XPS graphs of Cu 2p, one satellite peak is observed at 940 eV. Satellite peaks are observed due to a sudden change in coulombic potential as the photo ejected electron passes through the valence band.

According to the EDX map spectroscopies, we can conclude that doping process was successful for Mn, Zn and Cu metals and they are included in the crystal structure. Also, maps show the homogenic distribution of each atom in the structure.

The addition of metal dopants is also can be observed in the XRD graphs. Three different mol percentages was tested for the synthesis of BSCF-Zn to determine the best doping amount. Three mol values was determined as 0,1 0,3 and 0,5. Their effect on the crystal structure was analyzed by XRD method and particle sizes was calculated by Scherrer's equation. Average particle sizes (d) were calculated according to the Scherrer equation ($d = 0.94\lambda/B_{2\theta}\cos\theta_{max}$) from XRD data by B being the peak width and θ the peak position and Λ = 0.15418 for Cu K-alpha. Scherrer equation calculations shows that the particle sizes are as followed for BSCF-Zn synthesis; $d_{0.1\text{-}Zn}$ = 51,61 nm, $d_{0.3\text{-}Zn}$ = 51.62 nm and $d_{0.5\text{-}Zn}$ = 103.32 nm. According to the Scherrer equation calculations, average particle sizes are as followed for synthesized perovskite oxides; d_{BSCF}=28.68 nm $d_{BSCF\text{-}Zn}$=51.62 nm $d_{BSCF\text{-}Cu}$=20.69 nm and $d_{BSCF\text{-}Mn}$ = 34.97 nm. According to the particle size comparison, BSCF-Cu has the smallest particle sizes which means it has greater surface area. Particle size of pure BSCF synthesized is smaller in comparison to other synthesis methods in literature [58,59] and also in comparison to sol-gel synthesis previously mentioned in the literature. [34,37] From XRD pattern comparison at Fig. 13, there are slight shifts of main peaks which can be related to lattice size changes. Lattice sizes increase as the 2-theta shift to lower angles. According to Fig. 13, lattice sizes increase as followed; BSCF-Cu > BSCF-Zn > BSCF-Mn.

BET analysis was used for the determination of surface areas, pore size and pore volumes of synthesized perovskite oxides. Pure BSCF has a surface area of 1,07 m^2/g, since a higher surface are is important for catalytic reactions, dopings are also expected to increase the surface area of pure BSCF. According to BET results, surface area of BSCF-Cu is 1,35 m^2/g, BSCF-Zn is 1,70 m^2/g and BSCF-Mn is 4,30 m^2/g. The most dramatic change for surface is observed for Mn doping by approximately 4 times. Pore size for pure BSCF size determined as 186,08 Å. Although pore sizes decrees compared to pure BSCF, BSCF-Mn has the biggest size compared to other metal dopings with 135,76 Å. Mn doping also observed to be increase the pore size of püre BSCF from 0,005 cm^3/g to 0,015 cm^3/g.

HER potentials of transition metal-doped BSCF perovskite structures were determined as; -340 mV for BSCF-Cu, -380 mV for Mn and -390 mV for Zn according to LSV measurements. These potential values are slightly higher than the theoretical HER

potential of water which is 0 V (vs RHE.). To show the scan rate effect on catalytic activity of synthesized perovskites, 20 mV/s, 60 mV/s, 100 mV/s, 140 mV/s, and 180 mV/s scan rates were applied for 1 cycle from 0,12 to 0,17 V in 1 M KOH solution. According to CV measurements at different scan rates, pure BSCF showed maximum current densities at 140 and 180 mV/s. BSCF-Cu has the highest maximum current density at 180 mV/s and BSCF-Zn showed similar maximum current densities at 100, 140 and 180 mV/s. On the contrary, BSCF-Mn showed highest current density among all scan rates at 20 mV/s. All scan rate tests are concluded as expected except BSCF-Mn. As the Randles–Sevcik equation suggests, peak current is proportional to the square root of scan rate,[57] therefore it is expected that the higher scan rates show better maximum currents. This can be explained by increase in scan rate increases the diffusion rates to electrode surface increasing the obtained maximum current. Tafel plots were prepared from the LSV data and Tafel slopes were calculated. According to the calculations Tafel slopes of BSCF-Cu, BSCF-Zn and BSCF-Mn are; 190 mV/dec; 193 mV/dec and 178 mV/dec respectively. Tafel slope gives information about the kinetic rates of a catalytic reaction. Since BSCF-Mn has the smallest Tafel slope with 178 mV/dec, it is proven that BSCF-Mn has the fastest kinetic rates for hydrogen evolution reactions, therefore water splitting reactions. On the other hand, overpotential is one of the indicators for a good HER catalyst. In this study, it is shown that BSCF-Cu has the smallest overpotential compared with other perovskite oxides tested with 340 mV. It is proven that BSCF-Cu is the thermodynamically most favorable structure among pure BSCF, BSCF-Zn and BSCF-Mn.

According to the choronopotentiometry data, BSCF-Cu, BSCF-Mn and BSCF-Zn shows good stabilities at 50 mA/cm^2 current density for 5 hours. Most dramatic change among synthesized perovskites belongs to pure BSCF from -0,3 to -0,5. Stability of BSCF-Zn changes among 5 hours from 370 mV to 390 mV. BSCF-Cu shows increase in overpotential from 350 mV to 370 mV and BSCF-Mn shows increase as from 380 to 400 mV. Also, choronopotentiometry data confirms the overpotential trend between metal dopings, showing that Mn doping has the highest overpotential followed by Zn doping. As a conclusion of electrochemical measurements, Zn, Mn, and Cu doping increase the catalytic activity of BSCF towards hydrogen evolution reaction. Cu shows the best increase among metal dopings.

2.2.5. Conclusion

In this chapter of the study, different perovskites was synthesized to test their activity and stability for hydrogen evolution reaction. All perovskites was synthesized according to EDTA-Citrate complexation method. BSCF was doped with Zn, Mn and Cu metals. Firstly Zn was doped in different proportions to investigate effect of the doped amount on crsyatllite sizes. From XRD results, 0,3 mol doping showed better crystallite sizes and other metals was added to structure by 0,3 mol. Among all the synthesizes perovskites, Cu doping has the best effect on both catalytic activity and stability. BSCF-Cu showed 340 mV overpotential whereas BSCF has 340 mVin alkaline media at 50 mA/cm^2 current density. From overpotential values, we can simply conclude that Cu doping provides best structure as a HER catalyst. It needs much less energy to overcome water splitting reaction energy barrier. So, according to the experiemental results, it is pwoven that BSCF-Cu is a promising canditate as hdyrogen evolution reaction catalyst for future applications.

2.3. Oxygen Evolution Reaction: Synthesis and Characterization of Perovskite Oxide Catalysts

2.3.1. Synthesis of Perovskite oxide powders

All perovskite oxide catalysts used in this study was synthesized by the same EDTA-Citrate complexing method according to sol-gel route.

2.3.1.1. Synthesis of BSCF

- 0,04 mol of EDTA dissolved in 40 ml 1M NH_4OH solution.
- 0,02 mol of $Ba(NO_3)_2$ mixed with EDTA-NH_3 solution.

- 0,02 mol of $Sr(NO_3)_2$ 0,03 mol of $Co(NO_3)_2$ and 0,008 mol of $Fe(NO_3)_3$ were dissolved in 100 ml of water.
- $Ba(NO_3)_2$ -EDTA- NH_3 mixture and solutions of $Sr(NO_3)_2$, $Co(NO_3)_2$ and $Fe(NO_3)_3$ was added together to form precursor solution.
- 0,04 mol of citric acid was added to the mixed solution and pH was set to 5 by addition of NH_4OH.
- Final solution was stirred for 24 hours at 75ºC with 500 rpm.
- The gelled samples obtained were baked in a drying oven at 250°C for 24 hours.
- Finally, primary powder was calcinated at 800°C for 2 hours.

2.3.1.2. Synthesis of BSCF-Ag

- 0,04 mol of EDTA dissolved in 40 ml 1M NH_4OH solution.
- 0,02 mol of $Ba(NO_3)_2$ mixed with EDTA-NH_3 solution.
- 0,02 mol of $Sr(NO_3)_2$ 0,03 mol of $Co(NO_3)_2$ and 0,008 mol of $Fe(NO_3)_3$ were dissolved in 100 ml of water.
- $Ba(NO_3)_2$ -EDTA- NH_3 mixture and solutions of $Sr(NO_3)_2$, $Co(NO_3)_2$ and $Fe(NO_3)_3$ was added together to form precursor solution.
- $AgNO_3$ was added to final precursor solution.
- 0,04 mol of citric acid was added to the mixed solution and pH was set to 5 by addition of NH_4OH.
- Final solution was stirred for 24 hours at 75ºC with 500 rpm.
- The gelled samples obtained were baked in a drying oven at 250°C for 24 hours.
- Finally, primary powder was calcinated at 800°C for 2 hours.
-

2.3.1.3. Doping of perovskite oxide catalyst with several metals

For OER activity studies, BSCF was doped with silver for its known electrochemical stability in basic solutions and good electrical conductivity. Various

studies have been made on the ORR activity of Ag as catalyst. [60–64] OER activity of Ag was investigated by Li et al. in near-neutral potassium tetraborate (K2B4O7) electrolyte and they observed high activity and low overpotentials as 318 mV. [65]

Zhang et al. compared BSCF and BSCF-Ag for low temperature SOFC applications by screen printing method and showed that BSCF-Ag has double conductivities for all tested temperatures than pure BSCF. [66]

Ag doped BSCF was investigated for its ORR catalytic activity by Shao et al. in two different dopant percentages. The addition of Ag was made by dropping $AgNO_3$ solution to BSCF electrode and then reducing the Ag^+ to Ag by hydrazine addition. Two different percentages (3 and 15 wt %) was investigated and 3 wt. % Ag addition reduced both resistance and activation energy compared to pure BSCF. Excessive Ag loading reported to have negative effect also. They also reported that the O_2 adsorption and charge transport was improved. [67]

Although there are several studies on the catalytic activity of Ag doped BSCF for ORR, there are not any works done one its OER activity. As its shown that ORR and OER has similar activity descriptors such as reaction intermediate adsorption strengths, BSCF-Ag was prepared for OER activity tests in this work.

2.3.2. Bulk and Surface Characterizations

2.3.2.1. Scanning Electron Microscope and Energy Dispersive X-Ray Spectroscopy

Scanning Electron Microscopy (SEM) images were obtained via FEI QUANTA 250 FEG instrumentation to investigate surface morphologies of powders. 2500x and 5000x zooming are demonstrated at 50µ and 20µ respectively to show the porosity differences of BSCF, and BSCF-Ag perovskite oxide powders synthesized by the same sol-gel route. For SEM images, backscattered electron detector was used while for EDX analysis, X-Ray detector was used. With EDX, mappings and spectroscopy analysis were done.

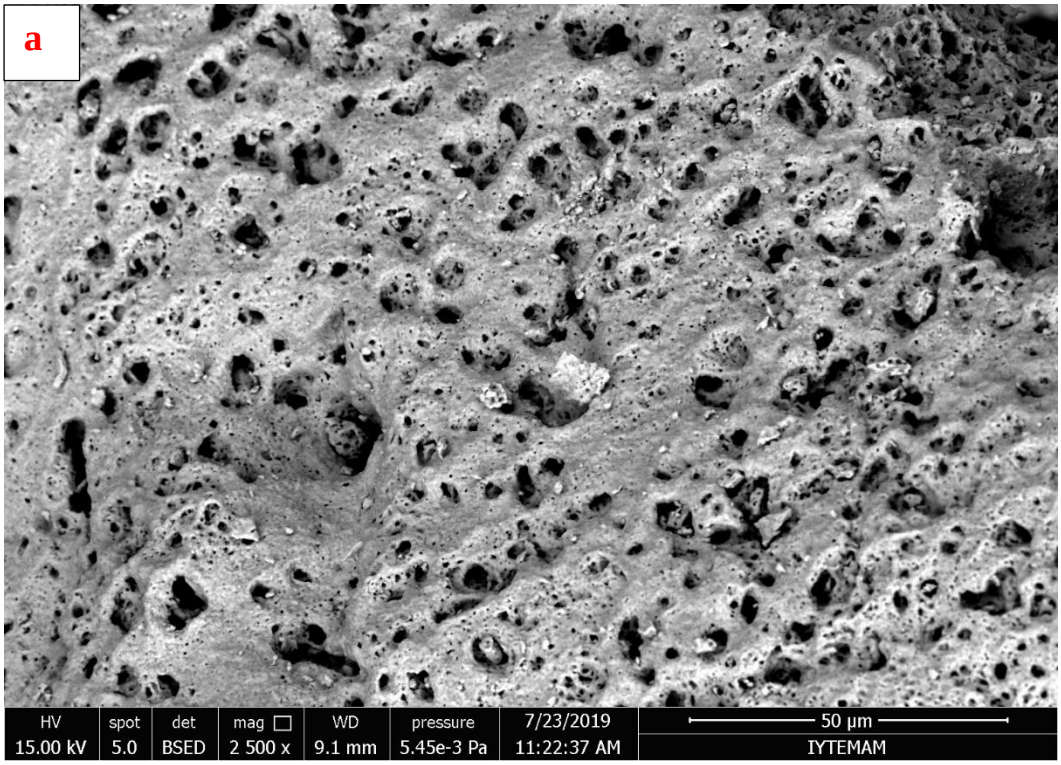

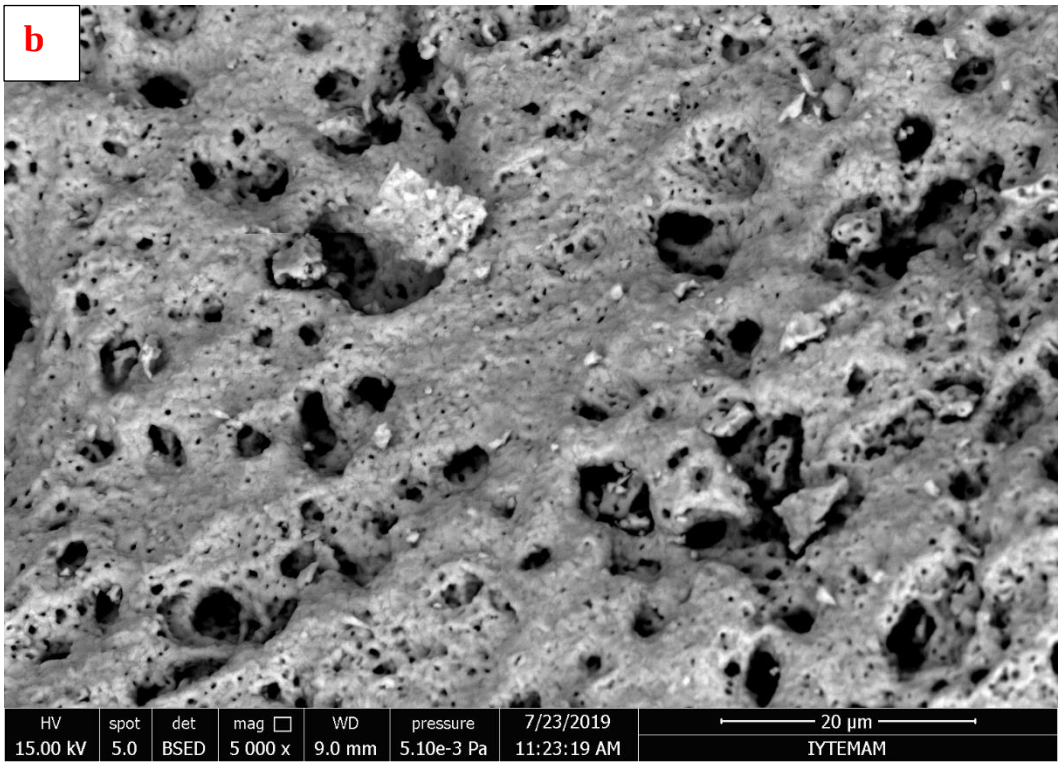

Figure 2.20. SEM images of BSCF powders obtained by backscattered electron detector at a) 2500x and b) 5000x zooming.

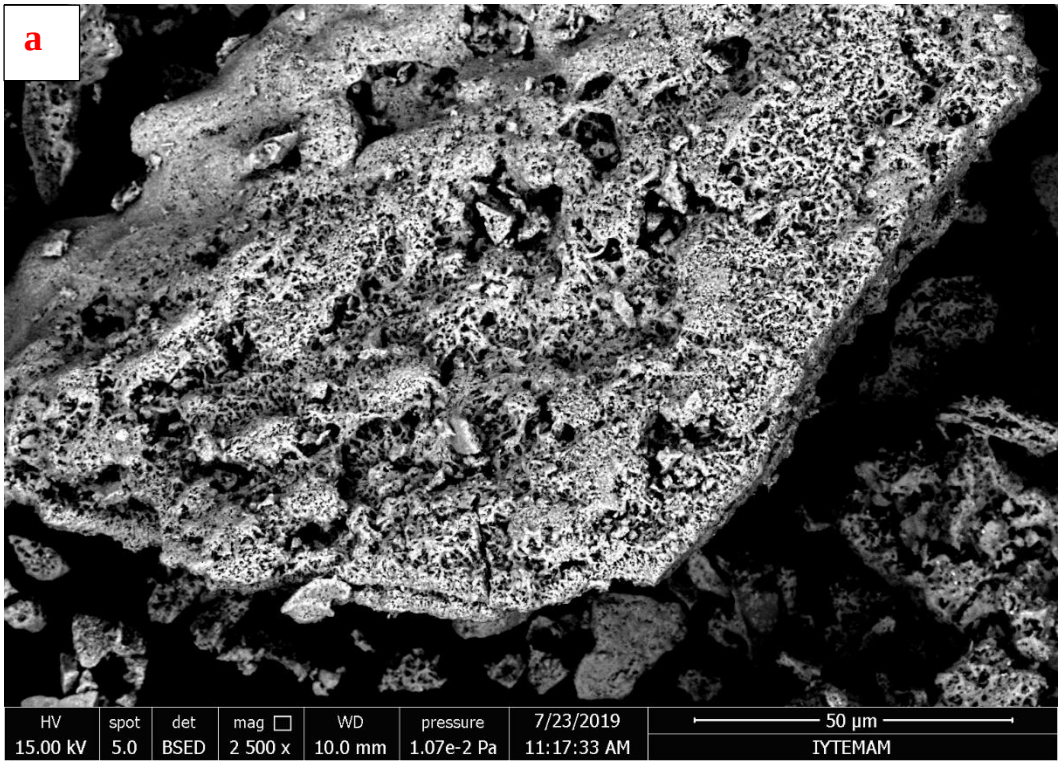

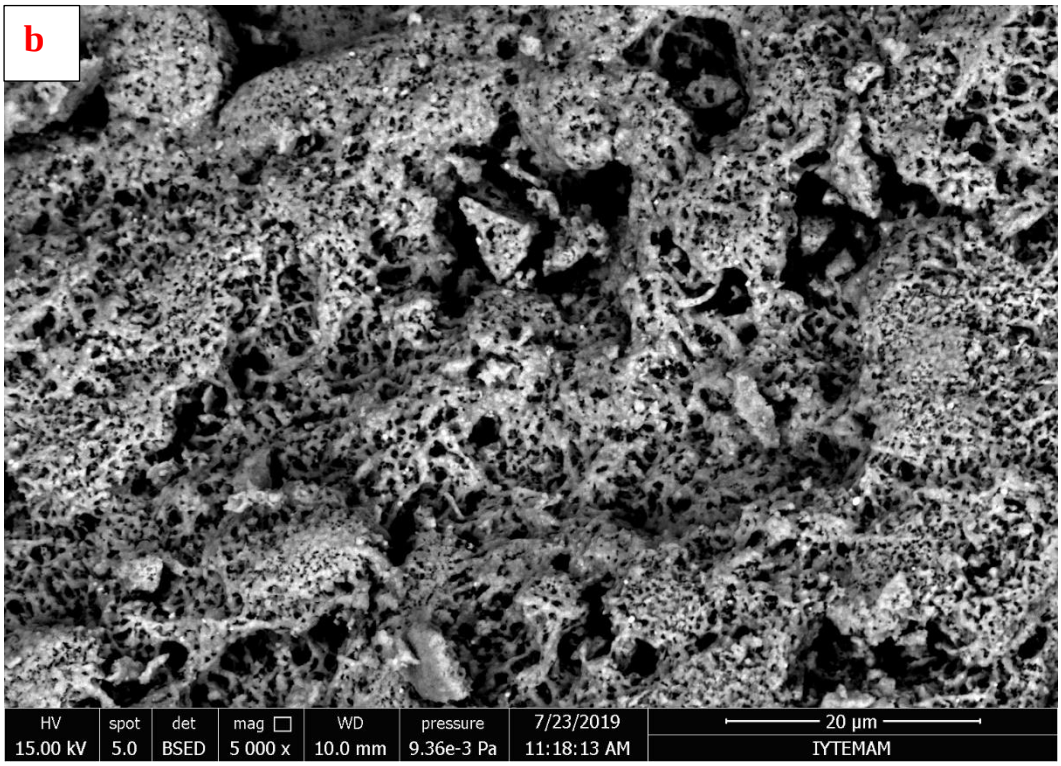

Figure 2.21. SEM images of BSCF-Ag powders obtained by backscattered electron detector at a) 2500x zooming and b) 5000x zooming.

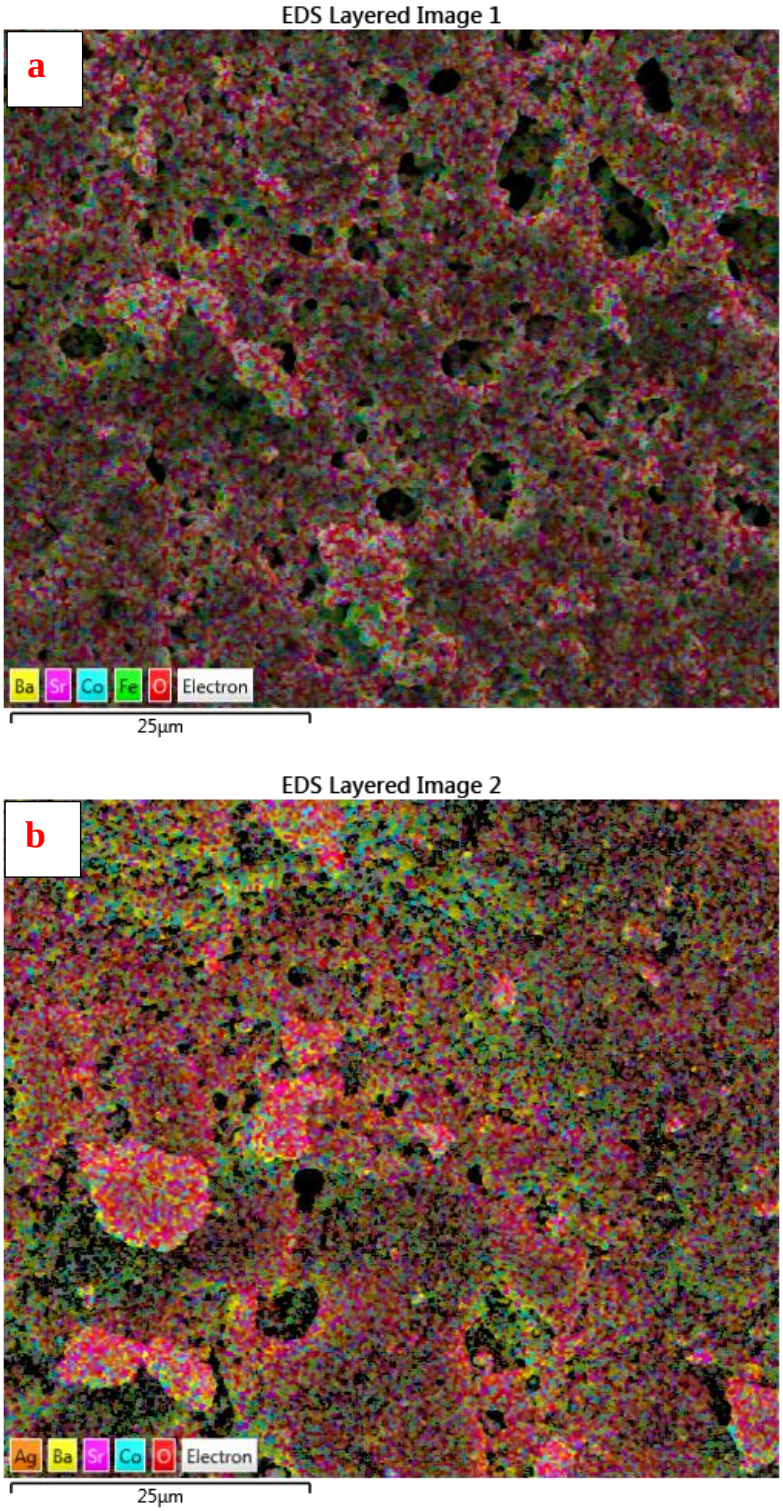

Figure 2.22. EDX maps of a) BSCF, b) BSCF-Ag showing the molecular level homogeneity of synthesized powders.

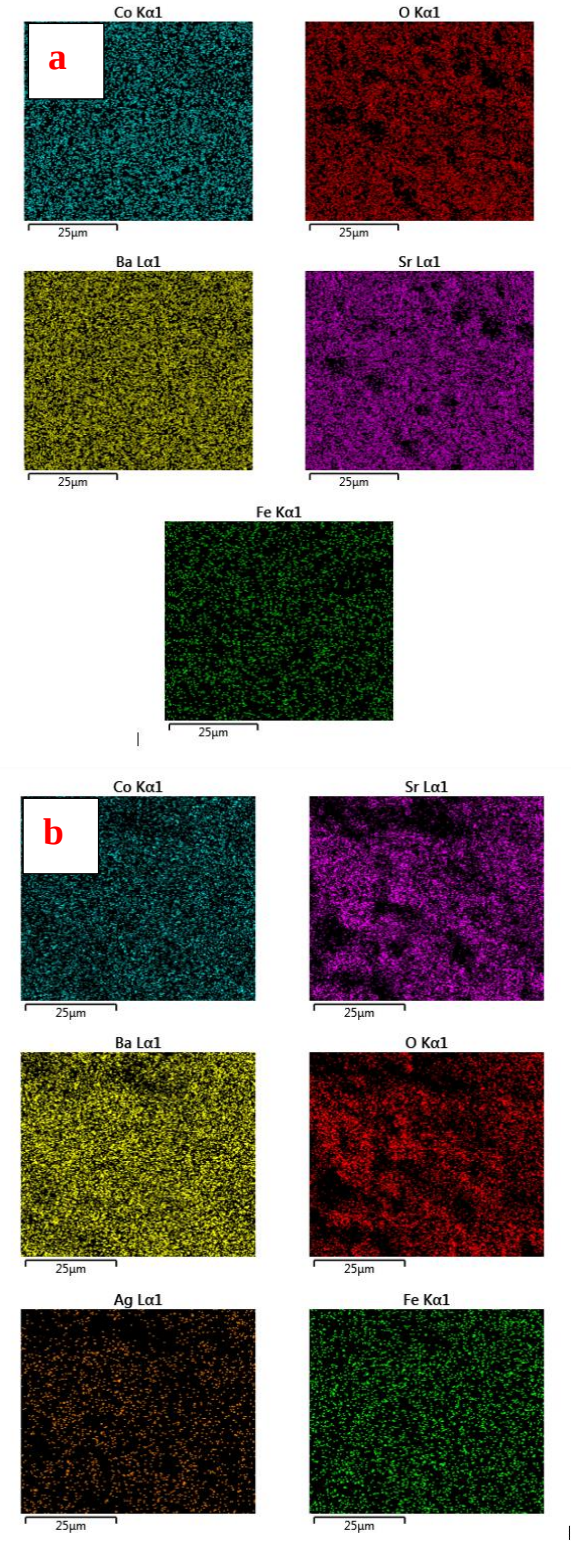

Figure 2.23. Distribution map of Ba, Sr, Co, Fe and Ag atoms of a)BSCF b) BSCF-Ag perovskite powders.

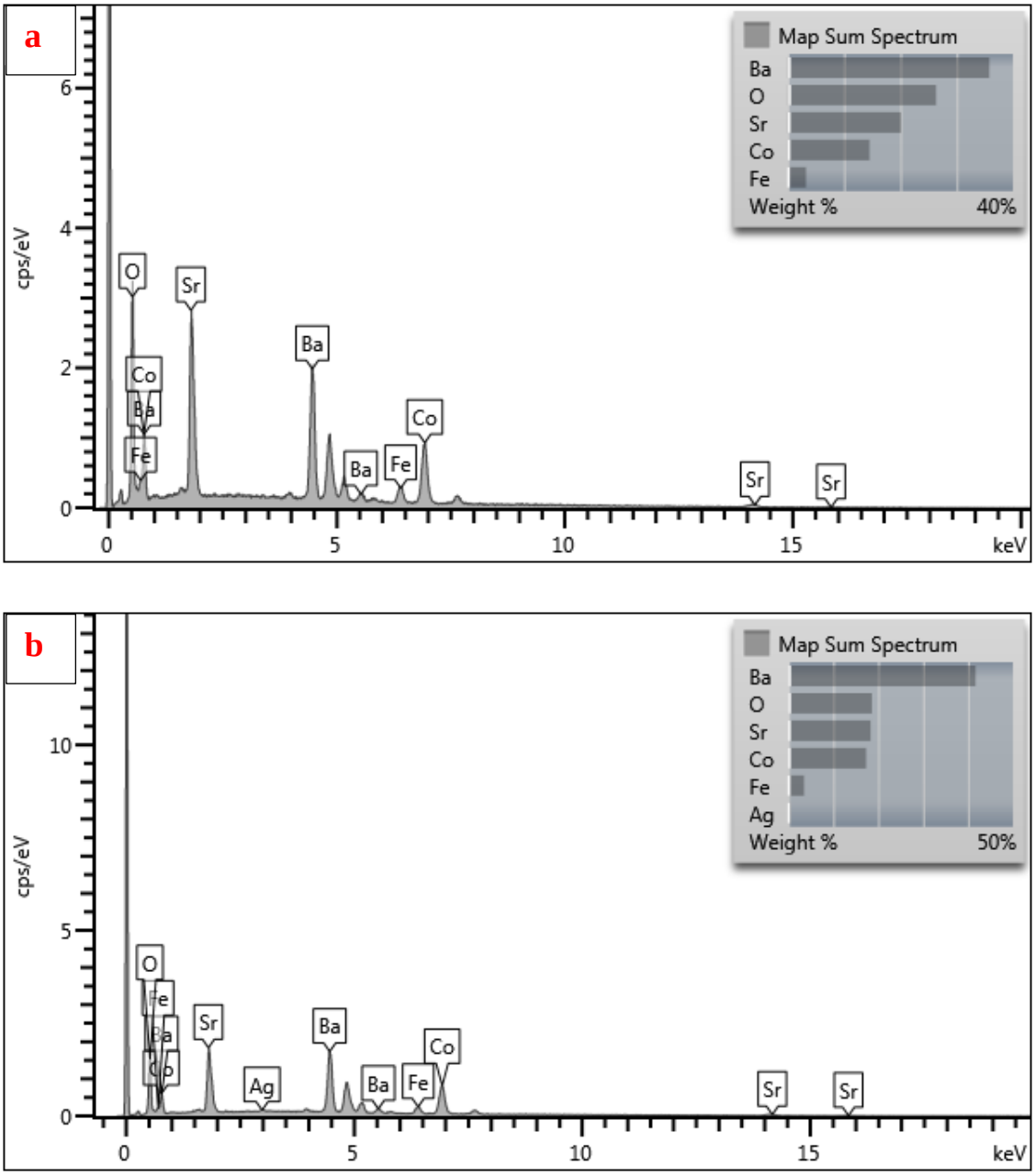

Figure 2.24. EDX map spectrum analysis of a) BSCF b) BSCF-Ag.

2.3.2.2. X-Ray Crystallography and Rietveld Analysis

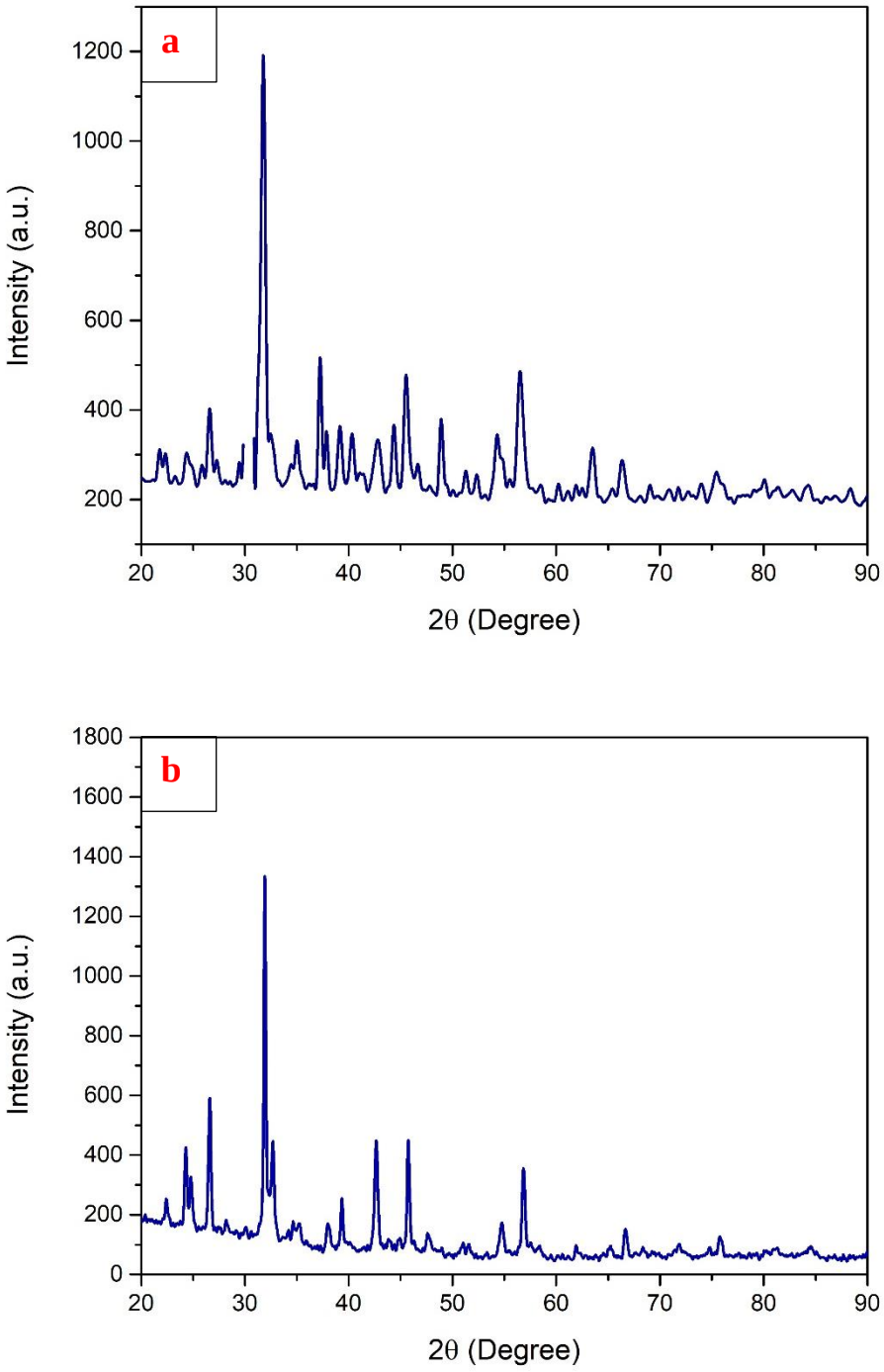

Figure 2.25. XRD graphs showing main peaks of a)BSCF at 31.74 and b) BSCF-Ag at 31.89.

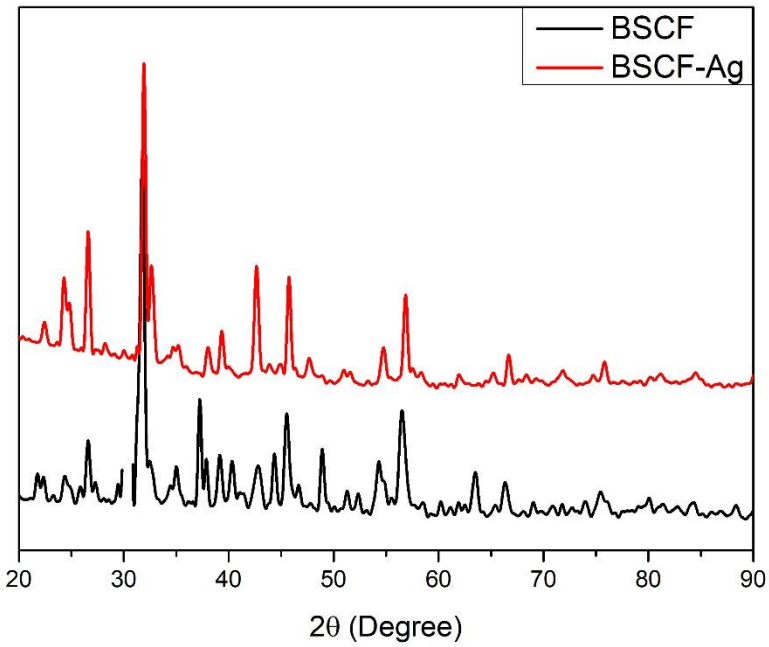

Figure 2.26. XRD peak comparisons of BSCF and BSCF-Ag powders.

Table 2.9. Rietveld refined parameters and reliability factors of perovskites.

Perovskite Type	**Space group**	**Lattice parameter**	**X^2**	**R_p (%)**	**R_{wp} (%)**
BSCF	*P*m-3m	a= 3.992	1.978	3.10	5.44
BSCF-Ag	*P*m-3m	a= 3.989	1.434	3.18	4.94

Table 2.9 shows the Rietveld analysis results of BSCF and BSCF-Ag. Rietveld analysis proves the cubic symmetry with Pm-3m space group as intended. Also small lattice parameter decrease was expected from graphical results of XRD analysis and proven with Rietveld analysis also.

2.3.2.3. X-Ray Photoelectron Spectroscopy

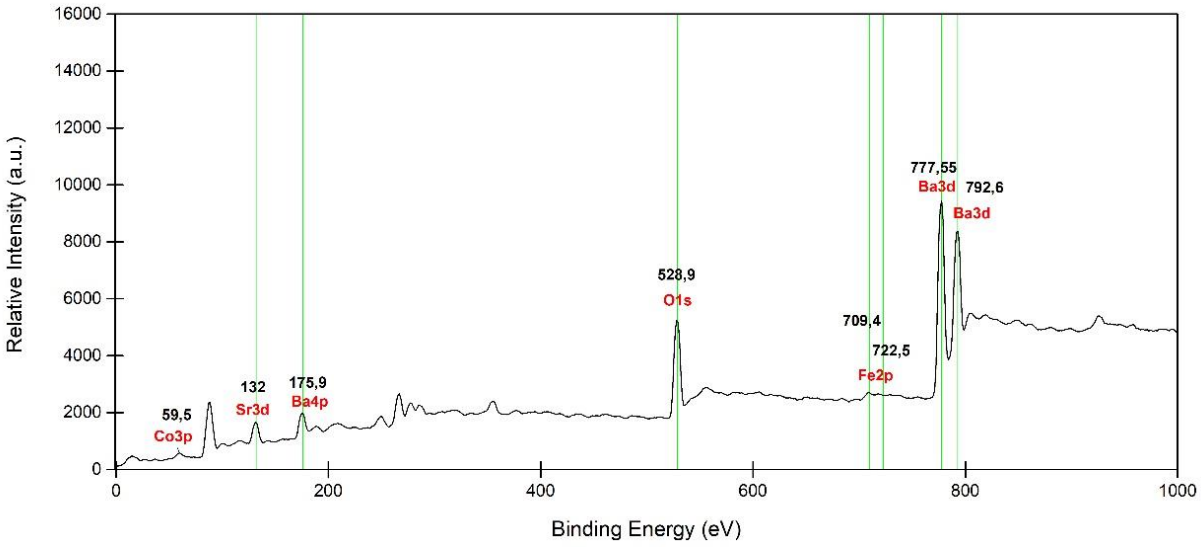

Figure 2.27. XPS graph of BSCF powder showing Ba (4p,3d), Sr (3d), Co (3p), Fe (2p) and O (1s) orbitals characteristic binding energy peaks.

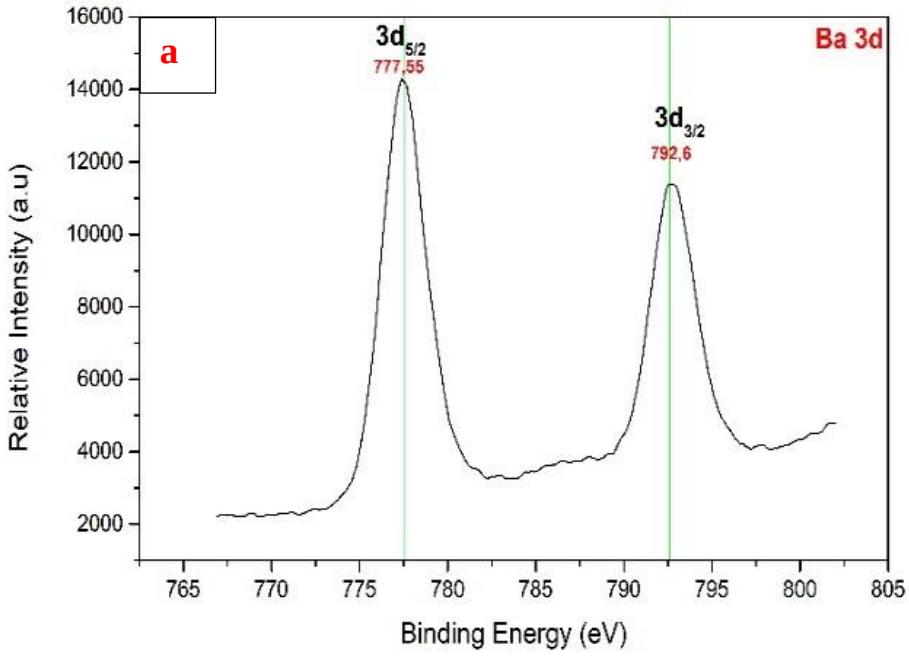

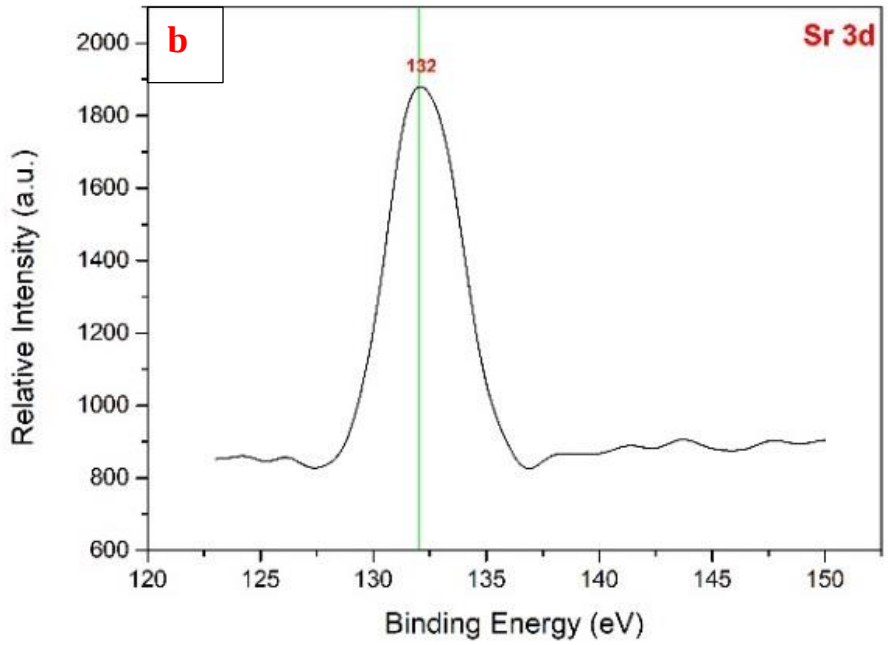
b
Sr 3d
132
Relative Intensity (a.u.)
Binding Energy (eV)
2000
1800
1600
1400
1200
1000
800
600
120
125
130
135
140
145
150

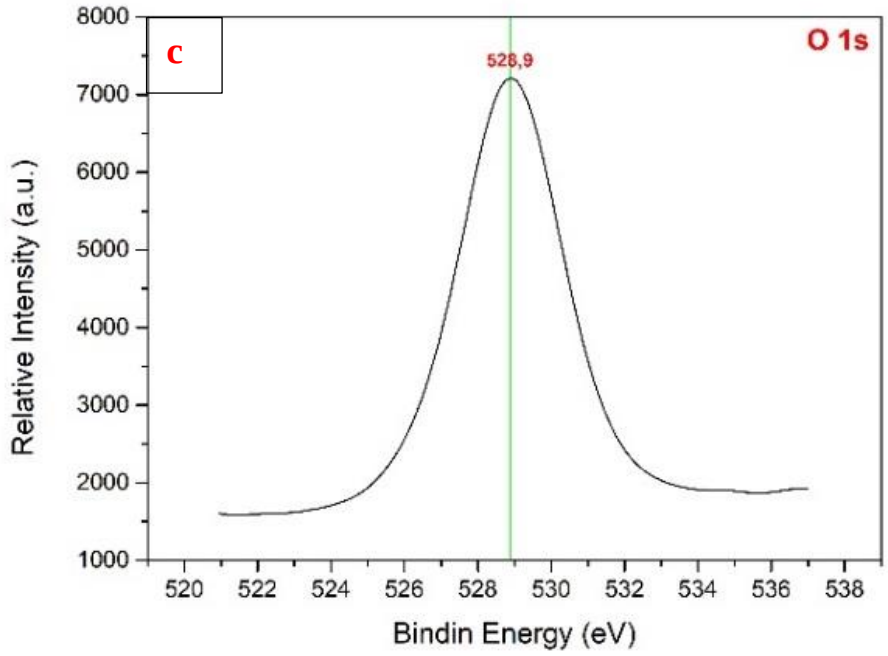
c
O 1s
528,9
Relative Intensity (a.u.)
Bindin Energy (eV)
8000
7000
6000
5000
4000
3000
2000
1000
520
522
524
526
528
530
532
534
536
538

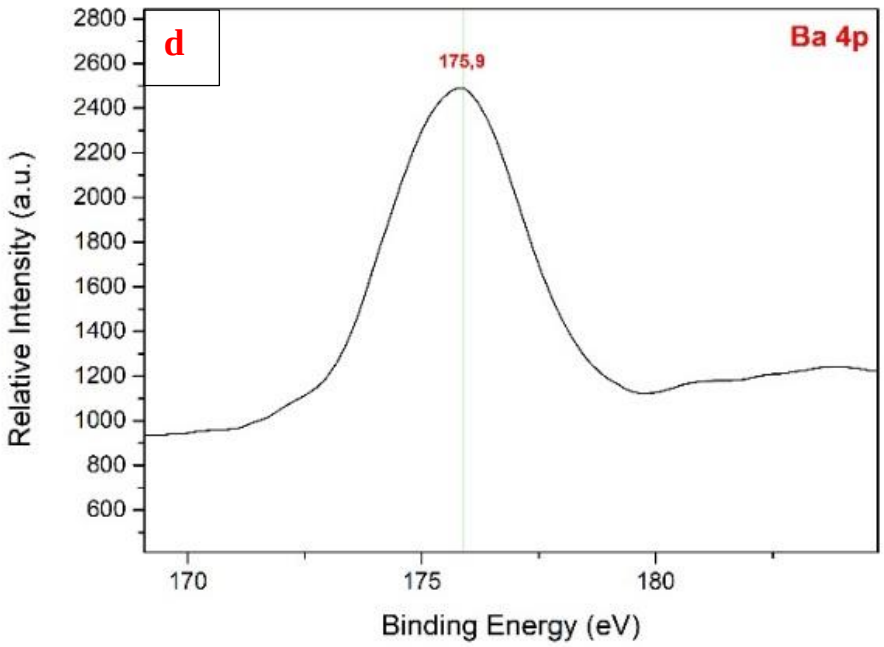
d
Ba 4p
175,9
Relative Intensity (a.u.)
Binding Energy (eV)
2800
2600
2400
2200
2000
1800
1600
1400
1200
1000
800
600
170
175
180

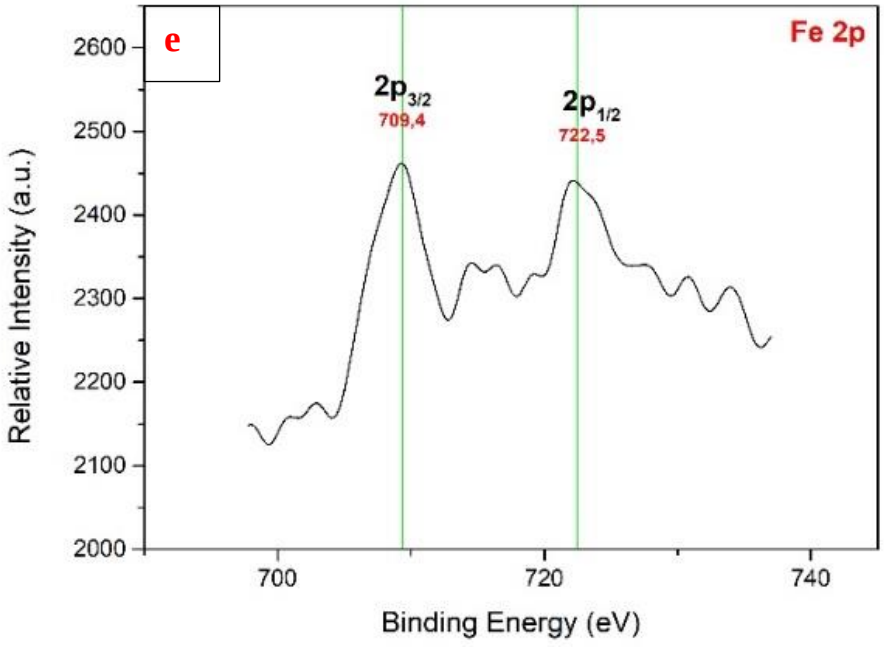
e
Fe 2p
2p3/2
709,4
2p1/2
722,5
Relative Intensity (a.u.)
Binding Energy (eV)
2600
2500
2400
2300
2200
2100
2000
700
720
740

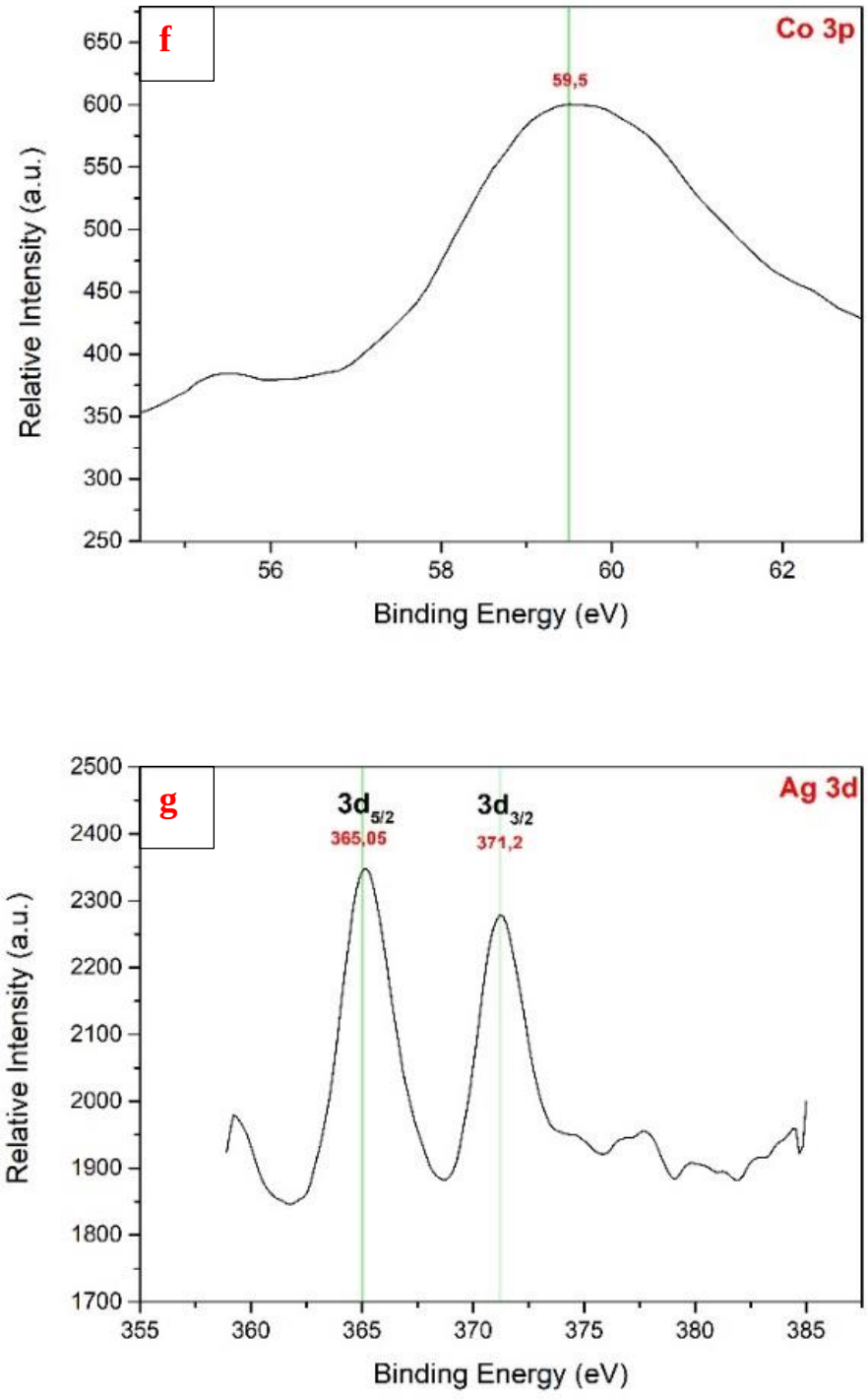

Figure 2.28. XPS graphs showing the characteristic peaks of existing electronic states of a) Ba – 3d, b) Sr – 3d, c) O – 1s d) Ba – 4p e) Fe – 2p, f) Co – 3p, g) Ag – 3d in the crystal structure .

2.3.2.4. Brunauer Emmett Teller Analysis

Table 2.10. BET Analysis results of BSCF and BSCF-Ag.

Perovskite Type	Surface Area (m^2/g)	Pore Size (Å)	Pore Volume (cm^3/g)
BSCF	1,07	186,08	0,005
BSCF-Ag	2,48	126,90	0,008

Table 2.10., shows the results of BET analysis. According to BET data, Ag increases the surface area approximately 2 times. Although Ag doping decreases the pore size, pore volume is increases slightly.

2.3.3. Electrochemical Characterization

Cyclic voltammetry and chronoamperometry measurements were carried out by using the Metro ohm PG-208 instrument. Ag/AgCl electrode was used as a reference electrode and Pt mesh was used as a counter electrode. Cyclic voltammetry and chronoamperometry measurements were both done in 1 M KOH solution. Chronoamperometry measurements were done at 1.6 V for 5 h. Cyclic voltammetry measurements were done between 1 – 1,8 V. All voltage values was normalized according to pH of 1 M KOH (pH = 14 at 25 °C)

2.3.3.1. Ink Preparation from Synthesized Perovskite Oxide Powders

Ink solutions were prepared by mixing 10 mg of BSCF powders with 100 µl of nafion and 1 ml of ethanol and 10 mg of carbon black for OER measurements of BSCF and BSCF-Ag powders. Both perovskite powders were prepared as inks in the same formulation.

2.3.3.2. Coating and Preparation of Electrodes

Perovskite powders were coated on Ni foam by Firstly, Ni foams were prepared in dimensions of 1x5 cm. Then, dispersed catalyst ink was coated on to Ni surface by drop coating with a loading of ~ 232 µg/cm^2.

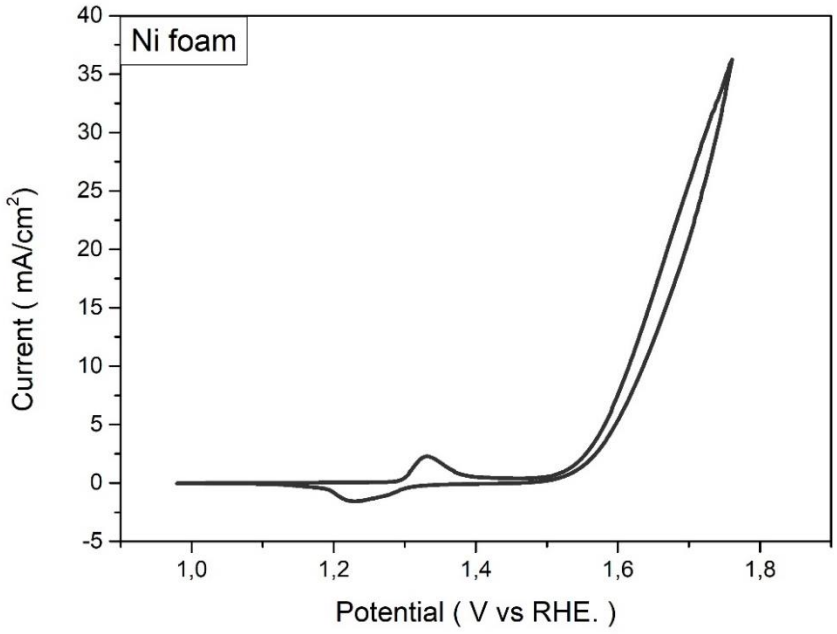

Figure 2.29. Un-coated Ni foam CV graph showing maximum current density of 35 mA/cm^2.

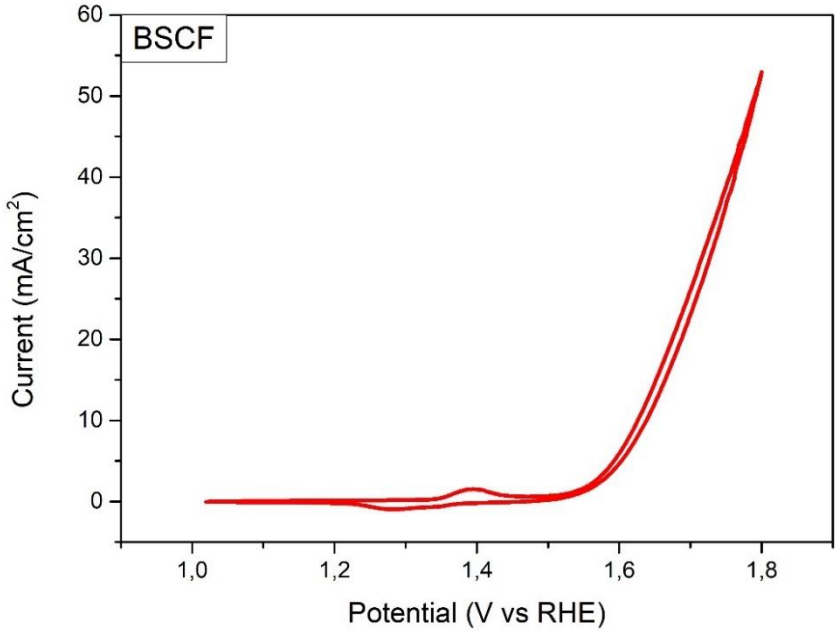

Figure 2.30. CV of BSCF coated on Ni foam between 1 - 1,8 V. Showing Maximum current density of 53 mA/cm^2.

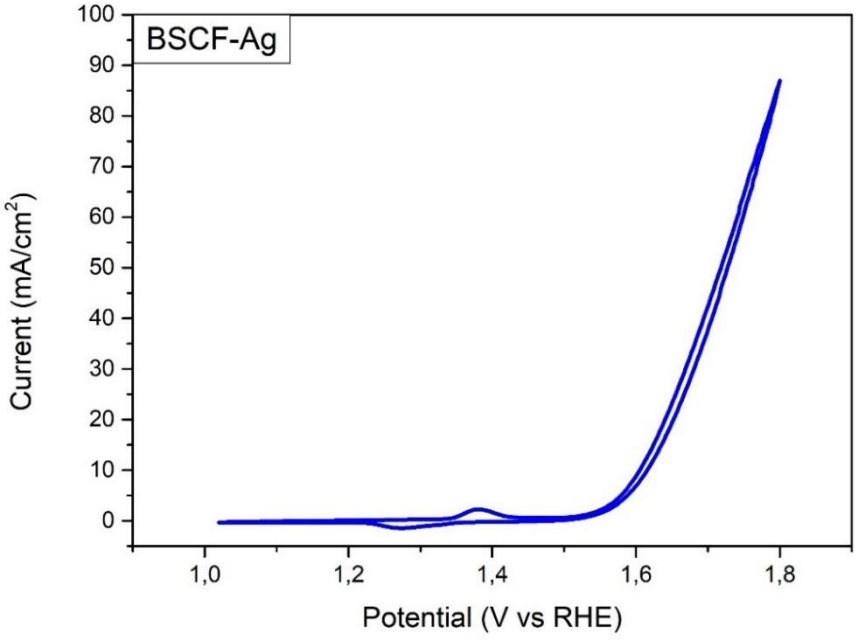

Figure 2.31. CV of BSCF-Ag coated on Ni foam between 1 - 1,8 V. Showing Maximum current density of 87 mA/cm^2.

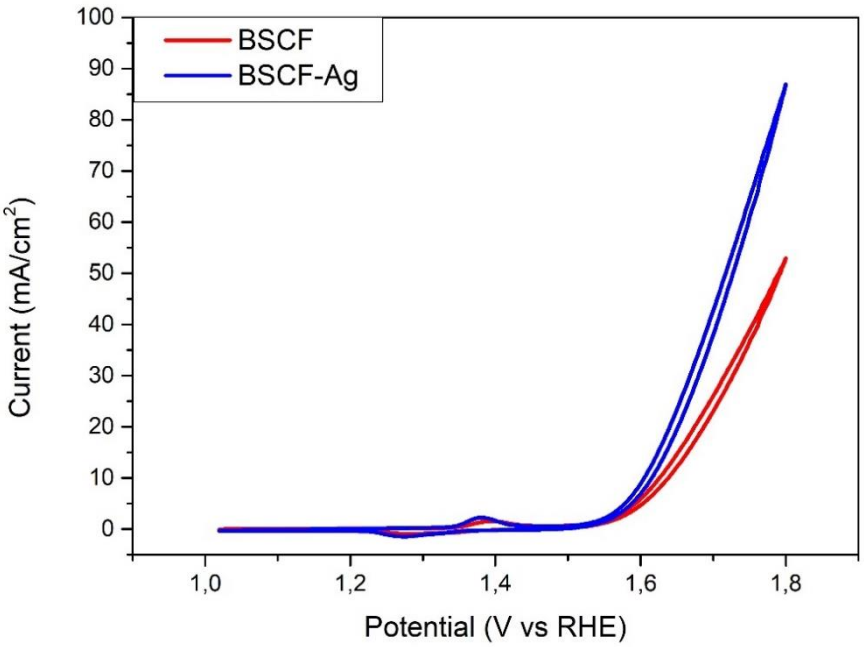

Figure 2.32. CV comparisons of pure BSCF and BSCF-Ag between 1 - 1,8 V. Showing onset potential for BSCF-Ag is smaller.

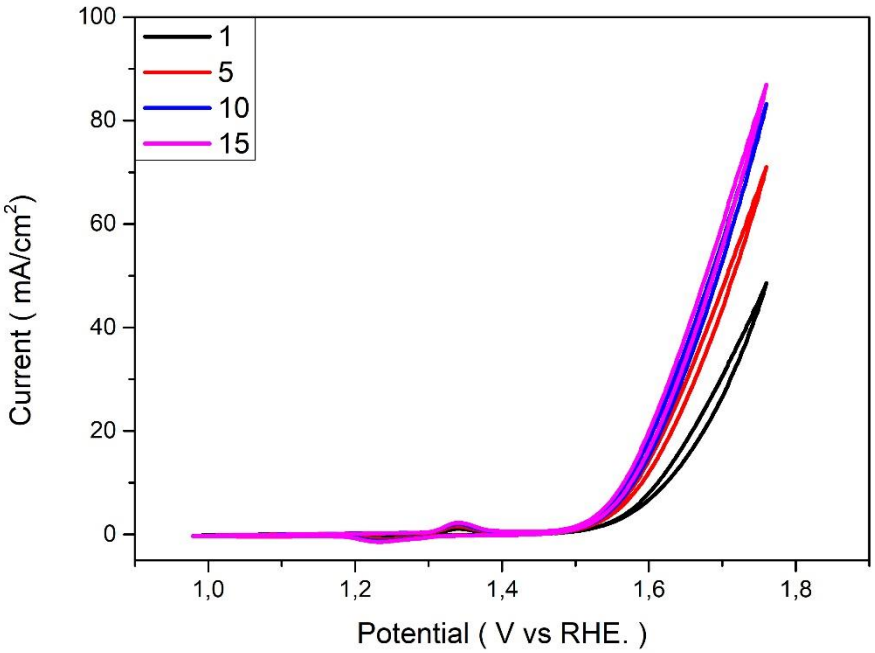

Figure 2.33. CV graph of BSCF-Ag coated on Ni foam between 1 - 1,8 V. Showing the effect of cycling times on the catalytic activity. 15th cycle shows better current densities and onset potentials than 1st cycle.

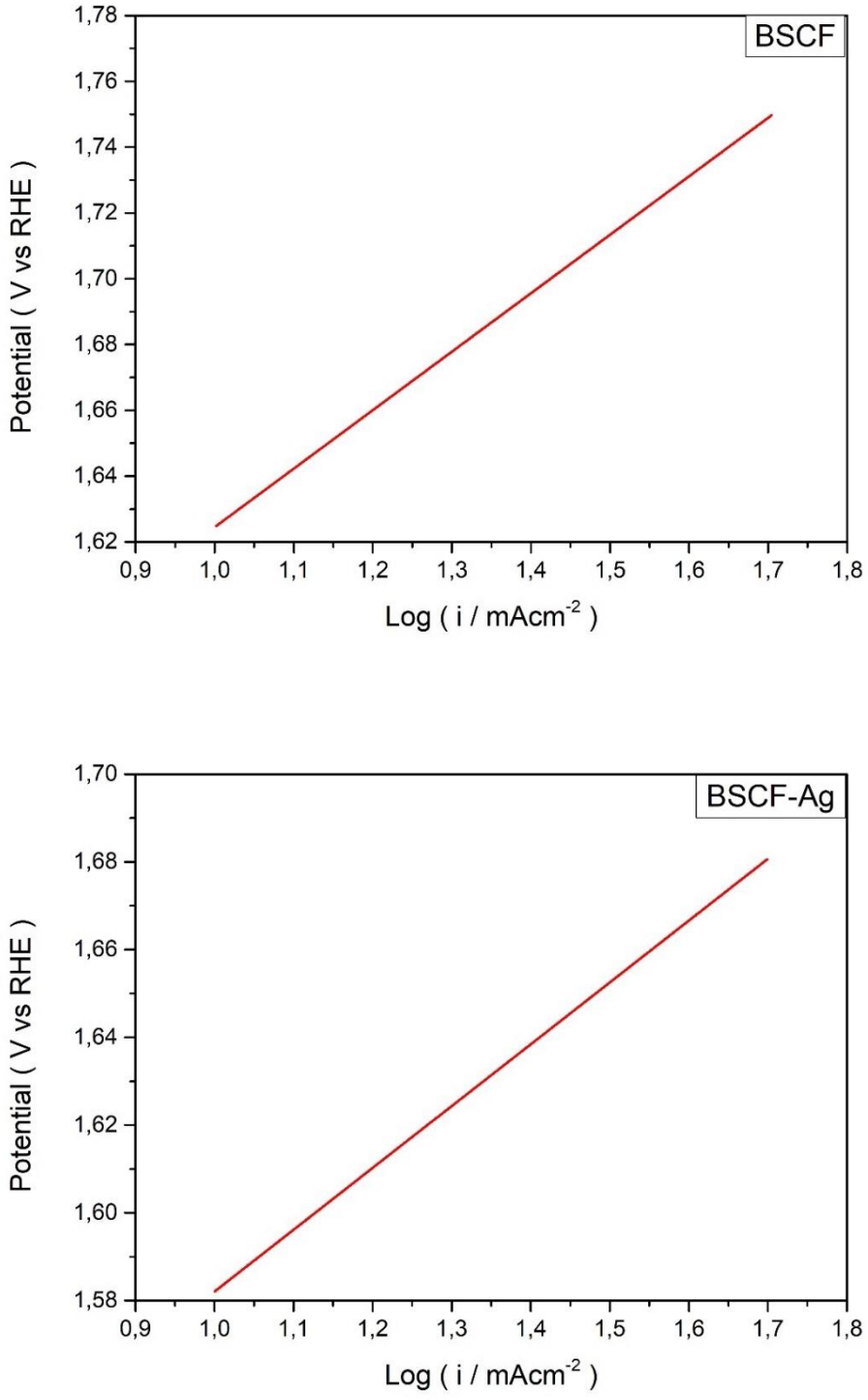

Figure 2.34. Tafel plots of BSCF and BSCF-Ag showing onset potential differences between 1 - 10 mA/cm^2.

Tablo 2.11. Tafel slopes and overpotentials of BSCf and BSCF-Ag for OER.

Perovskite Type	Tafel Slope (mV/dec)	Overpotential (mV)
BSCF	178	400
BSCF - Ag	141	350

Table 2.11. shows the results obtained from Tafel plots. From the Tafel plots, Tafel slopes and overpotentials were calculated. According to the table, BSCF-Ag decreases both Tafel slope and overpotentials of pure BSCF. Decreases in Tafel slopes and overpotentials indicate that BSCF-Ag structure is both thermodynamically and kinetically more favorable for oxygen evolution reactions.

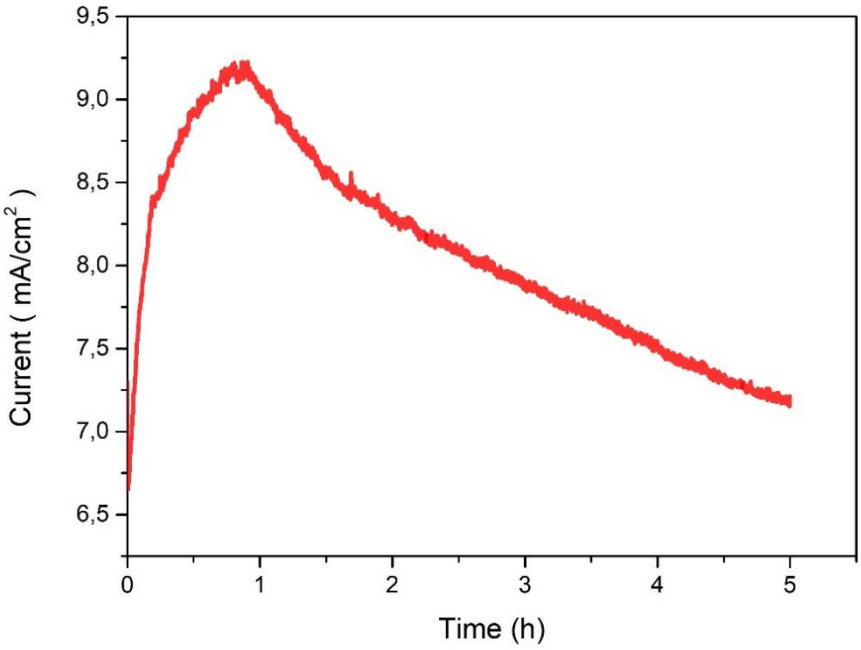

Figure 2.35. Chronoamperometry of pure BSCF coated on Ni foam at 1,6 V (corresponding to 10 mA) for 5 hours. showing an important decrease in the current density after 1,5 h.

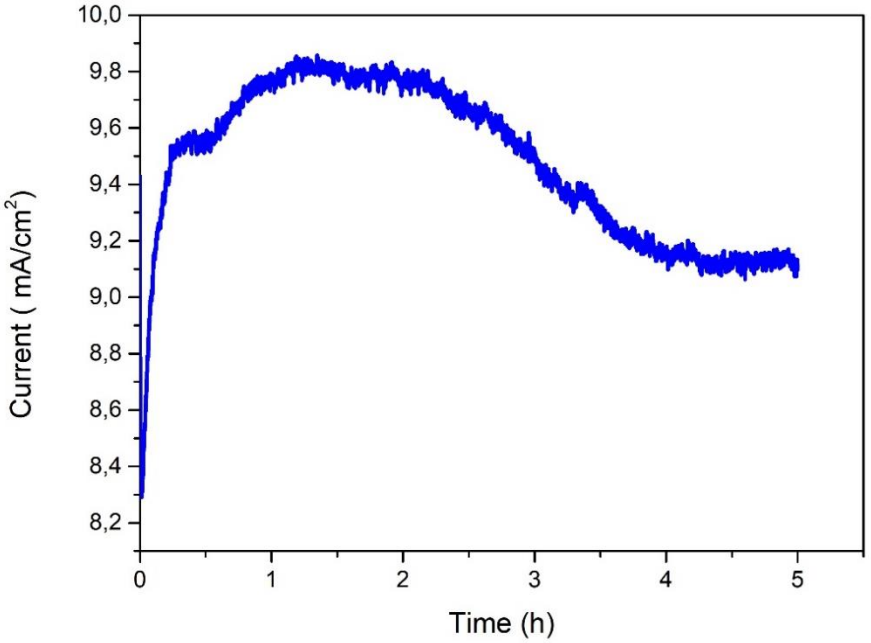

Figure 2.36. Chronoamperometry of BSCF-Ag coated on Ni foam at 1,6 V (corresponding to 10 mA) in 1 M KOH for 5 hours.

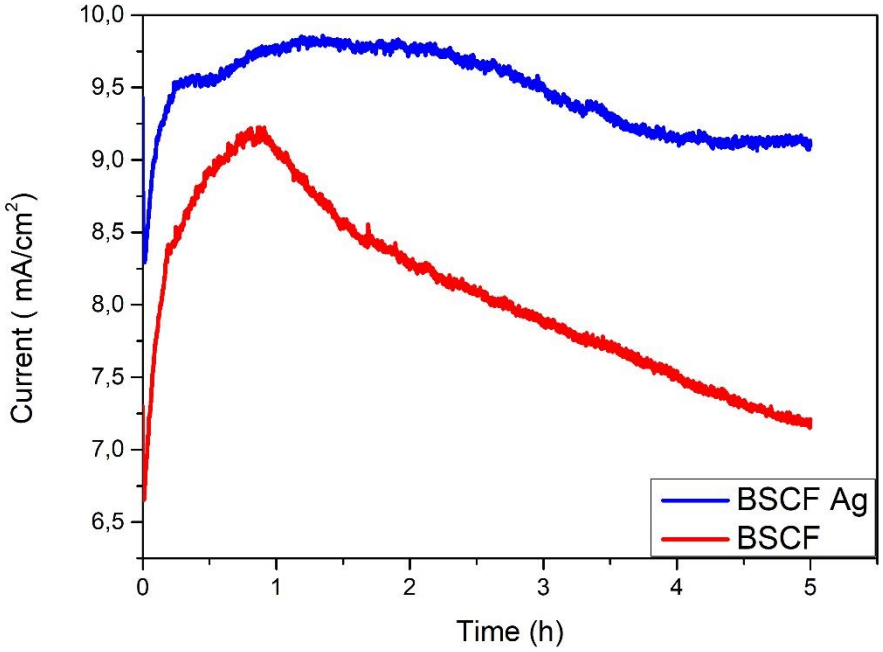

Figure 2.37. Stability comparison of BSCF and BSCF-Ag according to chronoamperometry measurements at 1,6 V in 1M KOH for 5 hours.

2.3.4. Results and Discussion

In this chapter of the study, OER activities of two perovskites was compared. BSCF was doped with Ag to increase its stability and catalytic activity towards OER.

BSCF and BSCF-Ag powders were synthesized by the EDTA-Citrate method. For the characterization of synthesized catalysts; XRD, BET, XPS, SEM and EDX methods were used. XPS graphs show the oxidation states of the metals in the BSCF and BSCF-Ag. In the XPS Ag 3d characteristic peaks observed. According to XPS results, we can conclude that Ag is present in the BSCF structure XRD data also prove the single phase of crystal structures of BSCF and BSCF Ag. Also, it proves the presence of Ag within the BSCF structure.

According to XRD data, the cell volume of BSCF is 635 A^3 and the cell volume of BSCF-Ag is 860 A^3. An increase in the cell volume shows that Ag is included in the crystal. As surface area increases, catalytic activity increases since the working sites are more in touch with the electrolyte. In Fig. 2.26 shows the XRD patterns of BSCF and BSCF- Ag, main peaks show a slight shift from 31.75 to 31.89 when Ag is added in the structure. This shift indicates a decrease in the lattice parameter. From the Rietveld refinement results, the lattice parameter for BSCF is a = 3,992 and for BSCF- Ag a= 3.989 which is consistent with the XRD data. Also, this shift can be caused by the increase in stress caused by addition of high radius element to structure. According to the Scherrer equation, crystallite size of BSCF-Ag is 64.52 nm. This small change in the lattice parameter can be due to change of Co oxidation state. Lattice parameters of synthesized BSCF and BSCF-Ag powders are consistent with previous literature works. [34]

SEM and EDX images were done to determine the surface morphology and homogeneity of BSCD and BSCF-Ag. SEM and EDX analysis show that Ag doping increases the surface are and both perovskite oxides are prepared by homogeneity at atomic level. Also, EDX map spectrums shows Ba, Sr, Co and Fe atoms present is intended percentages as well as Ag doping for BSCF-Ag.

According to BET results, Ag doping increases the surface area of BSCF from m^2/g to 2,48 m^2/g. Although pore volume decreased from 186,08 to 126,90 Å, pore volume increased slightly from 0,005 to 0,008 cm^3/g.

Firstly, Uncoated Ni foam was tested electrochemically by CV from 1 to 1,8 V in 1 M KOH and showed 35 mA/cm^2 current density at 1,8 V. Then two synthesized perovskites were compared by same methods. According to Fig. 2.30 BSCF shows 52 mA/cm^2 at 1,8 V and its onset potential is 1,53 V. Ag doping of BSCF was compared to pure BSCF in the Fig. 2.32 and it is clearly observed that the current density of BSCF was increased from 52 to 87 mA/cm^2. Since all other parameters including synthesis method, calcination time and electrode preparation method was kept same for the study, this increase is due to Ag addition to structure. Tafel plotes were prepared from LSV data to obtain Tafel slope and overpotential values of BSCF and BSCF-Ag for OER. LSV were also measured between 1 – 1,8 V in 1M KOH by three electrode system. According to the Tafel plots, pure BSCF has Tafel slope of 178 mV/dec and its overpotential is 400 mV at 10 mA. BSCF-Ag has Tafel slope of 141 mV/dec and 350 mV overpotential at 10 mA. Both overpotentials were calculated according to 1,23 V which is required for water splitting to oxygen. For OER studies, it is proven that Ag doping increases both thermodynamic and kinetic characteristics of pure BSCF by decreasing Tafel slope and overpotentials. According to the study, BSCF-Ag is a promising candidate as a OER catalyst.

For the stability measurements of synthesized perovskites, chronoamperometry was used. Chronoamperometry measurements were taken at 1,6 V which corresponds to 10 mA/cm^2 (Current density which must be achieved for solar to hydrogen efficiency of %10) in 1 M KOH. Since all measurements were taken in alkaline media, potentials were normalized to pH of electrolyte. In the chronoamperometry measurements shown in the Fig. 2.37, it is observed that the Ag doping also increased the stability of BSCF. Fig. 2.37 shows that BSCF-Ag stays stable at 9,8 V for 4 hours and after 4th hours its stability decreases for 6 %. Fig. 39 shows the stability test performed for pure BSCF for 5 hours at 1,6 V and from the data it can be calculated that the stability decreases 25 % after 1st hour of the measurement.

2.3.5. Conclusion

From the bulk and surface characterizations, it is proved that BSCF and BSCF-Ag was successfully synthesized by Sol-Gel synthesis. Also, atomic level homogeneity is achieved by maintaining the cubic crystal structure. In all electrochemical characterization tests including cyclic voltammetry and chronoamperometry for oxygen evolution reaction, Ag doping proved to be increased the stability and catalytic activity of BSCF perovskite. Although the stability of BSCF dropped dramatically after 1st hour, BSCF-Ag achieved to held high stability for longer hours. Also, from CV graphs, it is calculated that the current density achieved at the same voltages is almost doubled. This result show that BSCF-Ag can be an efficient candidate for OER applications.

CHAPTER 3

OVERALL CONCLUSION

In this study, the effect of various water-splitting catalysts was investigated for both oxygen and hydrogen evolution reactions. There are two main research subjects investigated, firstly HER activities of transition metal doped BSCF structures were investigated and secondly, OER activity of Ag doped BSCF was investigated.

For experimental part of this study combination of several transition metals with alkaline earth metals were investigated. Especially ABO3 type perovskites were the subject of this study. All perovskites studied synthesized by the Sol-Gel Method. BaSrCoFe being the starting perovskite, several dopants including Ag, Mn, Cu, and Zn were introduced to increase its electrochemical efficiency and stability. For the experimental research, surface, bulk, and electrochemical characterizations were performed. All the surface and bulk characterization tests were done on powder form of perovskites. X-Ray Diffraction Crystallography and Rietveld analysis were used to determine the crystal structure while X-Ray Photoelectron Spectroscopy was used to determine the elemental composition, electronic state, and binding energies of elements of the perovskites. Scanning Electron Microscope and Energy Dispersive X-Ray Spectroscopy were used to analyze the surface morphologies and composition, and Brauner-Emmet-Teller analysis was used to determine the surface areas and pore sizes of synthesized perovskites.

For the electrochemical characterizations; ink of BSCF perovskites was prepared by the same manners. Ni foam were used as substrates for the electrochemical analysis of perovskites. For the coating of Ni foam, drop coating was used. All electrochemical measurements were done in alkaline media at fixed pH and room temperature with a three-electrode configuration. Both hydrogen evolution and oxygen evolution reaction characteristics were investigated for different synthesized perovskites. As starting perovskite BSCF was chosen for its remarkable electrochemical activity for both HER and OER. For the HER investigations, transition metals with known cost efficiencies and good electrochemical activities were chosen as dopants. Copper, Manganese, and Zinc

were added to the BSCF structure to enhance its HER performance and stability. A comparison of the catalytic effects of dopants was done by their overpotentials. According to the cyclic voltammetry, linear sweep voltammetry, and chronopotentiometry analysis, BSCF-Cu showed better thermodynamic characteristics with lower overpotentials where BSCF-Mn showed faster kinetic rates with smaller Tafel slopes among all perovskite oxides synthesized.

Silver is used as a doping material for the enhancement of OER performance and stability of BSCF since it is known to provide lower overpotentials as a dopant. Cyclic voltammetry and chronoamperometry were used for the electrochemical characteristics of BSCF-Ag on Ni foam substrate. With the addition of Ag to BSCF structure, it is observed that the Tafel slopes and overpotentials decreased compared to pure BSCF. According to electrochemical tests, it is proven that BSCF-Ag is both kinetically and thermodynamically a better candidate than pure BSCF as OER catalyst.

REFERENCES

(1) Roulet, N. T. Peatlands, Carbon Storage, Greenhouse Gases, and the Kyoto Protocol: Prospects and Significance for Canada. *Wetl. 2000 204* **2000**, *20* (4), 605–615. https://doi.org/10.1672/0277-5212(2000)020[0605:PCSGGA]2.0.CO;2.

(2) International Energy Agency. World Energy Outlook-2017. **2017**.

(3) Statistical Review. *BP Stat. Rewiev World Energy* **2019**, *68*. https://doi.org/10.1001/jama.1973.03220300055017.

(4) Sivula, K.; Van De Krol, R. Semiconducting Materials for Photoelectrochemical Energy Conversion. *Nat. Rev. Mater.* **2016**, *1* (2). https://doi.org/10.1038/natrevmats.2015.10.

(5) Finnveden, G.; Nilsson, M.; Johansson, J.; Persson, Å.; Moberg, Å.; Carlsson, T. Strategic Environmental Assessment Methodologies - Applications within the Energy Sector. *Environ. Impact Assess. Rev.* **2003**. https://doi.org/10.1016/S0195-9255(02)00089-6.

(6) Giménez, S.; Bisquert, J. *Photoelectrochemical Solar Fuel Production: From Basic Principles to Advanced Devices*; 2016. https://doi.org/10.1007/978-3-319-29641-8.

(7) Baur, E.; Rebmann, A. Über Versuche Zur Photolyse Des Wassers. *Helv. Chim. Acta* **1921**, *4* (1), 256–262. https://doi.org/10.1002/hlca.19210040124.

(8) Kudo, A.; Miseki, Y. Heterogeneous Photocatalyst Materials for Water Splitting. *Chem. Soc. Rev.* **2009**, *38* (1), 253–278. https://doi.org/10.1039/b800489g.

(9) Chen, C.; Ma, W.; Zhao, J. Semiconductor-Mediated Photodegradation of Pollutants under Visible-Light Irradiation. *Chem. Soc. Rev.* **2010**, *39* (11), 4206–4219. https://doi.org/10.1039/b921692h.

(10) Murphy, A. B.; Barnes, P. R. F.; Randeniya, L. K.; Plumb, I. C.; Grey, I. E.; Horne, M. D.; Glasscock, J. A. Efficiency of Solar Water Splitting Using Semiconductor Electrodes. *Int. J. Hydrogen Energy* **2006**, *31* (14), 1999–2017.

https://doi.org/10.1016/j.ijhydene.2006.01.014.

(11) Lewis, N. S.; Crabtree, G.; Nozik, A. J.; Wasielewski, M. R.; Alivisatos, P.; Kung, H.; Tsao, J.; Chandler, E.; Walukiewicz, W.; Spitler, M.; Ellingson, R.; Overend, R.; Mazer, J.; Gress, M.; Horwitz, J.; Ashton, C.; Herndon, B.; Shapard, L.; Nault, R. M. *Basic Research Needs for Solar Energy Utilization. Report of the Basic Energy Sciences Workshop on Solar Energy Utilization, April 18-21, 2005*; 2005. https://doi.org/10.2172/899136.

(12) Soriano-López, J.; Schmitt, W.; García-Melchor, M. Computational Modelling of Water Oxidation Catalysts. *Current Opinion in Electrochemistry*. Elsevier B.V. January 1, 2018, pp 22–30. https://doi.org/10.1016/j.coelec.2017.10.001.

(13) McCrory, C. C. L.; Jung, S.; Ferrer, I. M.; Chatman, S. M.; Peters, J. C.; Jaramillo, T. F. Benchmarking Hydrogen Evolving Reaction and Oxygen Evolving Reaction Electrocatalysts for Solar Water Splitting Devices. *J. Am. Chem. Soc.* **2015**, *137* (13), 4347–4357. https://doi.org/10.1021/ja510442p.

(14) Subbaraman, R.; Tripkovic, D.; Strmcnik, D.; Chang, K. C.; Uchimura, M.; Paulikas, A. P.; Stamenkovic, V.; Markovic, N. M. Enhancing Hydrogen Evolution Activity in Water Splitting by Tailoring Li+-Ni(OH)2-Pt Interfaces. *Science (80-.).* **2011**, *334* (6060), 1256–1260. https://doi.org/10.1126/science.1211934.

(15) Elbert, K.; Hu, J.; Ma, Z.; Zhang, Y.; Chen, G.; An, W.; Liu, P.; Isaacs, H. S.; Adzic, R. R.; Wang, J. X. Elucidating Hydrogen Oxidation/Evolution Kinetics in Base and Acid by Enhanced Activities at the Optimized Pt Shell Thickness on the Ru Core. *ACS Catal.* **2015**, *5* (11), 6764–6772. https://doi.org/10.1021/acscatal.5b01670.

(16) Strmcnik, D.; Uchimura, M.; Wang, C.; Subbaraman, R.; Danilovic, N.; Van Der Vliet, D.; Paulikas, A. P.; Stamenkovic, V. R.; Markovic, N. M. Improving the Hydrogen Oxidation Reaction Rate by Promotion of Hydroxyl Adsorption. *Nat. Chem.* **2013**, *5* (4), 300–306. https://doi.org/10.1038/nchem.1574.

(17) Durst, J.; Simon, C.; Hasché, F.; Gasteiger, H. A. Hydrogen Oxidation and Evolution Reaction Kinetics on Carbon Supported Pt, Ir, Rh, and Pd Electrocatalysts in Acidic Media. *J. Electrochem. Soc.* **2015**, *162* (1), F190–F203.

https://doi.org/10.1149/2.0981501jes.

(18) Li, Y. MoS2 Nanoparticles Grown on Graphene: An Advanced Catalyst for the Hydrogen Evolution Reaction. *J. Am. Chem. Soc.* **2011**, *133*, 7296.

(19) BE Conway, L. B. Determination of Adsorption of OPD H Species in the Cathodic Hydrogen Evolution Reaction at Pt in Relation to Electrocatalysis. *J. Electroanal. Chem.* **1986**, *198*, 149.

(20) Hwang, J.; Rao, R. R.; Giordano, L.; Katayama, Y.; Yu, Y.; Shao-Horn, Y. Perovskites in Catalysis and Electrocatalysis. *Science*. American Association for the Advancement of Science November 10, 2017, pp 751–756. https://doi.org/10.1126/science.aam7092.

(21) Xu, X.; Chen, Y.; Zhou, W.; Zhu, Z.; Su, C.; Liu, M.; Shao, Z. A Perovskite Electrocatalyst for Efficient Hydrogen Evolution Reaction. *Adv. Mater.* **2016**, *28* (30), 6442–6448. https://doi.org/10.1002/adma.201600005.

(22) Durst, J.; Siebel, A.; Simon, C.; Hasché, F.; Herranz, J.; Gasteiger, H. A. New Insights into the Electrochemical Hydrogen Oxidation and Evolution Reaction Mechanism. *Energy Environ. Sci.* **2014**. https://doi.org/10.1039/c4ee00440j.

(23) Liu, P. F.; Yin, H.; Fu, H. Q.; Zu, M. Y.; Yang, H. G.; Zhao, H. Activation Strategies of Water-Splitting Electrocatalysts. *J. Mater. Chem. A* **2020**. https://doi.org/10.1039/d0ta01680b.

(24) Reier, T.; Oezaslan, M.; Strasser, P. Electrocatalytic Oxygen Evolution Reaction (OER) on Ru, Ir, and Pt Catalysts: A Comparative Study of Nanoparticles and Bulk Materials. *ACS Catal.* **2012**, *2* (8), 1765–1772. https://doi.org/10.1021/cs3003098.

(25) Suntivich, J.; Gasteiger, H. A.; Yabuuchi, N.; Nakanishi, H.; Goodenough, J. B.; Shao-Horn, Y. Design Principles for Oxygen-Reduction Activity on Perovskite Oxide Catalysts for Fuel Cells and Metal-Air Batteries. *Nat. Chem.* **2011**, *3* (7), 546–550. https://doi.org/10.1038/nchem.1069.

(26) Fabbri, E.; Mohamed, R.; Levecque, P.; Conrad, O.; Kötz, R.; Schmidt, T. J. Ba0.5Sr0.5Co0.8Fe0.2O3-δ Perovskite Activity towards the Oxygen Reduction Reaction in Alkaline Media. *ChemElectroChem* **2014**, *1* (2), 338–342.

https://doi.org/10.1002/celc.201300157.

(27) Suntivich, J.; May, K. J.; Gasteiger, H. A.; Goodenough, J. B.; Shao-horn, Y.; Calle-vallejo, F.; Oscar, A. D.; Kolb, M. J.; Koper, M. T. M.; Suntivich, J.; May, K. J.; Gasteiger, H. A.; Goodenough, J. B.; Shao-horn, Y. A Perovskite Oxide Optimized for Molecular Orbital Principles. *Science (80-.).* **2011**, *334* (6061), 2010–2012. https://doi.org/10.1126/science.1212858.

(28) Nassau, K. *Handbook on the Physics and Chemistry of Rare Earths, Vol. 14*; 1993; Vol. 28. https://doi.org/10.1016/0025-5408(93)90088-u.

(29) Shao, Z.; Xiong, G.; Tong, J.; Dong, H.; Yang, W. Ba Effect in Doped Sr(Co0.8Fe0.2)O3-Delta on the Phase Structure and Oxygen Permeation Properties of the Dense Ceramic Membranes. *Sep. Purif. Technol.* **2001**, *25* (1–3), 419–429. https://doi.org/10.1016/S1383-5866(01)00071-5.

(30) Shao, Z.; Halle, S. M. A High-Performance Cathode for the next Generation of Solid-Oxide Fuel Cells. *Nature* **2004**, *431* (7005), 170–173. https://doi.org/10.1038/nature02863.

(31) Chen, Z.; Ran, R.; Zhou, W.; Shao, Z.; Liu, S. Assessment of Ba0.5Sr0.5Co1-YFeyO3-δ (y = 0.0-1.0) for Prospective Application as Cathode for IT-SOFCs or Oxygen Permeating Membrane. *Electrochim. Acta* **2007**, *52* (25), 7343–7351. https://doi.org/10.1016/j.electacta.2007.06.010.

(32) Fisher, C. A. J.; Yoshiya, M.; Iwamoto, Y.; Ishii, J.; Asanuma, M.; Yabuta, K. Oxide Ion Diffusion in Perovskite-Structured Ba1-XSrxCo1-YFeyO2.5: A Molecular Dynamics Study. *Solid State Ionics* **2007**, *177* (39–40), 3425–3431. https://doi.org/10.1016/j.ssi.2006.03.060.

(33) Fabbri, E.; Nachtegaal, M.; Cheng, X.; Schmidt, T. J. Superior Bifunctional Electrocatalytic Activity of $Ba_{0.5}Sr_{0.5}Co_{0.8}Fe_{0.2}O_{3-\delta}$ /Carbon Composite Electrodes: Insight into the Local Electronic Structure. *Adv. Energy Mater.* **2015**, *5* (17), 1402033. https://doi.org/10.1002/aenm.201402033.

(34) Cheng, X.; Fabbri, E.; Kim, B.; Nachtegaal, M.; Schmidt, T. J. Effect of Ball Milling on the Electrocatalytic Activity of Ba0.5Sr0.5Co0.8Fe0.2O3 towards the

Oxygen Evolution Reaction. *J. Mater. Chem. A* **2017**, *5* (25), 13130–13137. https://doi.org/10.1039/c7ta00794a.

(35) Chen, G.; Zhou, W.; Guan, D.; Sunarso, J.; Zhu, Y.; Hu, X.; Zhang, W.; Shao, Z. Two Orders of Magnitude Enhancement in Oxygen Evolution Reactivity on Amorphous Ba0.5Sr0.5Co0.8Fe0.2O3−d Nanofilms with Tunable Oxidation State. *Sci. Adv.* **2017**, *3* (6). https://doi.org/10.1126/sciadv.1603206.

(36) Li, X.; He, L.; Zhong, X.; Zhang, J.; Luo, S.; Yi, W.; Zhang, L.; Hu, M.; Tang, J.; Zhou, X.; Zhao, X.; Xu, B. Evaluation of A-Site Ba2+-Deficient Ba1−xCo0.4Fe0.4Zr0.1Y0.1O3−δ Oxides as Electrocatalysts for Efficient Hydrogen Evolution Reaction. *Scanning* **2018**, *2018*. https://doi.org/10.1155/2018/1341608.

(37) Behrouzifar, A.; Asadi, A. A.; Mohammadi, T.; Pak, A. Experimental Investigation and Mathematical Modeling of Oxygen Permeation through Dense Ba 0.5Sr 0.5Co 0.8Fe 0.2O 3-δ (BSCF) Perovskite-Type Ceramic Membranes. *Ceram. Int.* **2012**, *38* (6), 4797–4811. https://doi.org/10.1016/j.ceramint.2012.02.068.

(38) Kautkar, P. R.; Shirbhate, S. C.; Acharya, S. A. Study on Structural Refinement and Electrochemical Behaviour of Ba0.5Sr0.5Co0.8Fe0.2O3-δ as Cathode Materials for Intermediate Temperature Solid Oxide Fuel Cells (IT-SOFC). *AIP Conf. Proc.* **2018**, *1953*, 8–12. https://doi.org/10.1063/1.5032904.

(39) Hung, I.-M.; Laing, C.-Y.; Ze, Y. Synthesis and Characterization of Ba 0.5 Sr 0.5 Co 0.8 Fe 0.2 O 3-δ for Intermediate Temperature Solid Oxide Fuel Cell Cathode by Solid-State Reaction, Pechini and Citrate-EDTA Complexing Methods. https://doi.org/10.1149/1.3205823.

(40) Heel, A.; Holtappels, P.; Hug, P.; Graule, T. Flame Spray Synthesis of Nanoscale La0.6Sr0.4Co 0.2Fe0.8O3-δ and Ba0.5Sr 0.5Co0.8Fe0.2O3-δ as Cathode Materials for Intermediate Temperature Solid Oxide Fuel Cells. *Fuel Cells* **2010**, *10* (3), 419–432. https://doi.org/10.1002/fuce.200900093.

(41) Fabbri, E.; Nachtegaal, M.; Binninger, T.; Cheng, X.; Kim, B. J.; Durst, J.; Bozza, F.; Graule, T.; Schäublin, R.; Wiles, L.; Pertoso, M.; Danilovic, N.; Ayers, K. E.;

Schmidt, T. J. Dynamic Surface Self-Reconstruction Is the Key of Highly Active Perovskite Nano-Electrocatalysts for Water Splitting. *Nat. Mater.* **2017**, *16* (9), 925–931. https://doi.org/10.1038/nmat4938.

(42) Deganello, F.; Liotta, L. F.; Marcì, G.; Fabbri, E.; Traversa, E. Strontium and Iron-Doped Barium Cobaltite Prepared by Solution Combustion Synthesis: Exploring a Mixed-Fuel Approach for Tailored Intermediate Temperature Solid Oxide Fuel Cell Cathode Materials. *Mater. Renew. Sustain. Energy* **2013**, *2* (1). https://doi.org/10.1007/s40243-013-0008-z.

(43) Liu, B.; Compounds, Y. Z.-J. of A. and; 2008, U. Ba0. 5Sr0. 5Co0. 8Fe0. 2O3 Nanopowders Prepared by Glycine–Nitrate Process for Solid Oxide Fuel Cell Cathode. *Elsevier*.

(44) Tan, L.; Gu, X.; Yang, L.; Jin, W.; Zhang, L.; Xu, N. Influence of Powder Synthesis Methods on Microstructure and Oxygen Permeation Performance of Ba0.5Sr0.5Co0.8Fe0.2O3- δ Perovskite-Type Membranes. *J. Memb. Sci.* **2003**. https://doi.org/10.1016/S0376-7388(02)00494-5.

(45) May, K. J.; Carlton, C. E.; Stoerzinger, K. A.; Risch, M.; Suntivich, J.; Lee, Y. L.; Grimaud, A.; Shao-Horn, Y. Influence of Oxygen Evolution during Water Oxidation on the Surface of Perovskite Oxide Catalysts. *J. Phys. Chem. Lett.* **2012**, *3* (22), 3264–3270. https://doi.org/10.1021/jz301414z.

(46) Esposito, S. "Traditional" Sol-Gel Chemistry as a Powerful Tool for the Preparation of Supported Metal and Metal Oxide Catalysts. *Materials (Basel).* **2019**, *12* (4), 1–25. https://doi.org/10.3390/ma12040668.

(47) Jeans, C. V. M OORE , D. M. & R EYNOLDS , R. C., Jr. 1997. X-Ray Diffraction and the Identification and Analysis of Clay Minerals. *Geol. Mag.* **1998**, *135* (6), 819–842. https://doi.org/10.1017/s0016756898501501.

(48) Mattox, D. M. *Handbook of Physical Vapor Deposition (PVD) Processing*; William Andrew, 2010.

(49) Abd Mutalib, M.; Rahman, M. A.; Othman, M. H. D.; Ismail, A. F.; Jaafar, J. Scanning Electron Microscopy (SEM) and Energy-Dispersive X-Ray (EDX)

Spectroscopy. In *Membrane Characterization*; 2017. https://doi.org/10.1016/B978-0-444-63776-5.00009-7.

(50) Brunauer, S.; Emmett, P. H.; Teller, E. Adsorption of Gases in Multimolecular Layers. *J. Am. Chem. Soc.* **1938**. https://doi.org/10.1021/ja01269a023.

(51) Parker, V. D. Chapter 3 Linear Sweep and Cyclic Voltammetry. *Compr. Chem. Kinet.* **1986**, *26* (C), 145–202. https://doi.org/10.1016/S0069-8040(08)70027-X.

(52) Bond, A. M.; Feldberg, S. W. Analysis of Simulated Reversible Cyclic Voltammetric Responses for a Charged Redox Species in the Absence of Added Electrolyte. *J. Phys. Chem. B* **1998**, *102* (49), 9966–9974. https://doi.org/10.1021/jp9828437.

(53) Wang, W.; Wei, X.; Choi, D.; Lu, X.; Yang, G.; Sun, C. Electrochemical Cells for Medium-and Large-Scale Energy Storage: Fundamentals. In *Advances in Batteries for Medium and Large-Scale Energy Storage: Types and Applications*; Elsevier, 2015; pp 3–28. https://doi.org/10.1016/B978-1-78242-013-2.00001-7.

(54) Kear, G.; Walsh, F. The Characteristics of a True Tafel Slope. *Corros. Mater.* **2005**.

(55) Zhang, X.; Motuzas, J.; Liu, S.; Diniz da Costa, J. C. Zinc-Doped BSCF Perovskite Membranes for Oxygen Separation. *Sep. Purif. Technol.* **2017**. https://doi.org/10.1016/j.seppur.2017.08.029.

(56) Fabbri, E.; Cheng, X.; Schmidt, T. J. Highly Active Ba0.5Sr0.5Co0.8Fe0.2O3- Single Material Electrode towards the Oxygen Evolution Reaction for Alkaline Water Splitting Applications. *ECS Trans.* **2015**, *69* (17), 869–875. https://doi.org/10.1149/06917.0869ecst.

(57) Bard, A. J.; Faulkner, L. R. Electrochemical Methods Fundamentals and Applications. 2nd Ed. *John Wiley&Sons, New Jersey, USA* **2001**.

(58) Toprak, M. S.; Darab, M.; Syvertsen, G. E.; Muhammed, M. Synthesis of Nanostructured BSCF by Oxalate Co-Precipitation - As Potential Cathode Material for Solid Oxide Fuels Cells. *Int. J. Hydrogen Energy* **2010**, *35* (17), 9448–9454. https://doi.org/10.1016/j.ijhydene.2010.03.121.

(59) Nuernberg, R. B.; Morelli, M. R. Synthesis of BSCF Perovskites Using a Microwave-Assisted Combustion Method. *Ceram. Int.* **2016**, *42* (3), 4204–4211. https://doi.org/10.1016/j.ceramint.2015.11.094.

(60) Zeng, L.; Zhao, T. S.; An, L. A High-Performance Supportless Silver Nanowire Catalyst for Anion Exchange Membrane Fuel Cells †. *J. Mater. Chem. A Mater. energy Sustain.* **2014**, *3*. https://doi.org/10.1039/c4ta05005c.

(61) Bidault, F.; Kucernak, A. A Novel Cathode for Alkaline Fuel Cells Based on a Porous Silver Membrane. *J. Power Sources* **2010**, *195* (9), 2549–2556. https://doi.org/10.1016/j.jpowsour.2009.10.098.

(62) Sleightholme, A. E. S.; Varcoe, J. R.; Kucernak, A. R. Oxygen Reduction at the Silver/Hydroxide-Exchange Membrane Interface. *Electrochem. commun.* **2008**, *10* (1), 151–155. https://doi.org/10.1016/j.elecom.2007.11.008.

(63) Lu, Y.; Wang, Y.; Chen, W. Silver Nanorods for Oxygen Reduction: Strong Effects of Protecting Ligand on the Electrocatalytic Activity. *J. Power Sources* **2011**, *196* (6), 3033–3038. https://doi.org/10.1016/j.jpowsour.2010.11.119.

(64) Salomé, S.; Rego, R.; Oliveira, M. C. Development of Silver-Gas Diffusion Electrodes for the Oxygen Reduction Reaction by Electrodeposition. *Mater. Chem. Phys.* **2013**, *143* (1), 109–115. https://doi.org/10.1016/j.matchemphys.2013.08.026.

(65) Wang, W.; Zhao, Q.; Dong, J.; Li, J. A Novel Silver Oxides Oxygen Evolving Catalyst for Water Splitting. *Int. J. Hydrogen Energy* **2011**, *36* (13), 7374–7380. https://doi.org/10.1016/j.ijhydene.2011.03.096.

(66) Zhang, Y.; Liu, J.; Huang, X.; Lu, Z.; Su, W. Low Temperature Solid Oxide Fuel Cell with Ba0.5Sr0.5Co0.8Fe0.2O3 Cathode Prepared by Screen Printing. *Solid State Ionics* **2008**. https://doi.org/10.1016/j.ssi.2008.02.008.

(67) Lin, Y.; Ran, R.; Shao, Z. Silver-Modified Ba0.5Sr0.5Co0.8Fe 0.2O3-δ as Cathodes for a Proton Conducting Solid-Oxide Fuel Cell. *Int. J. Hydrogen Energy* **2010**, *35* (15), 8281–8288. https://doi.org/10.1016/j.ijhydene.2009.12.017.